

# **Distribution of Liquid, Vapor and Ice in a Phase Budget of a Colorado Orographic Cloud System**

By  
Taneil Uttal

Department of Atmospheric Science  
Colorado State University  
Fort Collins, Colorado



**Department of  
Atmospheric Science**

Paper No. 388

DISTRIBUTION OF LIQUID, VAPOR AND ICE IN A PHASE  
BUDGET OF A COLORADO OROGRAPHIC CLOUD SYSTEM

By  
Taneil Uttal

This report was prepared with support provided by  
National Science Foundation Grant ATM-8109590  
Principal Investigator, Lewis O. Grant  
and the NOAA Weather Modification Program Office  
and Wave Propagation Laboratory

Department of Atmospheric Science  
Colorado State University  
Fort Collins, Colorado

May 1985

Atmospheric Science Paper No. 388

**ABSTRACT OF THESIS**  
**DISTRIBUTION OF LIQUID,VAPOR AND ICE IN A PHASE**  
**BUDGET OF A COLORADO OROGRAPHIC**  
**CLOUD SYSTEM**

In this thesis, the distribution of cloud water between the liquid, vapor and ice phases in an orographic cloud system is addressed. The case study presented considers the upper levels of a wintertime cloud in the mountains of northwest Colorado. The period studied is one of minimal synoptic scale influences. Therefore, an opportunity is provided to examine the water phase distributions in the cloud as a function of the topography.

A major task in this study involves the development of a method by which ice water contents can be determined. Model generated ice particle trajectories through temperature defined growth regimes are used to predict particle habits. These predictions are shown to correspond closely to measurements of habit made with a decelerator on board a cloud physics aircraft. The correlation is sufficient to allow the use of temperature to parameterize ice crystal types in the cloud. Habit stratification based upon temperature allows determination of the volume to mass relationships which are used in conjunction with crystal size spectra to calculate ice water contents. Vapor contents are determined from aircraft measurements and simple thermodynamic calculations, and liquid contents are measured directly with aircraft.

Major conclusions of this study are:

1. Model results and in-cloud observations of particle habit confirm that crystal trajectories in the upwind regions of the cloud are horizontal. This results in significant habit stratification which is expected on the basis of model trajectories.
2. The habit stratification observed upwind of the barrier is not observed on the lee side of the mountain due to mixing associated with gravity wave induced downdrafts.
3. Liquid contents attain a maximum over the barrier crest of  $0.10 \text{ g/m}^3$ .
4. Ice contents attain a maximum of  $1.5 \text{ g/m}^3$ . This maximum is downwind and lower in altitude than the liquid maximum.
5. Vapor contents and maximum ice contents are of comparable magnitude, however maximum liquid contents are lower by a factor of ten. This suggests that in the cloud studied liquid is a small difference between two large competing phases, ice and vapor.
6. Total water contents (ice + liquid + vapor) are quasi-constant in the cloud, except for decreases on the downwind side of the mountain due depletion by precipitation processes.

7. The case study presented has low potential for artificial modification to augment precipitation at the levels between 4000 m MSL and 6000 m MSL that were accessible to the aircraft. This does not preclude the possibility of cloud seeding potential in lower levels of the cloud.
8. Model results and in-cloud observations suggest that maximum snow fall rates will occur on the lee side of the Park Range where downdrafts increase precipitation of ice crystals out of the cloud.

This study introduces a method for extending the understanding of the physical structure of an orographic cloud systems and designing a successful program for augmentation of winter snow packs in the Rocky Mountains. Previous weather modification studies have relied on statistical results rather than on a firm understanding of the controlling microphysical processes. This thesis is part of a larger program of study dedicated to such an understanding.

Taneil Uttal

Department of Atmospheric Science

Colorado State University

Fort Collins, Colorado 80523

Spring, 1985

## **ACKNOWLEDGEMENTS**

My work has been in part supported by the NOAA Weather Modification Program Office directed by Merlin Williams and the NOAA Wave Propagation Laboratory, Radio Meteorology Program Area directed by David C. Hogg. In preparing this thesis I have been guided by the expertise of Professor Lewis O. Grant and Robert M. Rauber. My other committee members, Professor Tom McKee and Professor Viswanathan Bringi also made numerous contributions. Bill Moninger was the original instigator of my interest in meteorology, and his support has played no small part in the completion of this work. Thanks are due to the National Center for Atmospheric Research (NCAR) Computer Science Division and the NCAR Research Aviation Facility for support in processing of the data, and the NOAA Weather Research Program Area for permitting me to use their word processor. Other individuals who have aided my work, each in their own special way are Jan Davis, and Lucy McCall. The final word processing was skillfully executed by Rita Bonino and Ginnie Kulpa of Raven Systems and Research, Inc. Finally, appreciation and love to my husband Rusty Jesse who provided some of the drafting and all of the moral support for many many months.

This research is based upon work supported by the National Science Foundation under Grant # ATM8109590.

## TABLE OF CONTENTS

<u>CHAPTER</u>	<u>PAGE</u>
ABSTRACT.....	iii.
ACKNOWLEDGEMENTS.....	vi.
LIST OF TABLES.....	ix.
LIST OF FIGURES.....	x.
1. INTRODUCTION.....	1.
1.1 Statement of the Problem.....	1.
1.2 Background.....	2.
1.3 Applications of Phase Water Budgets to Weather Modification.....	9.
2. RESEARCH APPROACH.....	11.
3. THE EXPERIMENT AND INSTRUMENTATION.....	12.
3.1 Description of the C.O.S.E. project.....	12.
3.2 Instrumentation.....	14.
i. The Aircraft.....	14.
ii. The Ku-band Radar.....	16.
iii. The Radiometer.....	17.
iv. Rawinsonde Launches.....	17.
v. The Decelerator.....	17.
4. ANALYSIS TECHNIQUES.....	19.
4.1 Vapor Water Content Calculations.....	19.
i. Method.....	19.
ii. Limitations.....	20.
4.2 Note on Liquid Water Measurements.....	21.
4.3 Ice Water Content Calculations.....	22.
i. Background and Approach.....	22.
ii. Model Calculations.....	26.
iii. Equations Relating Crystal Size and Habit to Crystal Mass.....	28.

5.	RESULTS.....	30.
5.1	Synoptic Conditions - December 15, 1981...	30.
5.2	The Flight Track.....	40.
5.3	Model Results and In-cloud Observations...	41.
5.4	Distribution of Vapor, Liquid, Ice, Total Water and Associated State and Microphysical Data Along Horizontal Flight Legs.....	58.
i.	The 4100 Meter Flight Leg (Fig. 15A and 15B).....	59.
ii.	The 4500 Meter Flight Leg (Fig. 16A and 16B).....	62.
iii.	The 4800 Meter Flight Leg (Fig. 17A and 17B).....	65.
iv.	The 5100 Meter Flight Leg (Fig. 18A and 18B).....	68.
v.	The 5400 Meter Flight Leg (Fig. 19A and 19B).....	71.
vi.	The 5700 Meter Flight Leg (Fig. 20A and 20B).....	71.
vii.	The 6000 Meter Flight Leg (Fig. 21A and 21B).....	76.
5.5	Two Dimensional Distributions of Vapor, Liquid, Ice, Total Water and Associated Microphysical Data.....	76.
6.	DISCUSSION AND CONCLUSIONS.....	85.
6.1	Particle Trajectories.....	85.
6.2	Ice Studies.....	87.
6.3	Budget Studies.....	89.
7.	SUGGESTIONS FOR FUTURE RESEARCH.....	91.
8.	APPENDIX I.....	93.
9.	REFERENCES.....	95.



## List of Tables

<u>Number</u>		<u>Page</u>
1.	Comparison of Precipitation Efficiencies Calculated From Water Budget Studies.....	8.
2.	Ice Mass for Identical Spectra Assuming Different Crystal Habits.....	22.
3.	Crystal Length to Mass Relationships.....	29.
4.	Timetable of Aircraft Flight Track Manuevers.....	43.
5.	In-Cloud Crystal Habit Summary.....	49.
6.	Crystal Types Utilized in Classification Procedures.....	54.

## List of Figures

<u>Figure</u>	<u>Page</u>
1. Hypothetical Water Budget Curves.....	3.
2. The COSE Study Area.....	13.
3. 0600 GMT Surface Map for 15 December 81....	31.
4. 0000 GMT 500 mb Map for 15 December 81.....	32.
5. 1200 GMT Surface Map for 15 December 81....	33.
6. 1200 GMT 500 mb Map for 15 December 81.....	34.
7. 1800 GMT Surface Map for 15 December 81....	35.
8. Radiometer-Radar-Surface Snow Measurements.....	37.
9. Profiles of Equivalent Potential Temperature.....	38.
10. Profiles of Wind Speeds.....	39.
11. Flight Cross-Section: 15 December 81 CIC Flight.....	42.
12. Computer Modeled Parcel Trajectories for 15 December 81.....	44.
13. Computer Modeled Particle Trajectories for 15 December 81.....	45.
14. Ice Crystal Observations In-Cloud by Microphysics Aircraft.....	48.
15A. 4100 m MSL Flight Leg: Altitude, Pressure, VWC, LWC, IWC, Total Water, Topography.....	60.
15B. 4100 m MSL Flight Leg: Theta, Theta-e, Dew point, Temperature, 2-D Concentration Topography.....	61.
16A. 4500 m MSL Flight Leg: Altitude, Pressure, VWC, LWC, IWC, Total Water, Topography.....	63.

16B.	4500 m MSL Flight Leg: Theta, Theta-e, Dew point, Temperature, 2-D Concentration, Topography.....	64.
17A.	4800 m MSL Flight Leg: Altitude, Pressure, VWC, LWC, IWC, Total Water, Topography.....	66.
17B.	4800 m MSL Flight Leg: Theta, Theta-e, Dew point, Temperature, 2-D Concentration Topography.....	67.
18A.	5100 m MSL Flight Leg: Altitude, Pressure, VWC, LWC, IWC, Total Water, Topography.....	69.
18B.	5100 m MSL Flight Leg: Theta, Theta-e, Dew point, Temperature, 2-D Concentration Topography.....	70.
19A.	5400 m MSL Flight Leg: Altitude, Pressure, VWC, LWC, IWC, Total Water, Topography.....	72.
19B.	5400 m MSL Flight Leg: Theta, Theta-e, Dew point, Temperature, 2-D Concentration Topography.....	73.
20A.	5700 m MSL Flight Leg: Altitude, Pressure, VWC, LWC, IWC, Total Water, Topography.....	74.
20B.	5700 m MSL Flight Leg: Theta, Theta-e, Dew point, Temperature, 2-D Concentration Topography.....	75.
21A.	6000 m MSL Flight Leg: Altitude, Pressure, VWC, LWC, IWC, Total Water, Topography.....	77.
21B.	6000 m MSL Flight Leg: Theta, Theta-e, Dew point, Temperature, 2-D Concentration Topography.....	78.
22.	Vapor water contents.....	79.
23.	Liquid water contents.....	80.
24.	Ice water contents.....	82.
25.	Average crystal sizes.....	83.
26.	Crystal concentrations.....	84.

## 1. INTRODUCTION

### 1.1 Statement of the Problem.

The purpose of this thesis is to consider the spatial distribution of the water substance of an orographic cloud in the Colorado Rockies in a phase water budget. To facilitate this goal the meaning of the term "water budget" as it is used in this paper must be clarified. Earlier works on cloud water budgets have traditionally described the total water contents of cloud systems or examined the difference between total inflow and total outflow values without water phase distinctions. In this paper, "water budget" refers to the distribution of the water in the cloud into its respective phases of vapor, liquid and ice, with a distinction being made between in-cloud ice and ice phase precipitation.

One specific task is the development and testing of a method to determine ice contents in the cloud. This method is to be based on both model calculations and in-cloud observations. In addition, the spatial variation of vapor, liquid, and ice is examined in relation to the underlying topography. Given appropriate air stream conditions of increasing equivalent potential temperature and wind shear with height, lee waves can occur with amplitudes dependent on the shape of the mountain. Under the influence of the forced lifting that the waves produce, initially high vapor contents will condense to form increased amounts of liquid and ice. Two processes occur which favor the growth of the ice. 1) The ice begins to utilize the liquid in growth processes

slowing the rate of increase of total liquid contents in the updraft region, and 2) On the lee side of the mountain where strong downdrafts and reevaporation occurs, both the ice and the remaining liquid will be quickly depleted. However, reevaporation rates for liquid will be greater than for ice since supersaturations with respect to ice are lower than supersaturations with respect to water. Also, water droplets will be much smaller than ice in cold clouds and will evaporate more quickly. Because of these factors, it is expected that maximas in ice contents will be downwind of maximas in liquid. Assuming an absence of precipitation, the sum total of the vapor, liquid and ice components should remain constant throughout this process. This is shown schematically in Fig. 1. Since interest is focused on topographical effects of the mountain barrier, the cloud chosen for study was one in which there was a strong orographic wind component.

As an essential part of the budget study additional cloud features such as crystal concentrations, temperature structure, and average droplet and crystal size distributions in the cloud are characterized. Conclusions are made relating all elements of structure to the primary controlling factor, the underlying topography.

## 1.2 Background

The components of a water budget can either be calculated by theoretical modeling, based on dynamic and thermodynamic principles, or they can be measured by a combination of ground-based remote sensing and

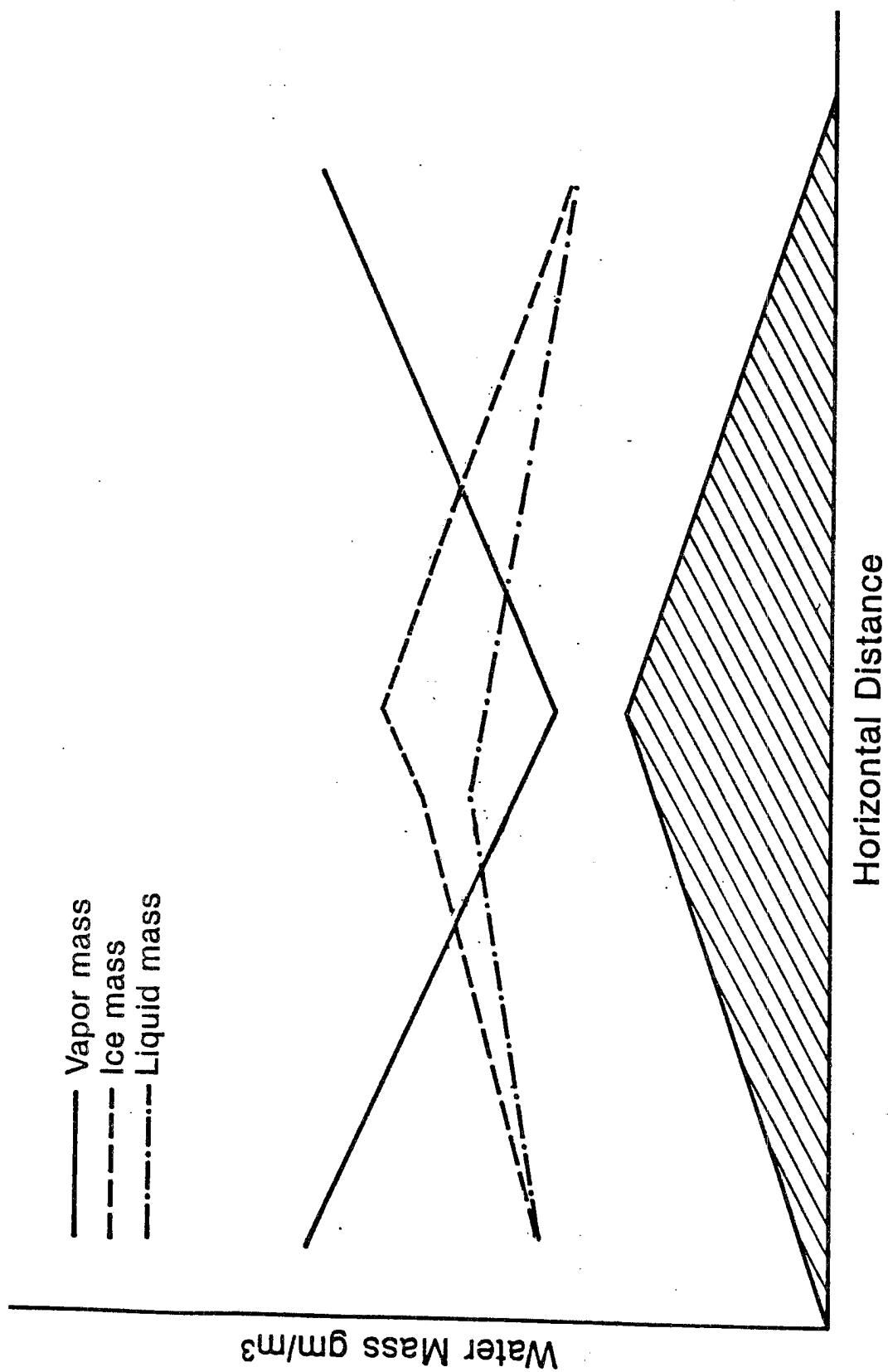


Figure 1. Hypothetical Water Budget Curves

airborne meteorological instruments. The former course of action has many problems. The primary difficulty is that a detailed knowledge of ice growth mechanisms, rates and conditions must be well understood theoretically if any kind of realism in the apportionment of the water content between the vapor, liquid and solid phases is to be accomplished. This is difficult since information on nucleation, when it occurs and in what concentrations is lacking. Therefore, field studies become a logical alternative to study the problem.

In the existing literature, little or nothing appears on the specific subject of phase water budgets in clouds. It is however extremely useful to examine the field work that has been done on the total water contents of cloud. In examining the problem of total water contents of clouds, several researchers have made full use of the scanty field measurements that have been available. In doing such work, two types of cloud systems that have been observed are 1) the orographic cloud and 2) the traveling midlatitude cyclone. The treatment of these two systems has been fundamentally different and an inspection of the different approaches applied yields insight into a fundamental difficulty.

In orographic clouds the problem of spatial variation of cloud water as a function of the uplift provided by an orographic barrier has been studied. In traveling cyclones the temporal variation of cloud water and precipitation is examined as a function of storm stage. These two kinds of studies emphasize two very different problems. In the first case the primary mechanism of change is a physical barrier, and the frame of reference in which change is examined is stationary with respect to that barrier. In the second case, the major effect on cloud

water distributions are dictated by synoptic development, and the frame of reference is Lagrangian, tracking the storm element of interest. Thus, a major problem emerges, the separation of variation in time from variation in space.

To consider both synoptic and orographic effects simultaneously, the complexity of the problem is greatly magnified. One of the works in which both factors were treated is that of Elliot and Shaffer (1962). They observed that a high variability was present in the ratio of mountain to coastal plain precipitation for a southern California location. On the basis of these ratios, the distinction was made between orographic precipitation and non-orographic precipitation. Orographic precipitation was defined as precipitation occurring in the mountains minus that occurring on the coast, which hypothetically results in the components of precipitation that occurred strictly as a function of the uplift created by the mountain barrier. The variances in coastal precipitation as compared to mountain precipitation was then related to air mass stability. The general trend emerged that a maximum orographic component of precipitation occurred in unstable air masses and a dominating non-orographic component of precipitation occurred in stable air masses.

Ensuing work on the water budgets of orographic clouds have typically been more limited in scope, the philosophy being that the synoptic effect and the orographic effect are best understood separately before the combined effect and interactions of the two can be investigated. In treating just the orographic case Elliot and Hovind (1964) presented the method of using rawinsondes to measure air moisture and flow parameters at the inflow and the outflow regions of a



barrier. Using the mixing ratios of cloud vapor, cloud water, and the wind component normal to the barrier, the total available condensate in the inflow is calculated by integrating vertically through the depth of the cloud. The process is repeated for the outflow region of the cloud, with the difference of the inflow total condensate minus the outflow total condensate being the total available condensate (C). The ratio of precipitation measured at the ground (P) to total available condensate (C) is defined as precipitation efficiency (P/C). Precipitation efficiency in this framework is lowered by the advection of cloud water and precipitation out of the immediate area of the barrier. The limitations of atmospheric sounding techniques, precipitation gage inaccuracies, and particle trajectories which place particles out of the region of interest contribute to inaccuracies in the measurements. Similar procedures have been followed by Rasmussen et al. (1969), Balick and Rasmussen (1972), Hindman et al (1981), and Riehl and Williams (1981).

Using a similar method, a more exact physical interpretation was developed by Dirks (1973) on the basis of three rather than two soundings, with the additional sounding located at the top of the barrier. Total available condensate was defined as the difference between upwind and mountain top integrated moisture profiles. Precipitation, rather than being measured at the ground was defined as the difference between the inflow and the outflow integrated moisture profiles. Dirks used aircraft measurements to accurately monitor cloud top height and, therefore, the amount of lifting of the air passing over the barrier. Precipitation efficiency was again defined as the ratio of precipitate to condensate, but the definition of precipitation and

condensate are different from those in the work by Elliot and Hovind. With the two sounding approach, total available condensate was defined as the difference between inflow and outflow moisture and precipitation is measured at the ground. In the three sounding approach total available condensate is the difference between inflow and mountain top soundings, and precipitation is given the definition allotted to total available condensate in the two sounding approach. In Dirk's work, a primary factor that contributed to a precipitation efficiency less than one was the reevaporization resulting in storage of potential condensate in the atmosphere. The problem of crystal trajectories is avoided because precipitation is not required to strike the ground in a specified area to be defined as precipitation. Therefore the usually bad assumption that all condensed water falls out immediately, and directly above the point of condensation, as is assumed in many orographic precipitation models, is circumvented. The problem of accurate measurement of precipitation over a mountainous region with a low density of gages is also avoided.

The method described by Elliot and Hovind (1964) focuses on the problem of advection hydrometeors away from the target area resulting in low precipitation efficiencies. The method described by Dirks (1973) emphasizes the underutilization of the available water resources due to storage of condensate and potential condensate in the atmosphere. Keeping these differences in mind it is instructive to examine the precipitation efficiencies which have been calculated for various types of storms. Data from several studies are summarized in Table 1. It is interesting to note that given advection processes it is theoretically possible for precipitation efficiencies greater than 100% to occur (Hobbs and Mateyba, 1981).

TABLE 1.

## Comparison of Precipitation Efficiencies from Water Budget Studies

Source	Location	Precipitation Efficiency
Elliott and Schaffer (1962)	Santa Yucz, CA	0.35
	San Gabriel, CA	0.67
Elliot and Hovind (1964)	Santa Yucz, CA	0.17
	(stable)	
	Santa Yucz, CA	0.26
	(unstable)	
	San Gabriel, CA	0.25
	(stable)	
	San Gabriel, CA	0.27
	(unstable)	
Dirks (1973)	Medicine Bow, WY	0.56
DeMott (1984)	Park Range, CO	0.05
	(stable)	
	Park Range, CO	0.39
	(unstable)	
Riehl and Williams (1981)	Wasatch Mtns, UT	0.63
Balick and Rasmussen (1972)	Leadville, CO	0.90

### 1.3 Applications of Phase Water Budgets to Weather Modification

In past weather modification projects, great reliance has been put on the hope that clear statistical trends by which the effects of cloud seeding can be verified will emerge. Unfortunately, precipitation data generates an extremely noisy signal, on the order of 200%, therefore modification of the precipitation signal is difficult to detect with any reliability, since artificial increases in snowfall are much smaller in magnitude (~10%) than the natural fluctuations. For meaningful statistical trends to emerge, data sets have to be collected over several years, and become prohibitively time consuming and expensive. Evaluation of weather modification potential is important however since even small increases in the amount of precipitation and winter snowpack in a given year would have positive results for the American Southwest and Mexico.

The microphysics of a cloud must be sufficiently understood in order that real and useful effects of precipitation augmentation can be studied and utilized. This implies a good understanding of cloud dynamics which controls particle trajectories in a cloud and thereby the environmental factors of specific humidity, temperature and pressure which influence particle formation, growth, and distribution. As such, understanding both large and small scale processes is imperative.

Precipitation efficiency is modified by both microphysical and dynamical factors including: 1) barrier size; 2) air mass stability; 3) liquid water content; 4) cloud condensation nuclei; 5) cloud droplet spectras 6) ice crystal concentrations; 7) cloud temperatures; 8) wind speeds which affect available crystal growth times; and, 9) three-

dimensional airflow dictating particle trajectories. As such it is a product of all of the ingredients of cloud physics which must be thoroughly understood before a firmly based theory of weather modification can be formulated.

Precipitation efficiency can be considered as a measure of the potential that a cloud has for modification. A cloud which already has extremely high ice contents as compared to liquid contents is naturally efficient and therefore a poor choice for seeding efforts. Conversely, a cloud with abundant supercooled water exhibits a much more promising environment for effective seeding operations. Part of this thesis will be to estimate the potential for modification of the particular cloud studied. The approach described is one that can be applied to future studies of different kinds of clouds.

## 2. RESEARCH APPROACH

The research approach involves a detailed analysis of a single case study. The data utilized in the study to develop the phase water budget was collected using an instrumented aircraft designed to measure environmental conditions as well as microphysical characteristics of the cloud. In the last ten years vast improvements have occurred in the quantity and quality of such airborne cloud physics instrumentation. Such sensors as the Particle Measuring Systems (PMS) 2-Dc probe developed by Knollenberg (1976), the Forward Scattering Spectrometer probe and the Fast Response Temperature probes yield the data elements necessary for measuring a phase water budget.

The measurement of liquid water is straight forward using a J-W Hotwire device. Vapor water contents is calculated from the dew point temperature and pressure. The greatest difficulty is the development of a satisfactory method for calculating ice water contents from available data. The method used is described in section 4.3 and is dependent on the characteristics of the individual cloud studied. The method is based on examination of particle trajectories through the cloud and the resulting relationship between the crystal habits and the temperature layers in the cloud.

The variation in space of cloud water in the vapor, liquid and solid phases are examined in relationship to one another. Trends are examined for different levels of the cloud and variations induced by the topography will be discussed.

### 3. THE EXPERIMENT AND INSTRUMENTATION

#### 3.1 Description of C.O.S.E. Project

The Cloud Orographic Seeding Experiment III (C.O.S.E. III) is part of an ongoing research program operated by Colorado State University (C.S.U.) in northwestern Colorado in the Park Range Mountains. The purpose of the experiment is the characterization of wintertime orographic clouds for both the scientific value as well as the application of such information to the understanding of modification potential. In the 1981-82 field season efforts were directed to a study of natural conditions in clouds and no artificial seeding occurred.

The primary mountain barrier where observations were made runs north to south with the prevailing flow pattern in the winter intersecting the barrier perpendicularly. The west to east flow is further enhanced by the channeling effects of the Yampa valley which runs east-west until it reaches the Park Range at which point it takes a sharp turn to the south (See Fig. 2). In the winter the Park Range is frequently embedded in a blanket cloud which forms as the flow is lifted orographically.

The C.O.S.E. III project utilized a large array of instrumentation including the Colorado International Corporation (C.I.C.) Cheyenne II and National Oceanographic and Atmospheric Administration (N.O.A.A.) P-3 aircrafts, vertically pointing K and KU-band radars, the Bureau of

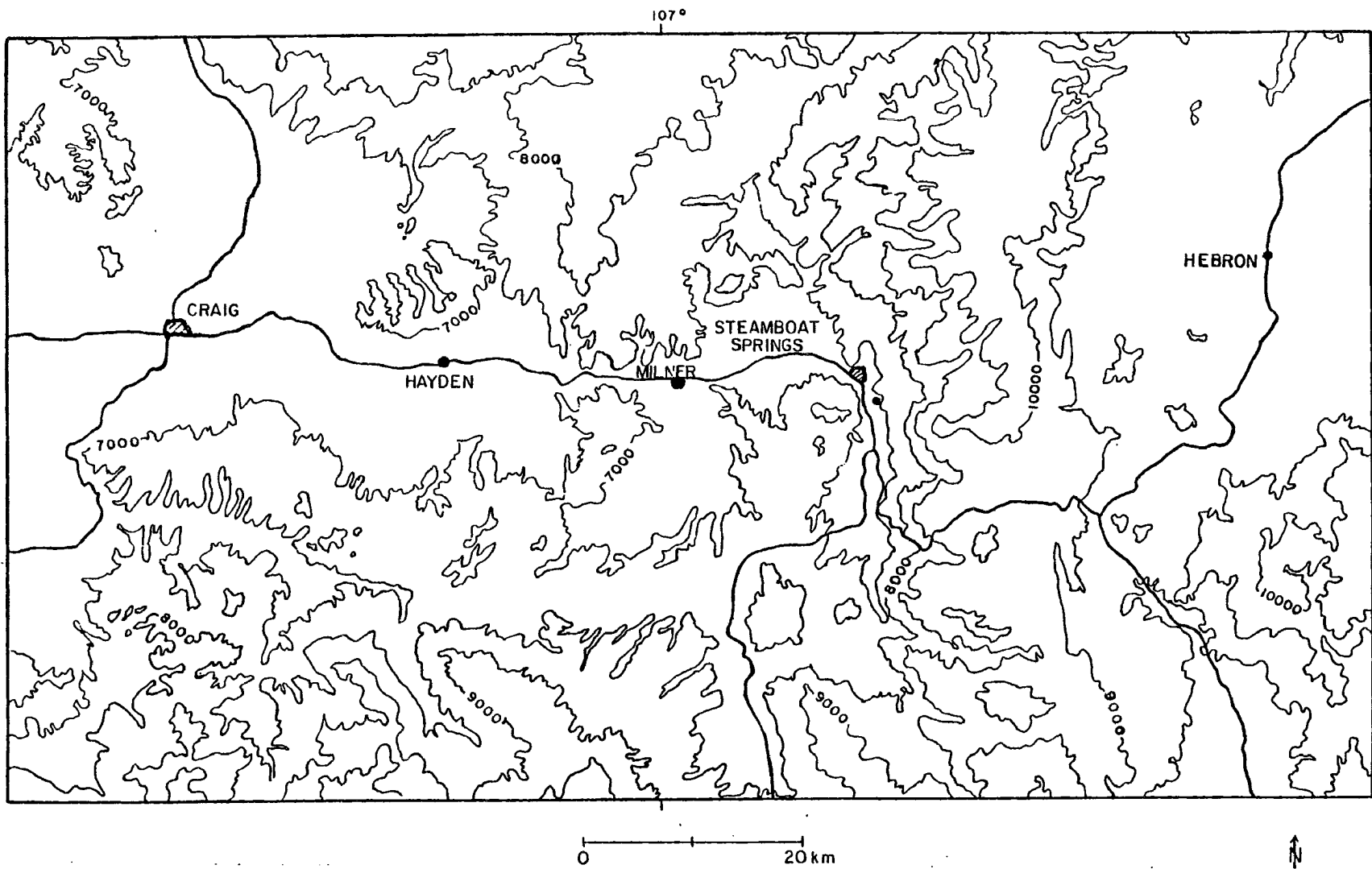


Figure 2. The COSE Study Area



Reclamation scanning C-band radar, the NOAA dual channel scanning radiometer, rawinsonde observations both upwind and downwind of the mountain, surface observation of ice crystals at three locations, high volume samplers for detection of atmospheric aerosols, the University of Utah lidar, and GOES West satellite data. The instruments which yielded data of immediate importance to this report are described in some detail in the following sections.

### 3.2 Instrumentation

#### i. The Aircraft

The C.I.C Cheyenne II aircraft was the primary instrument platform used in this study. A complete listing of instruments is found in Appendix I.

Instruments used in this study were the Rosemont temperature probe, the Cloud Technology J-W type liquid water content device, the Setra Systems Static pressure altimeter, the VOR azimuth and DME distance recorders, the Particle Measuring Systems (PMS) 2-D Optical Array probe (OAP), and the actual collection of ice crystals inflight with a particle decelerator. Particular attention is given to the PMS 2-D Optical Array Probe in the following section, since interpretation of the data from this instrument was critical to the method chosen for calculating ice water contents.

The two-dimensional optical array probe developed by Knollenberg (1976) consists of a 1.5 mW helium-neon (He-Ne) laser beam which impinges on a linear array of photo diodes. Particles passing between

the sensor array and the radiating laser will cast a shadow, and a record is made of which diodes lose 50% light intensity as a result of the blockage. As a particle moves through the array, it is recorded as a series of slices which can be reconstructed to yield the particle image. The linear array is composed of thirty-two photo diodes, each having a twenty-five micron diameter. The maximum sampling rate for the probe is 4 Mhz and is governed by the speed of the aircraft since the sampling volume is the cross sectional area of the probe ( $0.488 \text{ cm}^2$ ) multiplied by the true air speed. Particle size distributions can be used to develop size spectra in a specified number of channels.

Limitations of the probe that effect this work are as follows: (1) Particles smaller than 150 microns should be sized using a smaller depth of field (Heymsfeld and Parrish, 1979 and Baumgardner and Dye, 1983). Consequently, concentrations of small particles can be incorrect by as much as an order of magnitude. Since the primary interest of this study in this study is in total ice mass to which even large numbers of small particles make only a small contribution, this is not an important factor. However, there may be a significant effect in calculations of mean crystal sizes. (2) The maximum dimension that the probe can measure in the vertical dimension is 800 microns and in the horizontal dimension is 25,000 microns or greater. Therefore, very large crystals and aggregates can be grossly undersized when the particle passes through the sensor crosswise and the vertical dimension is used for sizing the crystal. This also implies that estimates of particle size will become much worse as the particle shape departs from spherical. (3) The sensor provides information on particle shape in only two dimensions rather than in three. Therefore the orientation of the

particles as it passes through the sensor is extremely important. For instance, a plate which passes edge on through the sensor will cast an image resembling a thin column or a needle. The aircraft channels flow in such a way as to create preferred crystal orientations, and therefore the mounting location of the probe on the plane can be extremely important (Beard, 1983).

#### ii. The Ku-Band Radar

The C.S.U. Ku-band radar was constructed and specifically designed by the Atmospheric Science Department for the observation of cold orographic clouds. The radar is fixed vertically and utilizes a 1.79 cm wavelength which is optimal for the detection of cloud ice particles. Since radar reflectivity is a function of particle diameter to the sixth power, the small supercooled water droplets in cold clouds do not make a significant contribution to the reflectivity measurement. Data is output in real time on a line printer in the form of a vertical reflectivity profile with a resolution of 100 meters and a total vertical extent of eight kilometers. The profiles are outputted at a rate of 30 seconds or an operator determined multiple of 30 seconds. The end result is a time height history of the vertical structure of the cloud reflectivity. Hardware specifications can be found in the C.O.S.E. III Operation Log (Rauber and Grant, 1982).

### iii. The Radiometer

The NOAA radiometer is a dual channel instrument designed for the measurement of both total integrated water vapor and cloud liquid water in a column determined by the orientation of the antenna beam. The radiometer operates passively, and depends for signal on the natural emissions of water vapor and liquid water at 20.6 GHz and 31.6 GHz respectively, which corresponding to the peak of wave absorption of the two measured parameters. Because microwave radiometers at these wavelengths do not respond to ice, it is assumed that the measured quantities include only water in the liquid or vapor state. The system has various scanning modes including: (1) fixed; (2) variable azimuth at fixed elevation; and, (3) 360 azimuth scans at fixed elevation. (Hogg et.al., 1983).

### iv. Rawinsonde Launches

Rawinsondes were released in Craig sixty kilometers upwind of the Park Range and also in Hebron just downwind of the barrier. (See Fig. 2). Releases occurred at three hour intervals during periods when the aircraft was over the study area

### v. The Decelerator

Samples of ice crystals were taken in the cloud with a divergent flow decelerator tube. The decelerator ratio is 11:1 and the collection efficiency is better then 50% for particles 30 microns or bigger, and

90% for particles 70 microns or bigger. The crystals impacted on a slide coated with mineral oil, with the exposure time controlled by the operator. Slides were stored in silicone in test tubes that were packed in dry ice. Slides were then photographed under magnification with excellent image quality. A more complete description of the instrument has been made by Cooper and Vali (1981).

#### 4. ANALYSIS TECHNIQUES

In this section, the methods used for calculation of the component parts of the phase water budget are discussed.

##### 4.1 Vapor Water Content Calculations

###### i. Method

Lowe (1977) has developed an approximating polynomial for the computation of saturation vapor pressures from temperature within the range  $-50^{\circ}\text{C}$  to  $+50^{\circ}\text{C}$ . The polynomial is of the form:

$$e_s = a_0 + T(a_1 + T(a_2 + T(a_3 + T(a_4 + T(a_5 + a_6 T))))),$$

with the numerical coefficients defined as:

$$a_0 = 6.107799961$$

$$a_1 = 4.436518521 \times 10^{-1}$$

$$a_2 = 1.428945805 \times 10^{-2}$$

$$a_3 = 2.650648471 \times 10^{-4}$$

$$a_4 = 3.031240396 \times 10^{-6}$$

$$a_5 = 2.034080948 \times 10^{-8}$$

$$a_6 = 6.136820929 \times 10^{-11}$$

This polynomial has been shown to compare favorably in accuracy to more precise calculations, and has the additional advantage of being economical computationally compared to other methods which typically require some form of exponentiation. For this study, actual vapor pressures (e) were required and therefore, dewpoint temperatures were substituted for temperature. The mixing ratio was calculated using:

$$w = 0.622 \frac{e}{p - e},$$

and density is calculated as a function of pressure and temperature:

$$D = D_0 \left( \frac{T_0}{T} \right) \left( \frac{P}{P_0} \right)$$

In the density calculation, a reference pressure of 600 mb and a reference temperature of  $-10^{\circ}\text{C}$  was assumed. Density multiplied by the mixing ratio yields the desired values of total vapor content in units of  $\text{g/m}^3$ .

## ii. Limitations

Examination of the state parameter data, indicated that upon several occasions when liquid water contents were in excess of  $.01 \text{ g/m}^3$  indicating water saturated conditions that  $T \neq T_d$ . This problem resulted partially because of the long response time of the dewpoint sensor, a Peltier cooled mirror, and partially as a result of the accuracy of the instrument ( $\pm 1^{\circ}\text{C}$ ).

Using another set of data when the FSSP was operational, a short test program was run to calculate the magnitude of the "dew point offset" by averaging all values of  $|T - T_d|$  when FSSP readings exceeded  $.01 \text{ g/m}^3$ . An average offset of  $.807^\circ\text{C}$  was obtained. This correction was not applied to the data set of interest on the basis of the fact that a  $.807^\circ\text{C}$  offset is less than the accuracy range of the the instruments.

#### 4.2 Note on Liquid Water Measurements

Ideally liquid water contents would have been obtained by direct measurement by both the FSSP and the J-W Hotwire probe, however, on the day of interest the FSSP was inoperative. Knollenberg (1972) compared the Hotwire values to the values obtained from integrating the spectrum of the Optical Array Probe, and concluded that agreement was excellent for small ( $<30$  microns) droplet populations as are expected for cold wintertime clouds. More recently, using data from a previous Park Range Study the J-W liquid water device has been compared to the FSSP by Rauber (1981). Comparisons have also been down between the J-W and the Axially Scattering Spectormeter Probe (ASSP) by Knollenberg (1972). The ASSP is also designed by PMS and is subject to similar operational problems as the FSSP. A discussion of both comparisons can be found in Rauber (1981), where it was concluded that the trends observed in LWC by the J-W are fairly reliable assuming that a clear air offset is subtracted from the values yielded by the instrument. The clear air offset is a value of water content that the J-W probe would register in clear air. Examination of the data on the day of interest indicated that the clear air offset was zero, and therefore no corrections on the data set were necessary.



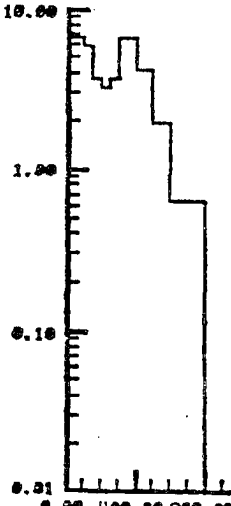
### 4.3 Ice Water Content Calculations

#### 1. Background and Approach

Calculation of ice water contents from 2D-c size spectra presents a major difficulty. This difficulty is a function of the disparate volumes of particles of similar sizes because of the variations in shape, density and structure of different particle habits. Therefore, not only a size spectra, but a knowledge of predominant crystal types is necessary to determine crystal masses. Significant variations in calculated mass can result from assuming different habits for identical size spectras (see Table 2).

Table 2.

#### Ice Mass for Identical Spectra Assuming Different Crystal Habits

Crystal Size Spectra	Solid Water Content	Habit
	0.034	Dendrite
	0.077	Plate
	0.089	Cold Column
	0.110	Warm Column

Currently, the particle measurement systems 2D-c Optical Array Probe (OAP) developed by Knollenberg (1976) for the detection and measurement of ice particles is a frequent airborne fixture on wintertime meteorological aircraft. In addition to particle size spectra and concentration measurements it is possible to obtain shadow graphs of particle images by the method described in Section 3.2. A number of researchers have developed elegant algorithms for detection of habit from the shadow graphs including area to length ratios (Heymsfeld and Parrish, 1979), fourier analysis (Duroure, 1982) and eigenvector analysis (Hunter, 1982). These efforts have been hampered by the the same problems involved in crystal sizing: particle orientation, and high occurrences of crystal fragments, irregular images, and problem images such as aggregates and streakers. In addition, since the sensor require 50% occlusion of a diode to trigger, crystal edges are often fuzzy, making the shape unclear. All these factors create difficulties in correctly interpreting imaged particles. At this time a truly reliable form detection scheme that can be universally applied to a variety of cases has not been developed.

The alternative approach developed in this thesis is to assume knowledge of crystal habit on the basis of temperature. It has become established fact that ice crystal habits are primarily controlled by temperature with a dependence for secondary characteristics on supersaturation with respect to water. Habit regimes as a function of the two parameters have been defined in different laboratories, including Magono and Lee (1966), Nakaya (1954) and Kobayasi (1961), with good agreement. Based on these experiments it has been established that the basic crystal shape is hexagonal with growth either occurring along

the basal plane to produce plate-like crystal or along the prism plane to produce column-like crystal. Transition temperatures, or those temperatures at which a crystal changes from plate-like to column-like growth modes or vice versa are near  $-4^{\circ}\text{C}$ ,  $-9^{\circ}\text{C}$ , and  $-22^{\circ}\text{C}$ . In addition a subset of the plate-like growth mode occurs between  $-12^{\circ}\text{C}$  and  $-16^{\circ}\text{C}$  where crystals assume dendritic characteristics.

More recently Fukuta (1984) has developed a "revised Nakaya" diagram based on work conducted at the University of Utah's wedge-shaped ice thermal diffusion chamber, (Fukuta, Kowa, and Gong, 1982). Crystal habits have been quantified with the parameter  $2a/c$  where "a" is the basal plane radius, and "c" is the prism axis length. The general trends of earlier works has been verified; however, shifts from the traditional transition temperatures have been detected. Notably, Kobayashi's diagram indicated  $2a/c$  maxima at  $-8^{\circ}\text{C}$  and minima at  $-13^{\circ}\text{C}$ . Fukuta's work indicates that these values more realistically occur at  $-5^{\circ}\text{C}$  and  $-15^{\circ}\text{C}$ .

Because of problems posed by fallout, mixing, turbulence and advection the problem of trying to correlate the distribution of crystal habits to specific temperature defined growth regimes in a cloud is potentially disastrous. Some researchers have indeed observed and noted cases in which cloud crystal shapes were too complex to correlate to specific growth regimes (Cooper and Vali, 1981). At the same time, many other observations indicate that under proper conditions, there is good to excellent agreement between observed ice crystal habits and those that would have been theoretically expected on the basis of local conditions. This phenomena has been documented in Great Lakes storms by Juisto and Weickman (1973) who observed that crystal types gathered at

the ground and in cloud by aircraft were consistent with the temperature and humidity profiles yielded by rawinsondes. In storms over Japan, Tazawa et.al. (1973) and Magono and Lee (1973) made use of a cloud-sonde to gather ice crystals on a rotating film while simultaneously making measurements of temperature and humidity with a rawinsonde. Taking into account the fall patterns of the particles, these researchers also came to the conclusion that observed particle habits were very much in keeping with theoretically expected ones. This habit information was used to calculate solid water contents which in turn were shown to vary in an orderly way with storm stage.

Ice water contents were also calculated by Heymsfield and Knollenberg (1972) for cold cirrus clouds and by Knollenberg (1972) in jet contrails. These formations are populated almost entirely with crystals of bullet shapes, and this habit information was used in conjunction with size spectra data from a 1-D probe to calculate the ice masse contents (IMC) in the clouds. The equations utilized in these calculations were of the form:

$$IMC = FR(I,J)N(I)M(I,J),$$

where  $FR(I,J)$  is the fraction of particles in size class  $I$  and habit class  $J$ ,  $N(I)$  is the number of particles in size class  $I$ , and  $M(I,J)$  is the mass of particles in size class  $I$  and habit class  $J$ . (Heymsfield and Parrish, 1979).

## ii. Model Calculations

Since the traveled path of the ice crystal through different temperature regimes is of primary importance in this analysis, a model was used to predict particle trajectories for particles of different habits and masses released at different start altitudes. Calculations involved two models developed by Rauber (1981) and are based on the work of Queney (1948) on mountain lee waves. The first model uses the governing equations of vertical momentum, horizontal momentum, continuity, and the thermodynamic energy equation and employs the boussinesq approximation in an orographic environment. This approach detailed by Smith (1979) results in an adiabatic, steady state, frictionless vertical velocity equation. The final form of the vertical velocity equation is:

$$w = \frac{-2 axhu (acos(lz) - xsin(lz))}{a^2 + x^2} - \frac{ahu}{a^2 + x^2} \sin(lz),$$

where  $w$  = vertical velocity,  $a$  = half width of mountain,  $x$  = horizontal coordinate,  $h$  = height of mountain,  $u$  = perturbation horizontal velocity,  $l$  = scorer parameter, and  $z$  = vertical grid coordinate in model. Using the measured horizontal velocities from rawinsonde soundings and the calculated vertical velocities, parcel trajectories can be predicted for a particular cloud.

The second model utilizes  $w$  to calculate crystal trajectories. Crystals are assumed to nucleate 60 km upwind of the barrier and growth by vapor diffusion is assumed. The trajectories are determined by advecting the crystal with the horizontal wind field, while at the same

time letting it fall as a function of the predicted vertical velocity field and the terminal velocity determined by particle habit and size. Growth equations are derived by considering the equilibrium conditions between latent heat production due to mass growth by conversion of vapor to ice and the rate of molecular diffusion of heat away from the crystal. Using this method growth equations are developed for different kinds of crystal habits. Six types of crystal types are considered in the model. They are: (1) columns; (2) capped columns; (3) capped columns when end-plates are so large that the column is assumed to fall like a plate; (4) plates; (5) dendrites; and, (6) plates that fall into a dendritic regime and become dendrites. Growth equations for these different crystal types are taken from Cotten (1970). Saturation vapor pressures can be varied in the model to simulate the growth condition extremes ranging from ice saturation to water saturation conditions. A complete description is found in Rauber (1981).

The model results are subject to limitations. The flow is assumed to be exactly from the west, and the restriction to two dimensions requires that blocking effects are nonexistent. The model terrain is a simple single barrier with a characteristic width and height. Therefore the effects of secondary terrain features is lost, and the flow field is much smoother than would be realistically expected. Certain rough assumptions are made about fall and growth characteristics when a particle passes between different growth regimes. For instance, when a column grows end-plates of sufficient size, it will begin to fall as a plate. Plates that fall into dendritic regimes become dendrites with immediate changes in growth and fall speed characteristics. No riming or aggregation processes are included. Despite these limitations the

similarity in basic trajectory characteristics for a wide range of particle sizes and a wide range of start altitudes for different clouds suggests that an essentially correct trajectory is being calculated.

### iii. Equations Relating Crystal Size and Habit to Crystal Mass

Assuming a knowledge of crystal habit and size, the problem becomes one of calculating crystal mass. Davis (1974) has developed a series of equations relating snow crystal volumes to size, and Heymsfield (1972) has devised corresponding equations relating crystal density to size for various habits. These equations can be combined to get a measure of crystal mass as a function of size.

Since each major crystal type has many subdivisions, a comparison was made between resulting masses of crystals of similar habits. For instance, using Mogono-Lee nomenclature, pla was compared to plb, cle was compared to clf and plc-s was compared to pld. The variance in mass within a major type was on the order of 10-25%. This variance was considered small enough to warrant the use of only one major equation relating mass to length for each of four basic categories. Therefore the four major categories of cold columns (cle/clf), warm columns (cle/clf), plates (pla/plb), and dendrites (plc-s/pld) was developed. The equations for the calculation of ice mass for each of these categories are shown in Table 3. The distinction between columns grown in the  $-22^{\circ}\text{C}$  region and the  $-9^{\circ}\text{C}$  region was necessary because of a significant difference in density between the cold and the warm columns.

Table 3.

## Crystal Length to Mass Relationships

## Dendrites

(P1e/P1d)

$$m = 5.823 \times 10^{-3} d^{2.415}$$

 $d < 100 \mu\text{m}$ 

$$m = 4.93 \times 10^{-4} d^{2.045} + 9.40 \times 10^{-4} d^{2.175}$$

 $100 \mu\text{m} < d < 300 \mu\text{m}$ 

$$m = \left(\frac{d}{1000}\right)^{-0.377} \times (3.22 \times 10^{-4} d^{2.645} + 6.14 \times 10^{-4} d^{2.175})$$

 $300 \mu\text{m} < d$ 

## Plates

(P1a/P1b)

$$m = 8.25 \times 10^{-3} d^{2.475}$$

all ranges of  $d$ 

## Cold Columns

(C1e/C1f)

$$m = 3.95 \times 10^{-2} d^{2.854}$$

 $d < 28 \mu\text{m}$ 

$$m = 2.85 \times 10^{-2} \times \left(\frac{d}{1000}\right)^{-0.0915} \times d^{2.854}$$

 $28 \mu\text{m} < d < 100 \mu\text{m}$ 

## Warm Column

(C1e/C1f)

$$m = 3.95 \times 10^{-2} d^{2.854}$$

 $d < 14 \mu\text{m}$ 

$$m = 3.72 \times 10^{-2} \times \left(\frac{d}{1000}\right)^{-0.014} \times d^{2.854}$$

 $14 \mu\text{m} < d$



## 5. Results

### 5.1 Synoptic Conditions - December 15, 1981

On the 15th of December, at 0600 GMT a weak high-pressure system was located in the four corners area of Southwest Colorado which had been stationary for approximately 15 hours. The remains of a low pressure system which had moved north of the study area the previous day, stalled in midwestern Nebraska. The associated cold front extended from the Nebraska low to southwestern Wyoming where it became a warm front associated with a storm system off the coast of the northern Continental United States (Fig. 3). Associated with the system was an area of enhanced moisture located along a strong mid-level jet (Fig. 4), which was positioned along the warm frontal boundary. At 1200 GMT (Fig. 5) three hours preceding the aircraft flight, the system had moved inland to eastern Washington state. The warm front moved south, but was still located north of the study area. The zone of enhanced moisture (Fig. 6) moved eastward and into the study area. During this time a primarily orographic induced stratiform cloud existed in the warm sector which included the study area. During the period of study, when the microphysics aircraft was aloft, the low pressure system moved across the state of Idaho. Both the warm and cold frontal boundaries remained north of Colorado (Fig. 7).

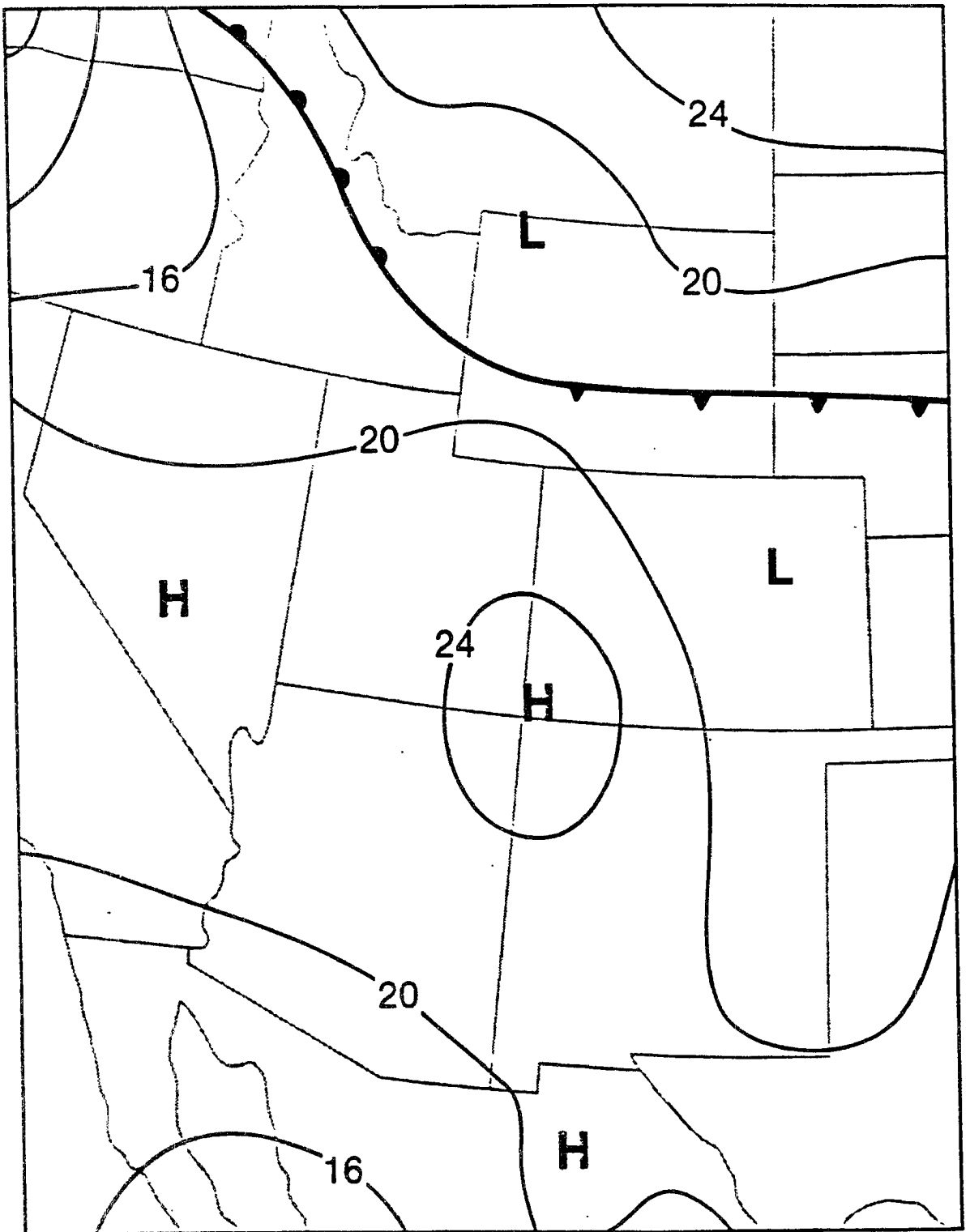


Figure 3. 0600 GMT Surface Map for 15 December 81

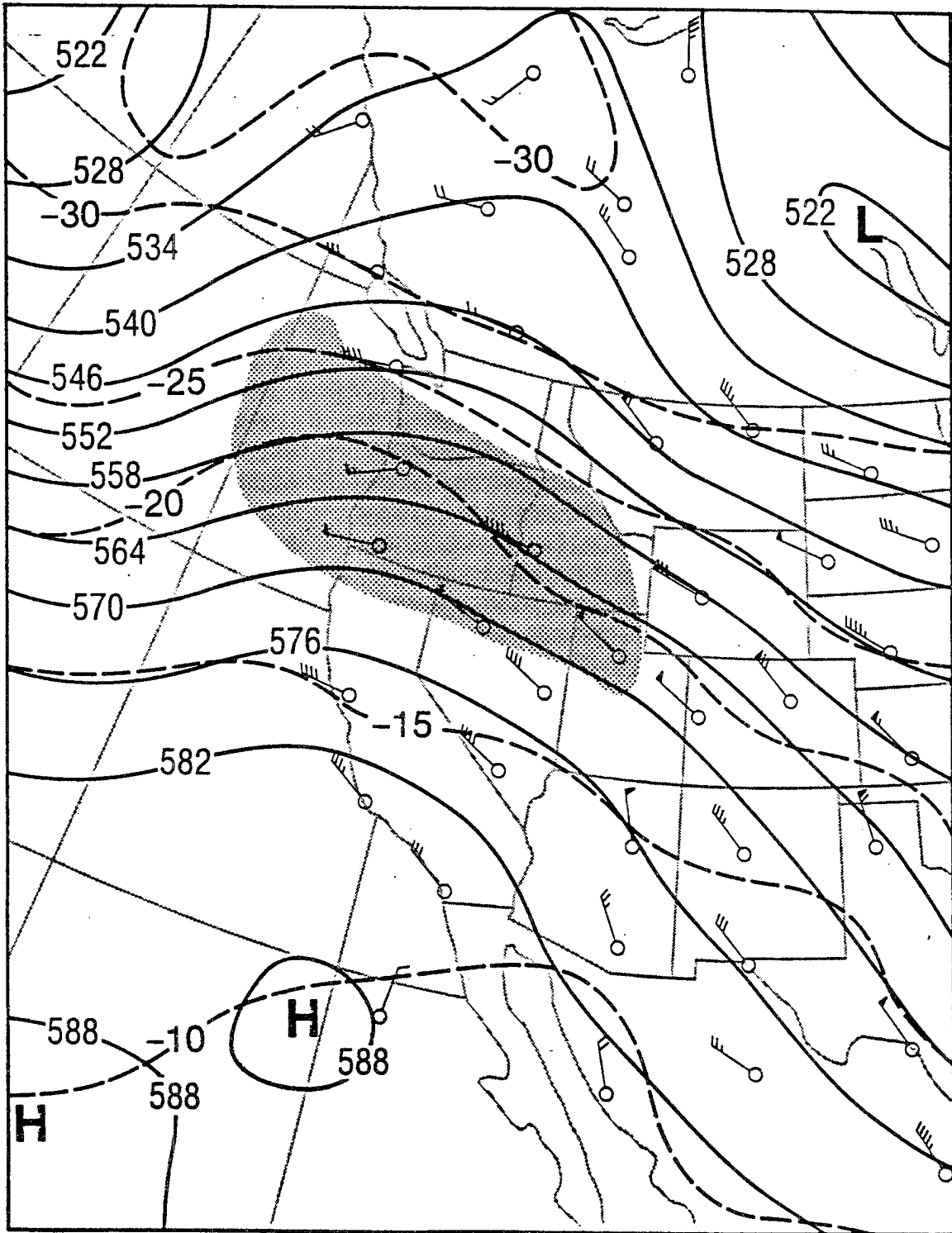


Figure 4. 0000 GMT 500 mb Map for 15 December 81

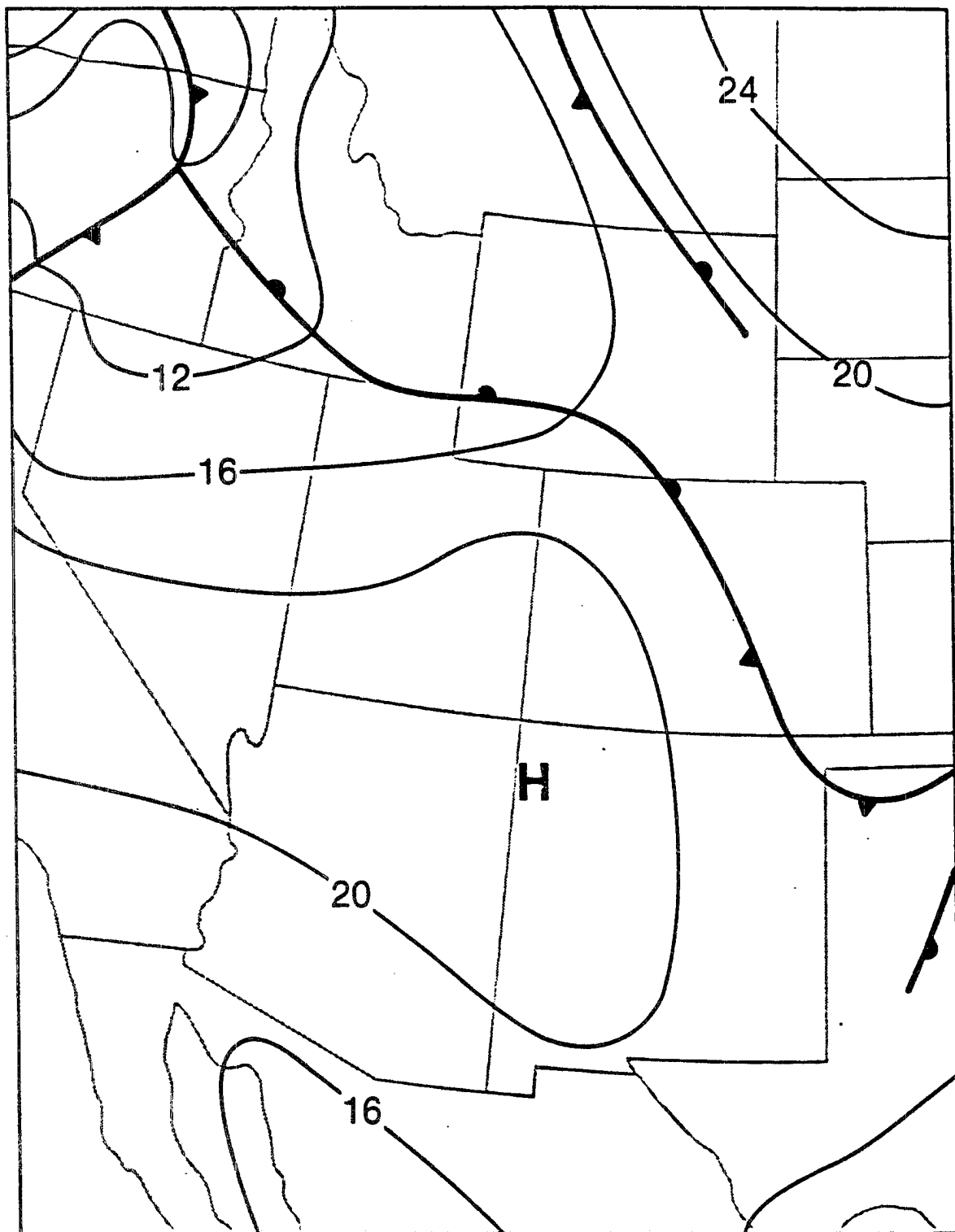


Figure 5. 1200 GMT Surface Map for 15 December 81

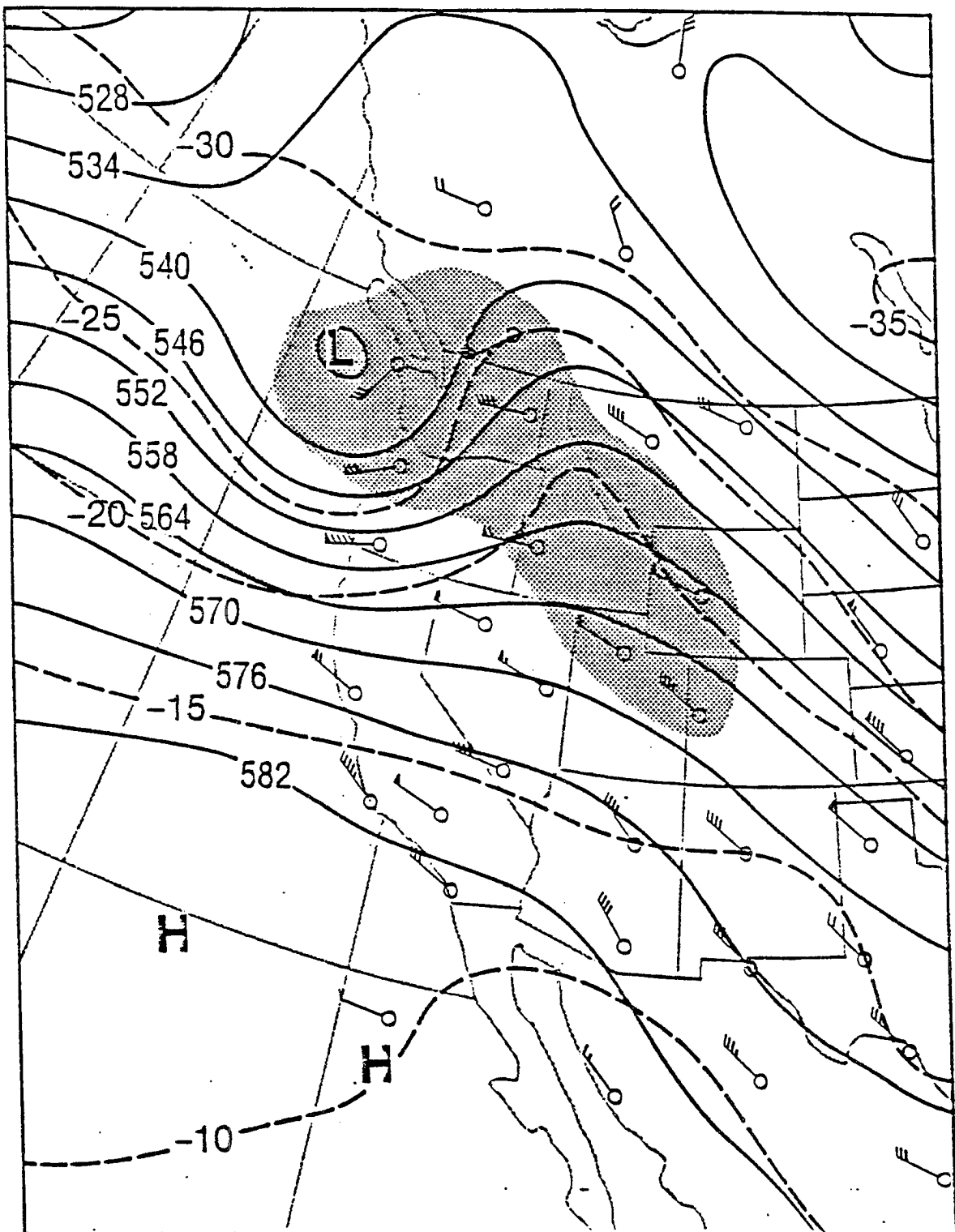


Figure 6. 1200 GMT 500 mb Map for 15 December 81

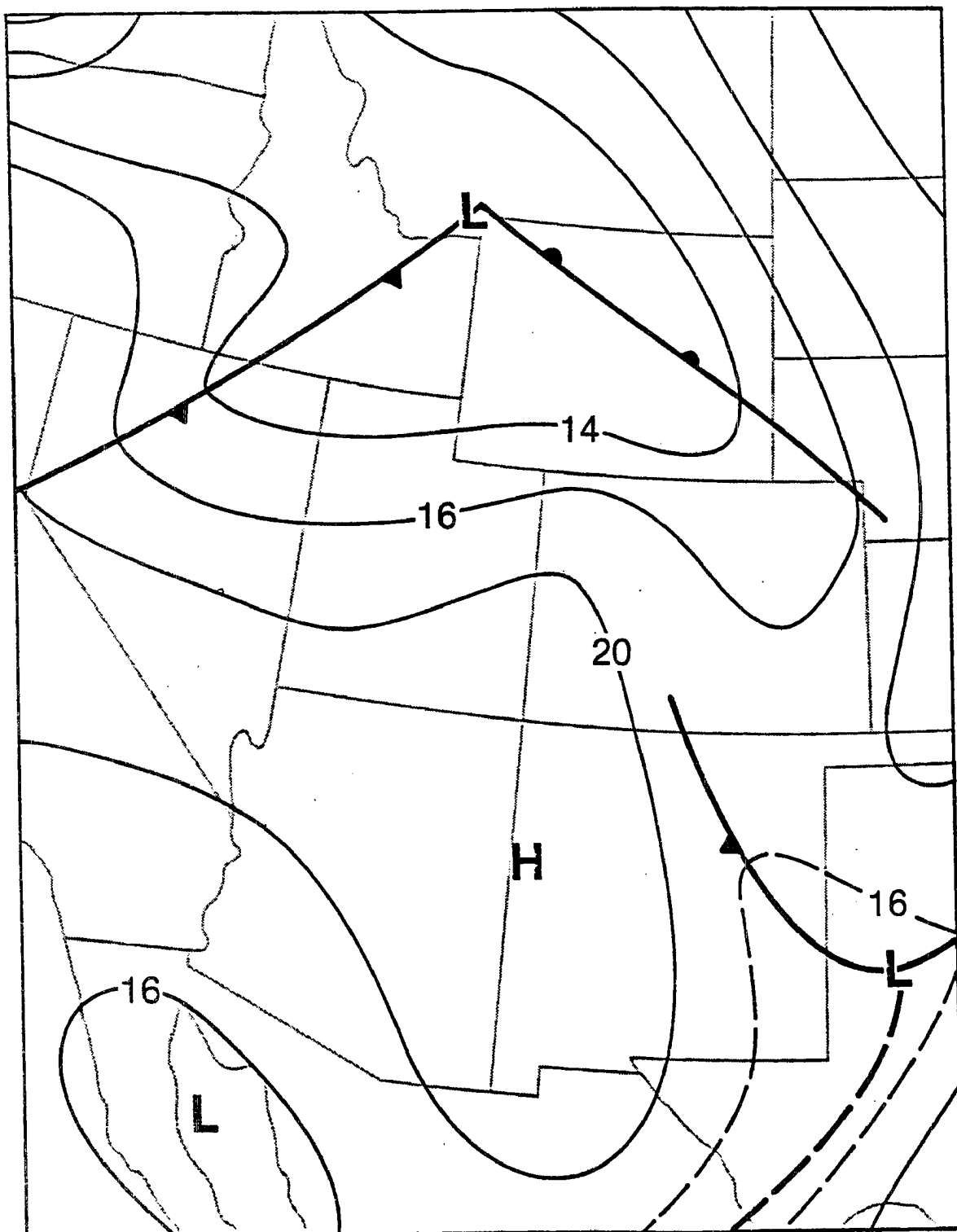


Figure 7. 1800 GMT Surface Map for 15 December 81

The synoptic analysis shows that no major synoptic changes occurred during the period of study. Since steady state conditions are of importance to the study, variations in the immediate cloud are also examined on the basis of local meteorological measurements. In Fig. 8, three types of data are displayed with the time period of interest bracketed by the heavy lines at 1500 GMT and 1740 GMT. At top, integrated values of liquid water are plotted as a function of the scanning azimuth angle and time. Maxima values which occur between  $40^{\circ}$  and  $200^{\circ}$  reflect the orographic effect, while the maxima at 1430 GMT, 1700 GMT and 1830 GMT indicate temporal variations in the cloud advecting through the area. The lack of radiometer data between 1600 GMT and 1640 GMT was caused by temporary instrument failure. In the second part of Fig. 8., cloud top heights above the Ku-Band radar are plotted, and in the third part surface snowfall rates measured by an observer at the radar site are plotted. Because of the sensitivity range of the 1.79 cm radar the cloud tops are indicative only of the extent of ice in the cloud and not of supercooled liquid water droplets. Inspection of Fig. 8 shows that maxima in radar cloud top heights at 1520 GMT and 1740 GMT correspond to minimum values of integrated liquid water measured by the radiometer. An inverse relationship between radar cloud top heights and precipitation is also apparent with periods of low cloud tops related to maximum precipitation rates. Cloud bases on December 15th, 1981 were around 2500 m MSL below the top of the mountain.

Figures 9 and 10 show profiles of equivalent potential temperature and wind speeds from rawinsonde launches made just before and after the study period. Fig. 9 indicates a generally neutral atmosphere with only

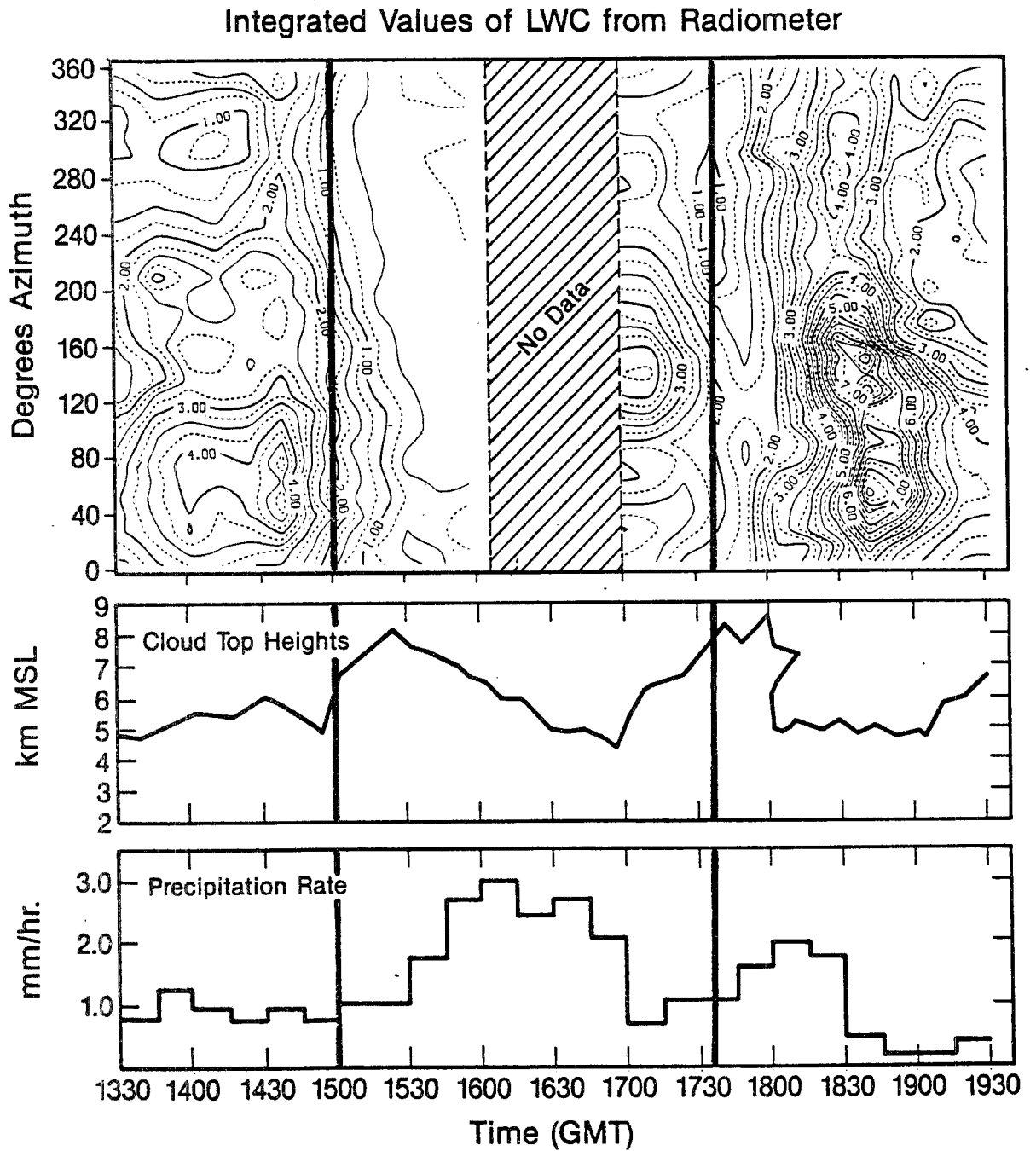


Figure 8. Radiometer-Radar-Surface Snow Measurements



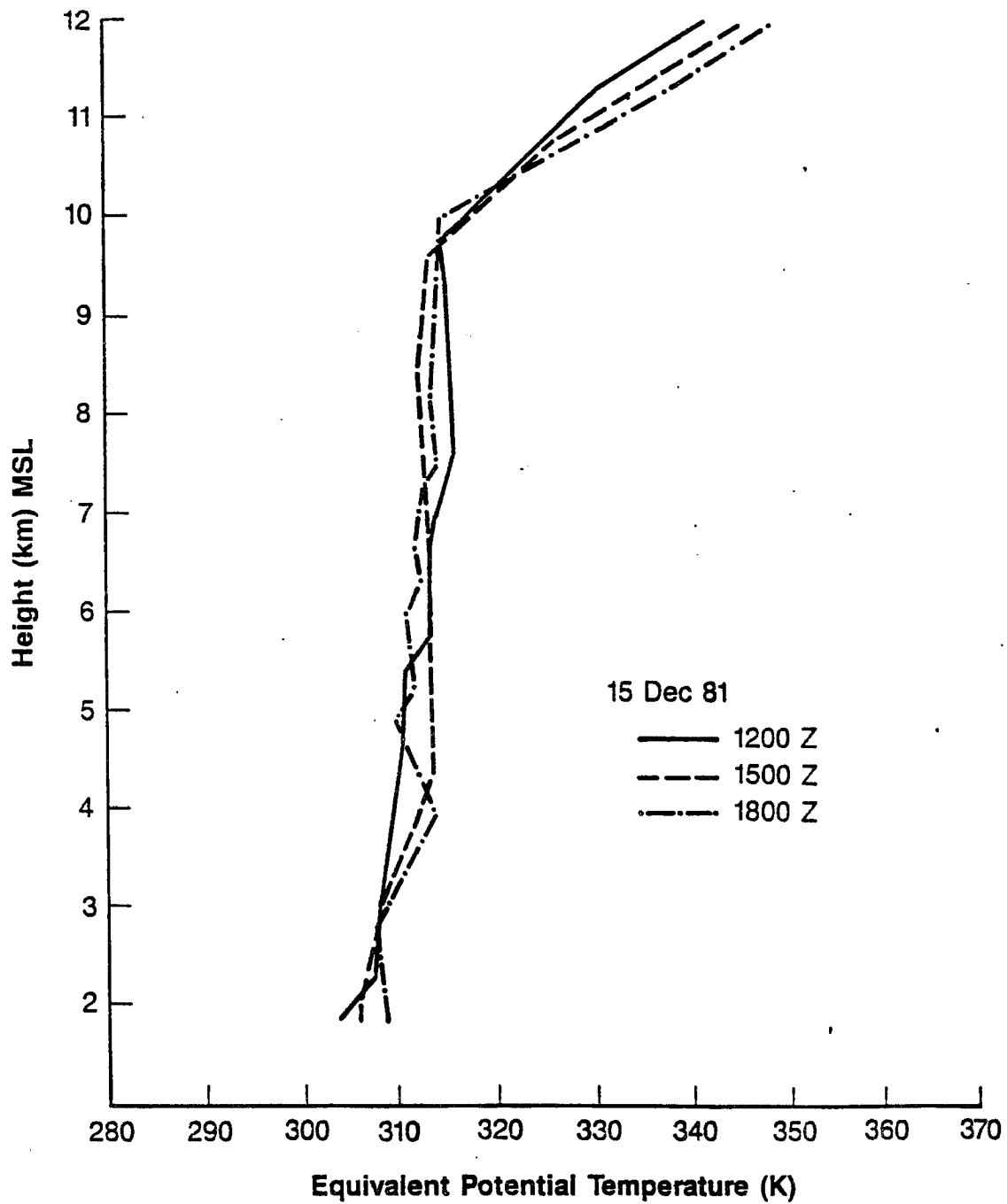


Figure 9. Profiles of Equivalent Potential Temperature

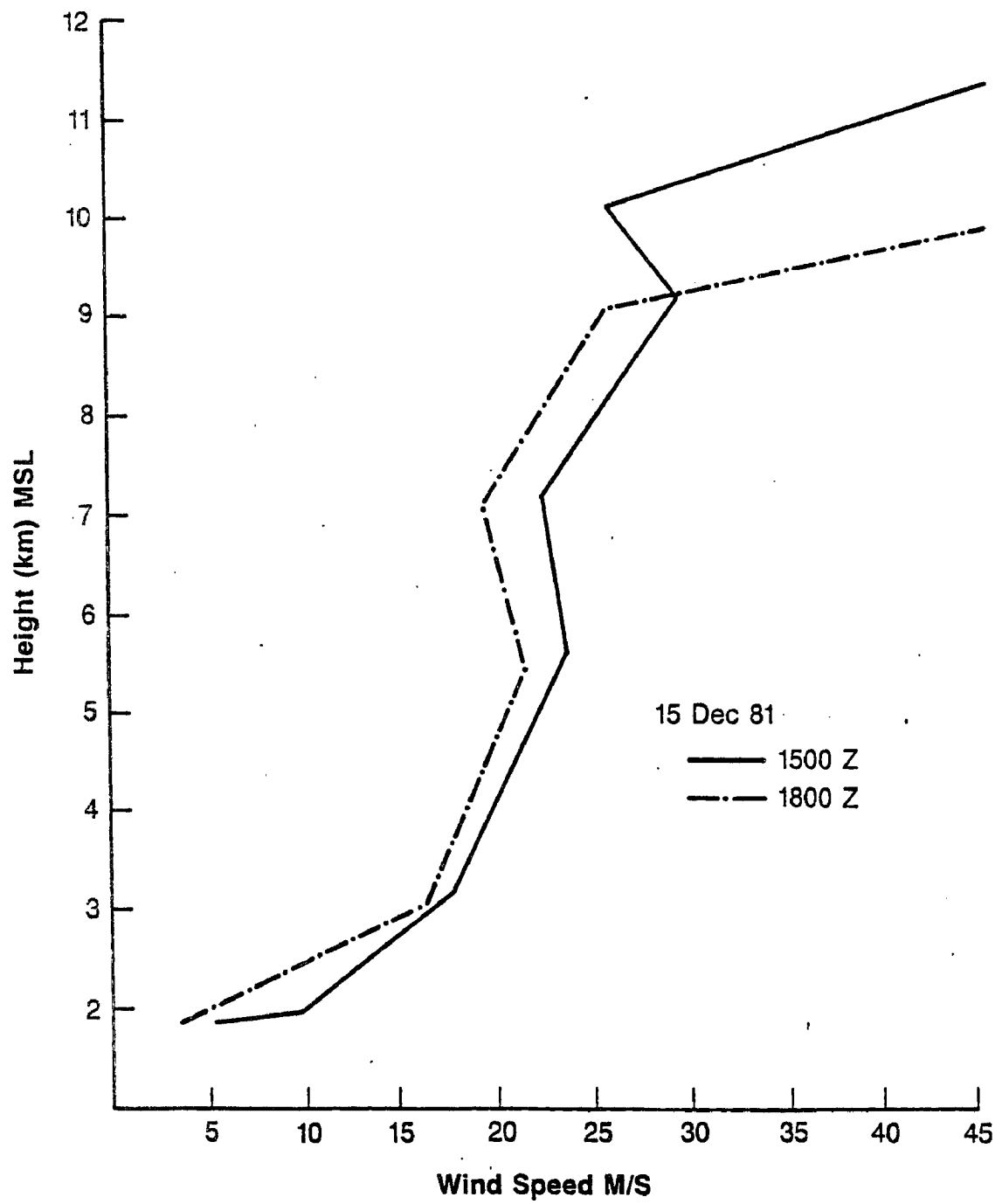


Figure 10. Profiles of Wind Speeds

weak potential instabilities. This result was confirmed by aircraft measurements that showed no more than a  $1.5^\circ$  variation in equivalent potential temperature between 4000 MSL and 6000 MSL throughout the entire aircraft cross section. Wind speed profiles were also extremely similar before and after the aircraft flight.

While the synoptic analysis indicates that there were no frontal passages during the study period, information from the radiometer, radar, and surface observations indicate that conditions were not perfectly steady state. On the basis of the essentially neutral atmosphere and the consistent wind speed profiles, the variations have been interpreted as advection of moisture through the area with a minimum of convective instabilities. Two steps were taken to remove the greater effects of the temporal variation. (1) The aircraft altitudes were plotted as a function of cloud top height to assure that the aircraft was in cloud at all times and (2) the period between 1640 GMT and 1710 GMT which appeared to have the greatest anomalies was not included in the data set. Overall, on the basis of this analysis it is contended that conditions were reasonably steady state and appropriate for this study.

## 5.2 The Flight Track

The inherent difficulty in measurement of cloud parameters with aircraft relates to the limited sampling space occupied by the aircraft in relation to the cloud. Because of the inability of the plane to be at every point in the cloud at the same instant, spatial variations are often difficult to separate from temporal variations. In addition, the

aircraft limitations of speed, range and altitude, and the constraints imposed by maintaining safe altitudes prohibit sampling of the entire cloud volume. The flight track design was therefore aimed at obtaining an optimum description of the cloud.

The aircraft flight track was confined to a vertical plane parallel to the prevailing airflow and perpendicular to the primary barrier. The emphasis was on fully covering a vertical cross section with a series of horizontal flight legs and vertical soundings. The horizontal flight legs occurred between 4000 and 6000 meters MSL at intervals of 300 meters, with endpoints originating 60 km upwind of the barrier and terminating over the leeward slope of the barrier. Four vertical soundings were performed. These were made at: (1) 60 km upwind of the barrier; (2) 20 km upwind of the barrier; (3) immediately over the windward slope of the barrier; and, (4) over the leeward slope of the barrier. The flight track is shown in Fig. 11, and a timetable of executed moves is listed in Table 4. The execution of the soundings was carefully timed in real time so that the soundings at different locations roughly tracked the same column of air based on the speed of the 650 mb flow.

### 5.3 Model Results and In Cloud Observations

The model was used to determine parcel and particle trajectories. The model was initialized with a rawinsonde made at 1500 GMT on December 15, 1981. Results from these runs are presented in Figs 12 and 13. The rawinsonde sounding used to initialize the model is indicated on Figure 12. On the basis of the model runs which indicate horizontal crystal

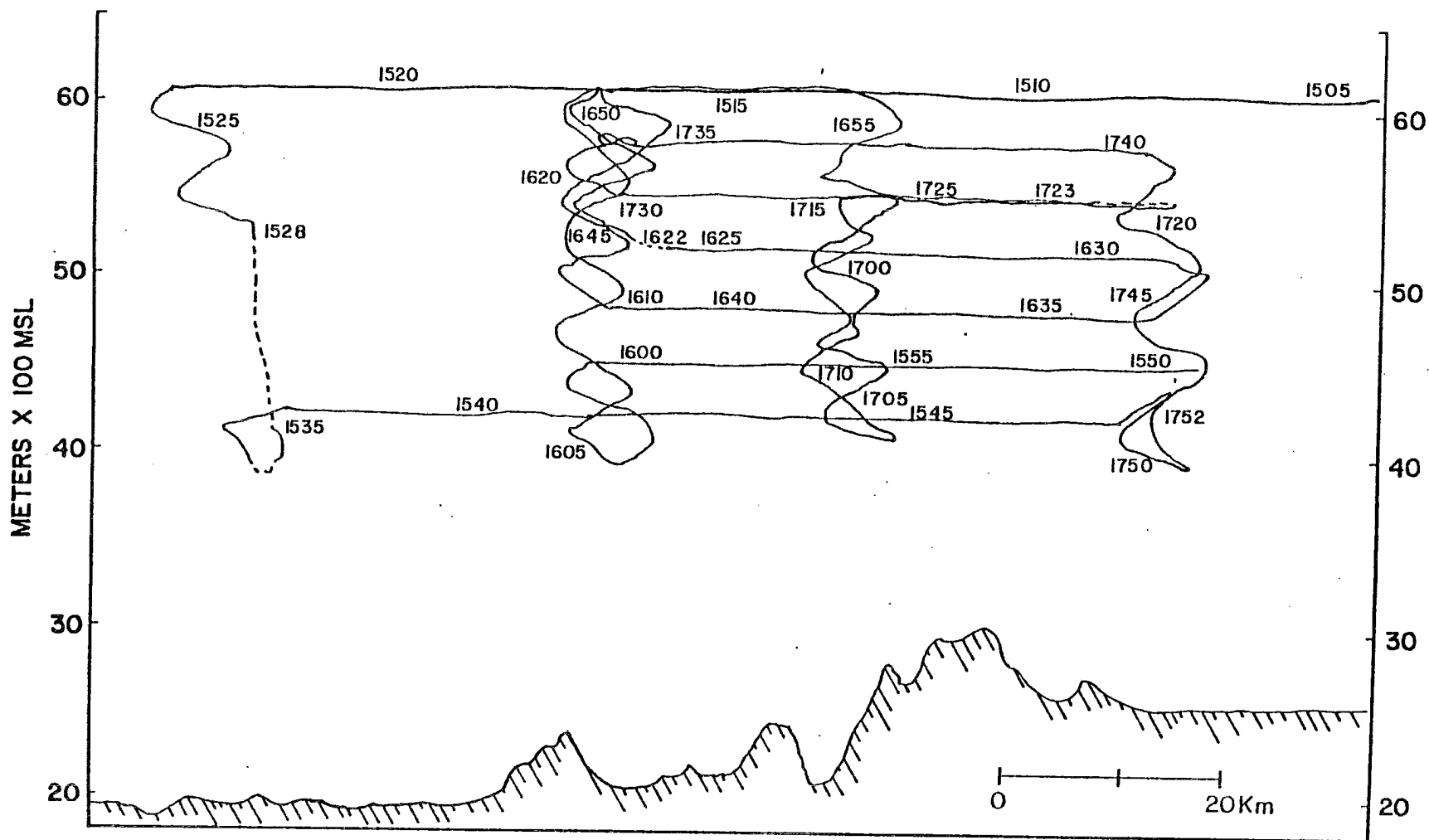


Figure 11. Flight Cross-Section: 15 December 81 CIC Flight,  
Indicated Times in GMT.

Table 4.  
 Timetable of Aircraft Flight Track Maneuvers

<u>Time</u>	<u>HHMM (GMT)</u>
1506-1523	6000 meter flight leg
1523-1535	Tape rewind
1538-1548	4100 meter flight leg
1551-1601	4500 meter flight leg
1605-1616	Sounding over Milner - ascending
1616-1621	Sounding over Milner - descending
1621-1624	Tape rewind
1624-1635	Cloud tops dropped - data not utilized
1636-1640	4800 meter flight leg
1642-1649	Sounding over Milner - ascending
1655-1706	Sounding over Steamboat Springs - descending
1706-1715	Sounding over Steamboat Springs - ascending
1719-1723	Tape rewind
1723-1730	5500 meter flight leg
1734-1741	5800 meter flight leg
1740-1750	Sounding over Hebron - descending

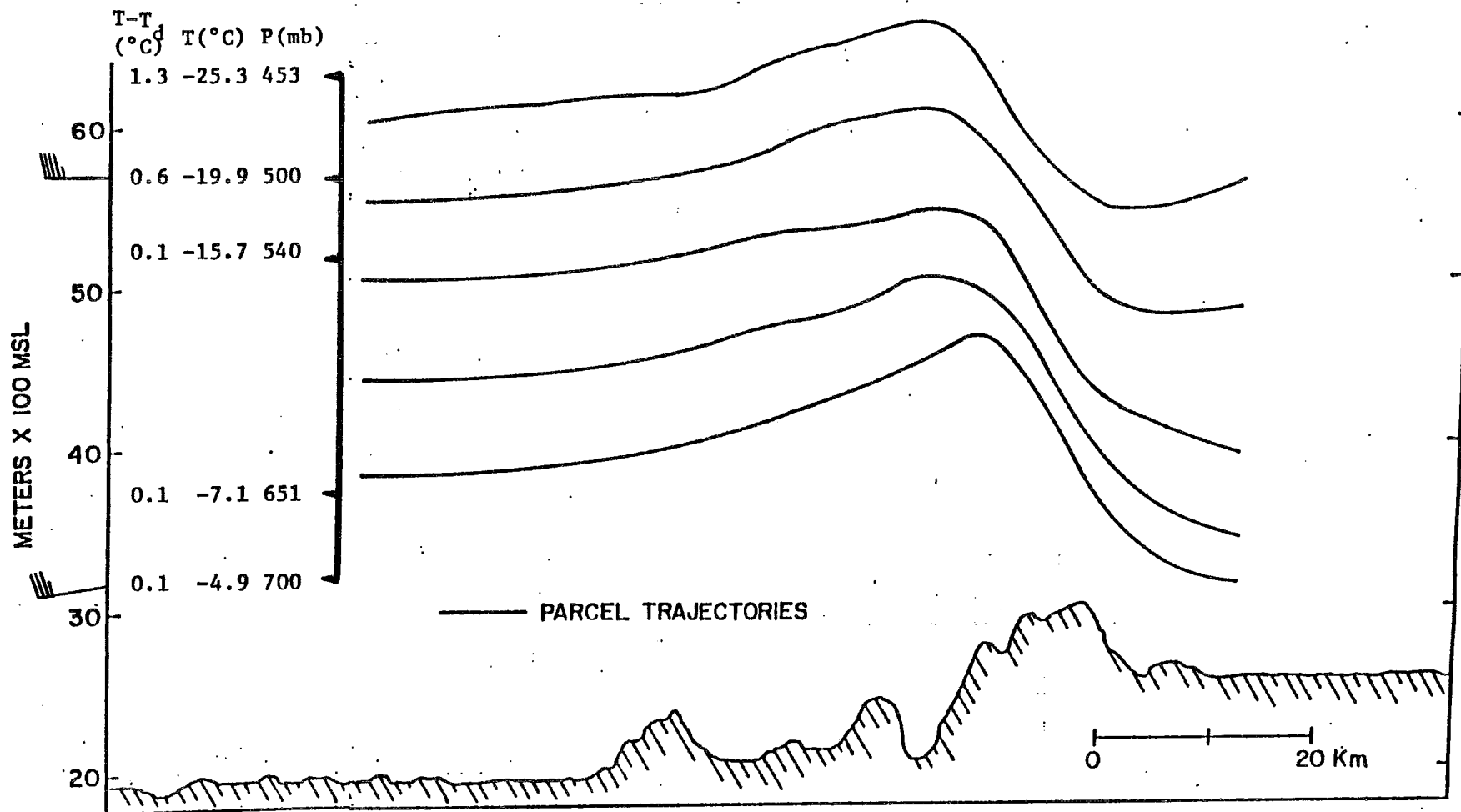


Figure 12. Computer Modeled Parcel Trajectories for 15 December 81  
Sounding used to initialize model indicated on left side,  
wind speed, wind direction, dewpoint depression, temperature,  
and pressure.

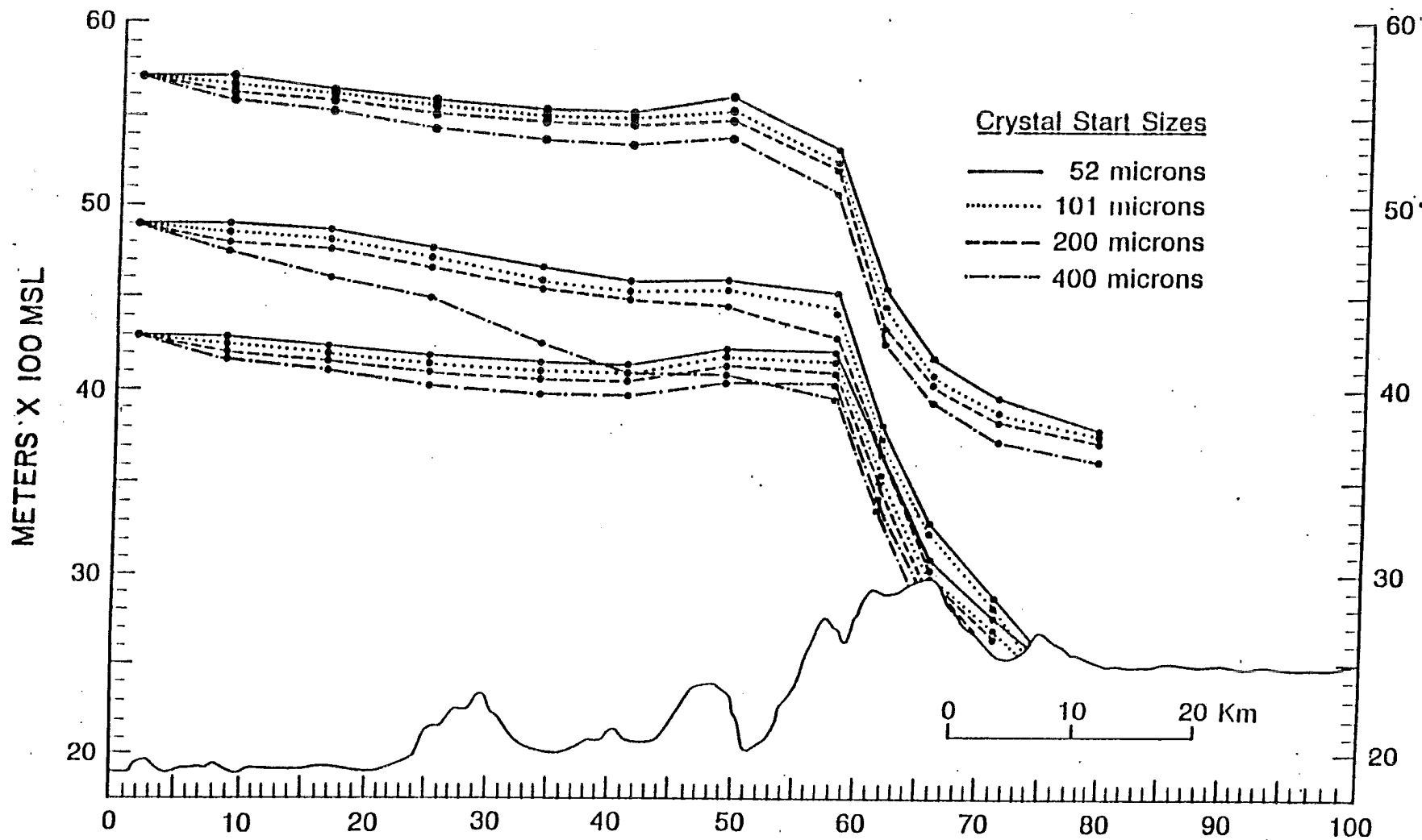


Figure 13. Computer Modeled Particle Trajectories for 15 December 81



trajectories, it was expected that significant habit stratification would occur in the cloud. To test this theory an examination was made of in-cloud measurements of ice crystals.

The results of the temperature measurements and the tally of crystal observed on decelerator slides at each of fourteen observation points are presented in Fig. 14 with detailed notes on each observation point in Table 5. On Fig. 14, the black dots indicate the position of the observation in the cloud, the bold faced number represents the total number of crystals counted in each respective sample, and the number in parenthesis correspond to the observation number in Table 5. In the boxes associated with each observation point the types of crystal observed are indicated and the associated number above each crystal represents the percentage that the crystal made up of the whole. The arrows on the right hand side of the diagram indicate the extent of the four major habit regimes. The crystals collected on decelerator slides were divided into the 20 categories shown in Table 6. This classification is a simplification of the 80 crystal categories developed by Magono and Lee (1966). The simplification has been assumed since the 20 categories give more than sufficient habit resolution for the purposes of the ice content calculation and a higher degree of specification was not possible from the slide photographs. The observations fell into three major categories indicated by the letters A, B, and C by each box in Fig. 14. A description of each of these categories follows:

Figure 14. Ice Crystal Observations In-Cloud by Microphysics Aircraft

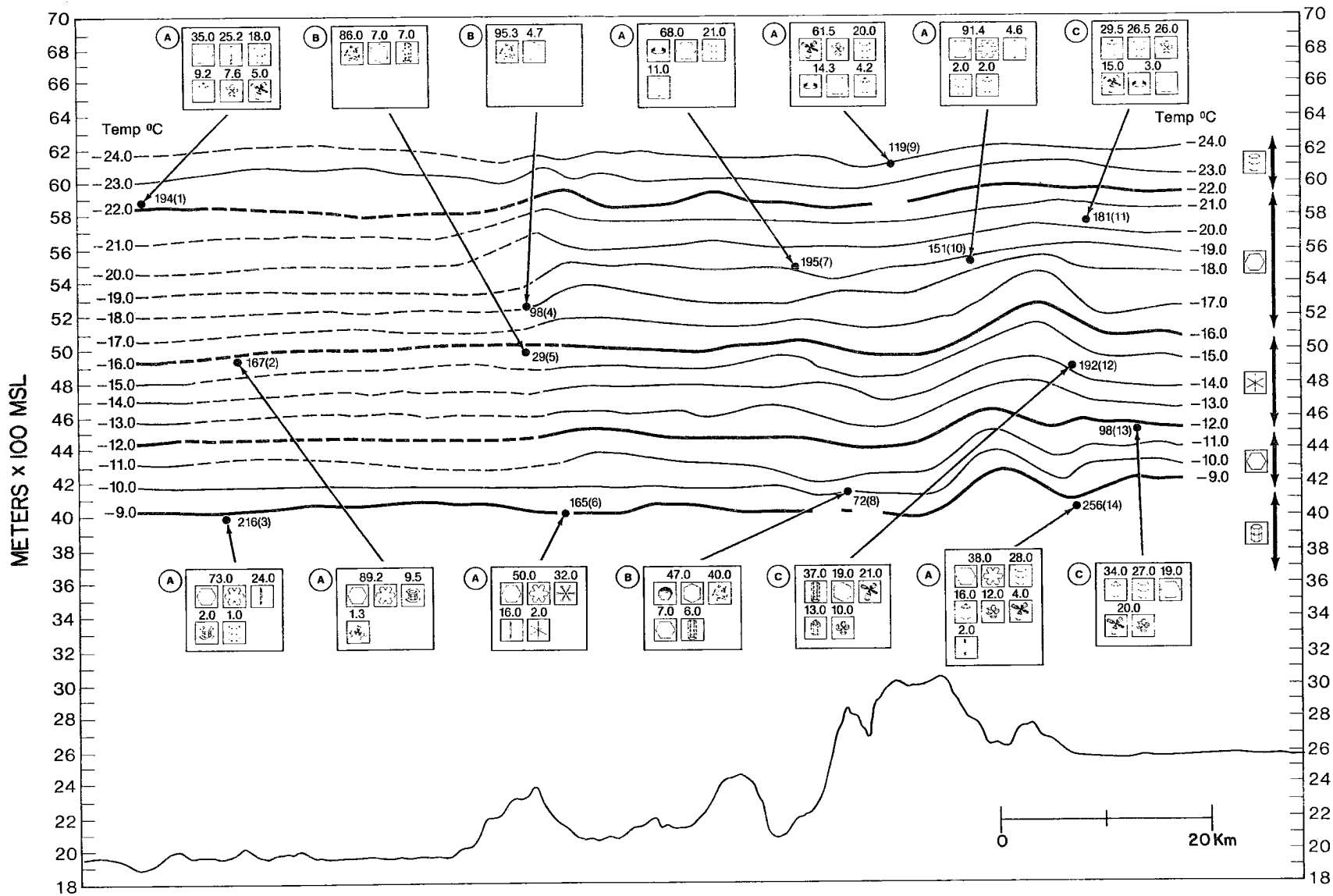


Table 5.  
In-Cloud Crystal Habit Summary

A = expected particle  
B = rimed particles  
C = downdraft region

Observation #	Temperature	Theoretical growth regime	Observed habits	Comments
1 A	-22.5°C	Clg/Clf/Cle/C2a/C2b Nla/Nle/Pla/Plb/Plc	9.2% bullets* 18% columns* 12.7% combo of bullets and columns* 25.3% needles* 35% plate-like  * 65.2% column-like	Sample taken right at the major transition zone between column-like and plate-like growth regimes. It is reasonable that 2/3 of the crystals counted come from the upper growth regime.
2 A	-15.8°C	Pla/Plb/Plc/CP1a/P2c CP2a/Clg/Plc/Pld	88% plates/sector broad branches 1.2% plates w/extensions 9.5% capped columns 1.2% capped bullets	Measurement taken just at transition zone, virtually all of the crystals measured, 88% were from the higher plate-like zone. Not quite down to the temperature zone where the dendritic growth regime begins.
3 A	-8.8°C	Pla/Plb/Plc/Clg Nla/Cle/Clf	73% plates/sectors 24% needles 3.5% columns/bullets	Sample taken right at a major transition zone between plate-like and column-like growth regime. Majority of particles from upper growth regime, but evidence of particles from lower growth regime.

4 B	-18°C	Pla/P1b/P1c/Clg P1d/P2c/	See comments, mostly II	Sample consisted almost entirely of ice particles Possible bad sample - shattered or melted. Only detectable particles were heavily rimed. This is possibly a high LWC zone as it is just prior to the smaller secondary barrier.
5 B	-15.8°C	Pla/P1b/P1c/Clg	See comments, mostly II	Not a very informative slide. Some Clg particles are detected, mostly ice par- ticles. Located in the high LWC zone induced by the the secondary barrier.
6 A	-9.0°C	Pla/P1b/P1c/Clg N1a/Clc/Clf	50% plates and sectors 16% needles 32% dendrites with plate-like extensions	66% of the particles ob- served (50% plates and sectors) and 16% needles are from the upper growth regime in this transition level observation. In addition, there are 32% dendrites from a higher growth regime. ~400 meters above the observation, however they all have sector and plate- like extensions from the intervening growth regime. Possible effects of a downdraft on lee side of small upwind barrier.







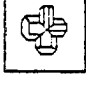








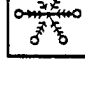




7 A	-19°C	P1b/P1b/P1c/C1g	70% plate-like 30% column and needle like	Majority of crystals (70%) are those that would have been predicted on the basis of the theoretical growth regime.
8 B	-10°C	P1a/P1b/P1c/C1gh	54% plate-like 6% column-like *40% ice particles or shattered particles.  *difficult to count therefore a very qualitative measurement	This sample is right over the crest of the barrier in the theoretical zone of maximum LWC over the primary barrier. Heavy riming is evident, graupel like particles, heavily rimed plates and columns.
9 A	-23.6°C	C1g/C1f/C1e/C2a C2b/N1a/N1e/	61% combo of bul- lets and columns 20% columns 14% plates 4.2% bullets	85% column-like crystals. Aircraft at ~6100 m near top of aircraft cross section where correlation is ex- pected to be the best.
10 A	-18.5°C	P1a/P1b/P1c/C1g	91% plates and sectors 9% columns and needles	Sample deep within a sector/ plate region - sample ob- servations correspond excel- lently (91%) with theoretical habit regime. No riming is observed despite the fact that the sample is po- tentially in a high LWC zone near to primary barrier crest.

11 C	-20.3°C	Pla/P1b/P1c/C1g	96% column-like 3% plate-like	Almost all of the sample was from a growth regime higher than that predicted by temperature at the observation point. Again, the point is in a region where model predicts strong downdraft due to gravity waves.
12 C	-14.3°C	P1e/P1f/P2c Pla/C1g	81% column-like 19% plate-like	The location of the observation is centered between the -9 to -22 plate-like growth regime. However, the particles observed were 81% from a growth regime 1200 meters above the observation point. This point is the best example of the strong downdraft effects predicted by the Rauber model.
13 C	-11.6°C	Pla/P1b/P1c/C1g/ P1e/P2c	20% bullet and column combos* 26% columns* 34% bullets* 19% plates  * 80% column-like	This observation point is firmly embedded in a plate-like growth regime. However, the primary particle habit observed is column-like. The observation point is on the less side of the mountain where strong gravity waves occur.
14	-8.5°C	N1a/C1e/C1f/N1e Pla/P1b/P1c	62% column-like 38% plate-like	Since this observation point is again in the downdraft region it is difficult to determine whether the column-like particles (62%)

are from the upper or the lower column growth regime. There is some evidence that they might be from the upper growth regime since bullets were observed. These are more characteristic of the  $<-22^{\circ}\text{C}$  growth regime.



Table 6. Crystals Utilized in Classification Procedures

Crystal	Magono-Lee Classification	Temperature Growth Regime	Crystal	Magono-Lee Classification	Temperature Growth Regime
	C1f	-5 to -10 and -20 to -30		CPla	Column Grows -20 to -30 Plates grow -9 to -22
	C1e	-25 to -35		CP2a	Bullets grow -25 to -35, Plates grow -16 to -12
	C2a	-25 to -35		N1a	-5 to -9
	C2b	-5 to -10 and -20 to -30		R1c	Same as Pla with Riming
	C1g	-25 to -35		R1b	Same as C1f with Riming
	Pla	-9 to -12 and -16 to -22		I1	Ice Particles
	Plc	-9 to -12 and -16 to -22		N1e	-5 to -10
	Plb	-9 to -12 and -16 to -22		P2c	grows -12 to -16, Plates -9 to -12
	Plc	-12 to -16		R4a	Graupel
	Pld	-12 to -16		-	Same as Cld with Riming

Category A

In Category A the observed crystal habits were predominantly those that would have been predicted on the basis of temperature, and were unrimed. 65% to 91% of the particles in the Category A samples were of a type consistent with the temperature at which the observation occurred, with an average of 77% of expected crystal types for the seven Category A samples. Three of the seven Category A samples occurred close to the major habit transition zones of  $-9^{\circ}\text{C}$  and  $-22^{\circ}\text{C}$ . In observations 1 and 3 roughly two thirds of the sample was composed of particles from the upper growth regime, and the remaining third were particles from the lower growth regime. The average percentage of temperature predicted particles habits for observations 2,7,9 and 10 which occurred deep within a single growth regime was significantly better than for the entire class A group at 86%.

Category B

Particles in Category B were highly rimed and/or interspersed with irregular ice particles.

Category C

Category C observations were those that would not have been predicted on the basis of temperature alone. Observation 12 occurred at

a point that was deeply embedded in the temperature region of plate like particles. It occurred more than 900 vertical meters from any source of column like crystals, yet contained 81% columns. Observations 11 and 13 also well within plate-like growth regions contained between 80% and 96% columns in the various combinations of bullets, bullet rosettes, columns and various column assemblages.

The distribution of crystal is reasonable when compared with the theoretical crystal trajectories developed in the model runs (See Fig. 13). Category A particles, or those which possess habit characteristics consistent with temperature regime all occurred in the upwind portion of the flow where particle trajectories were essentially horizontal. The near horizontal trajectories parallel the horizontal isotherms, and therefore particles travel in a consistent temperature environment and can develop homogeneous habit characteristics. Category B samples were collected just above the crest of either Mt. Werner or the crest of a smaller ridge located 15 km upwind of the Park Range. In previous studies in the Park Range (Rauber et al., 1984) maximum liquid water contents in orographic clouds were found to be near mountain crests due to enhanced vertical motion in these regions. Riming in these regions on December 15, 1981 strongly affected the characteristics of the particle sample. Particles were often so heavily rimed that the original habit was no longer distinguishable.

Category C particles can also be interpreted on the basis of model results. All Category C samples were composed of bullet type crystal and were located to the lee of the barrier crest. Model results indicate that in the areas immediately following the barrier strong downward motions occur in the form of mountain induced gravity waves.

According to Fig. 13 it is not unreasonable to expect a crystal to drop over 1000 vertical meters while only traversing four or five kilometers horizontally. Therefore, one would expect the crystal samples taken in this region to be predominantly of a type prescribed by a higher and colder growth regime being swept down by the prevailing downdraft. Fine structure in the flow can also be detected in the characteristics of the particle habits. In observation 6, 84% of the sample contained crystals from the upper growth regime, possibly forced down by a downdraft in the lee of the small upwind barrier. Observation 9 which occurred high in the cold column regime is distinguished by the occurrence of plates, 300 vertical meters above the plate regime. This would result from the orographic lifting of the airflow just prior to the barrier crest.

From these data, it is reasonable to use temperature and model particle trajectories to predict the crystal habit for the entire cross section to the west of the barrier. The aircraft measurements and the model predictions have both indicated that significant vertical habit stratification occurs in the upper regions of the cloud in the areas upwind of the Park Range. In addition, it has been shown that the downdraft region following the barrier will be populated with columns from the higher growth regimes. This habit information is combined with crystal size spectras from the Knollenberg 2D-c cloud probe to calculate ice contents using the method described in section 4.3. These ice contents are discussed in the following section in the context of the entire cloud water budget.

#### 5.4 Distribution of Vapor, Liquid, Ice and Associated State and Microphysical Data Along Horizontal Flight Legs

This section describes measurements along the seven horizontal flight segments of altitude, pressure, temperature, potential temperature, equivalent potential temperature, dewpoint temperature, ice crystal concentrations, and liquid water contents as measured by the aircraft. In addition, the values of ice and vapor contents which have been calculated and values of total water content (liquid + ice + vapor) are shown. Since topography is considered to be a major control on these values, exact measurements of the height of the barrier directly under the aircraft is plotted as a function of the distance and angle measurements from the Hayden vortac.

Because the data was plotted as a function of time and the plane was moving alternatively east to west or west to east, a reference arrow at the bottom of each diagram indicates which direction is east. The seven horizontal flight segments are presented separately in ascending order with height. In each of the discussions, the area of interest is divided according to topography into three categories. These are: (1) the windward side of the mountain; (2) the region directly above the crest of the mountain; and, (3) the leeward side of the mountain where the region of strong down draft occurs. These regions are marked with the symbols PBR, PreBarrier Region; BCR, Barrier Crest Region; and DDR, Down Draft Region, respectively.

i. The 4100 Meter Flight Leg (Fig. 15A and 15B)

In the lowest flight leg vapor contents show a decline under the effects of forced condensation in the BCR with a total loss in vapor mass from  $2.08 \text{ g/m}^3$  to  $1.30 \text{ g/m}^3$  of  $0.78 \text{ g/m}^3$ . After moving into the DD region, vapor water contents increase to  $1.75 \text{ g/m}^3$ . The total loss in vapor after condensation reevaporation process appears to be on the order of  $0.33 \text{ g/m}^3$ . Ice water contents through the PBR oscillate around an initial value of  $0.60 \text{ g/m}^3$  with no detectable trend of increases or decreases, however a substantial increase occurs in the BCR where an ice water maxima of  $1.53 \text{ g/m}^3$  is achieved. this sharp increase corresponds closely in location and magnitude with the decrease in the vapor water contents in the BCR. In the DDR, ice water contents fall sharply to zero corresponding to the rise in vapor water contents. The increase of vapor mass in that region of  $0.5 \text{ g/m}^3$  only accounts for about a third of the loss in ice water and it is presumed that the remaining  $1.0 \text{ g/m}^3$  of ice is lost in precipitation processes in the strong downdraft.

Liquid water does not show the expected trend of increasing sharply in the BCR, but increases gradually from  $0.04 \text{ g/m}^3$  to  $0.06 \text{ g/m}^3$  in the PBR and then falls off sharply in the late PBR and DDR to  $0.01 \text{ g/m}^3$  as evaporation occurs. The total loss of liquid mass in the DDR is  $0.05 \text{ g/m}^3$  which indicates a net loss of  $0.03 \text{ g/m}^3$  between the PBR and the DDR, due to ice growth processes and evaporation. The decrease in liquid content occurs downwind of the decrease in ice content. On the basis of the 4100 meter flight leg, liquid water contents appear to be two orders of magnitude lower than the corresponding ice and vapor

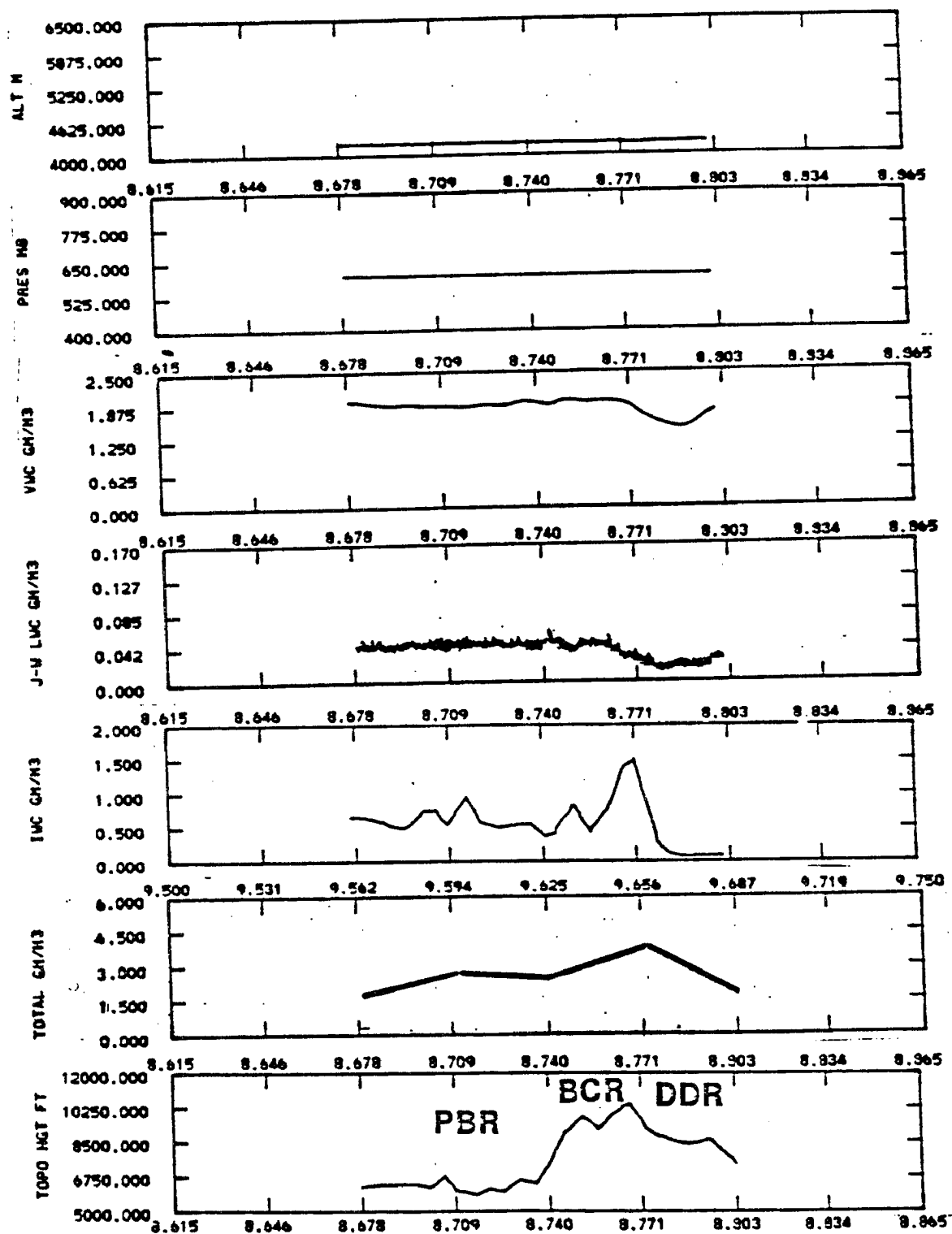


Figure 15A. 4100 Meter MSL Flight Leg: Altitude, Pressure, VWC, LWC, IWC and Topography

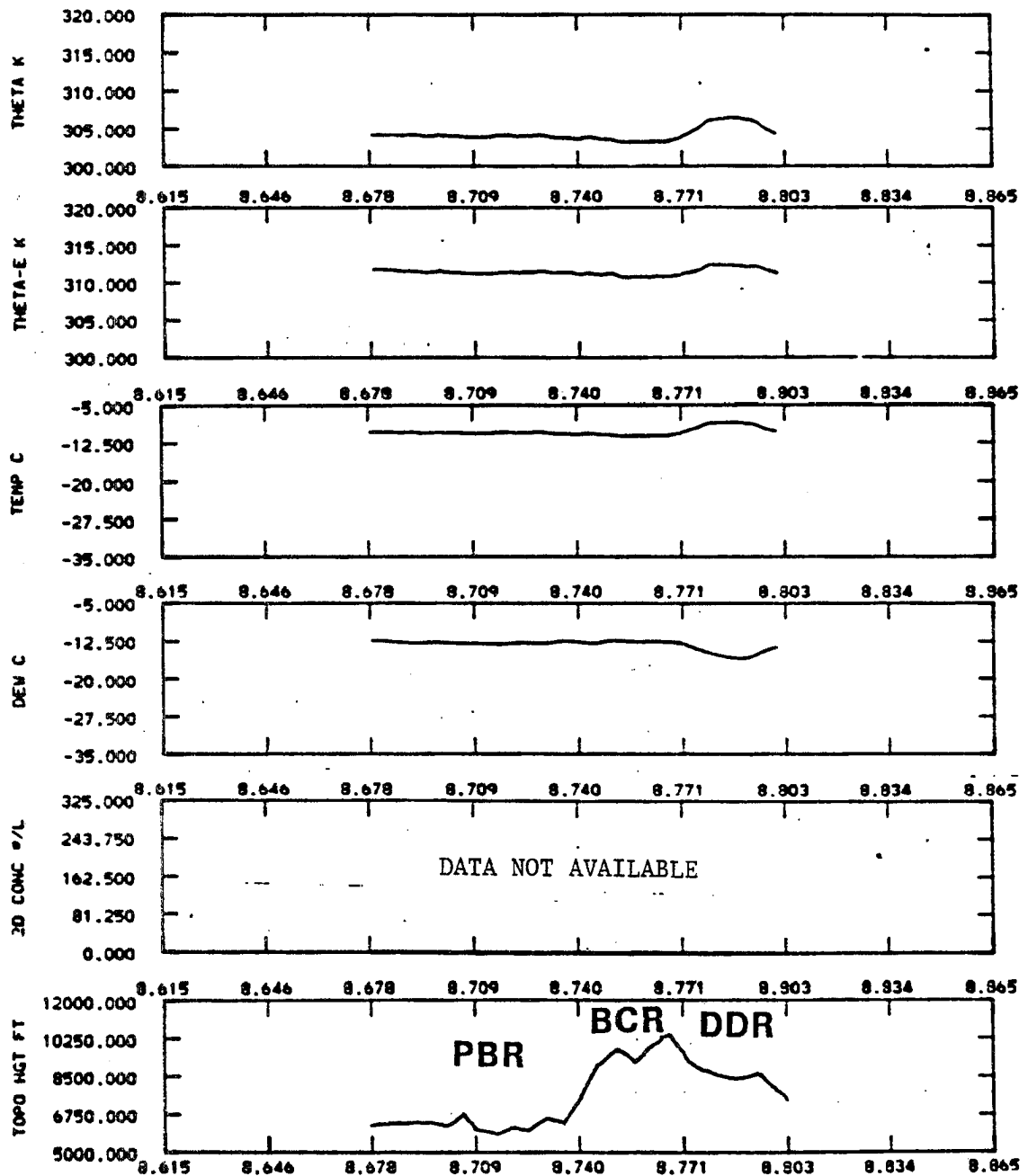


Figure 15B. 4100 Meters MSL Flight Leg: Theta, Theta-e, Temperature, Dewpoint, 2-D Concentration and Topography



contents. Therefore the trends in liquid water are not expected to be as tightly coupled as the vapor and ice trends which show a strong inverse relationship. Total water contents (ice + liquid + vapor) increase through the PBR and BCR from  $2.7 \text{ g/m}^3$  to  $3.7 \text{ g/m}^3$  due to the large increase in ice contents just over the BCR. This indicates that water substance is advecting in from out of the plane of the flight leg to support ice growth processes. In the DDR, total water contents fall off to  $1.7 \text{ g/m}^3$  suggesting that precipitation is removing a significant fraction of the cloud water from that altitude.

Crystal concentrations remain essentially constant at 60/liter through the BCR indicating that increases in total ice contents were due to growth of already existing crystals rather than nucleation of new crystals. Liquid water contents fall off before ice water contents in the DDR.

#### ii. The 4500 Meter Flight Leg (Fig. 16A and 16B)

Vapor contents show no noticeable decrease in the PBR, holding steady at a value of  $1.75 \text{ g/m}^3$ , however a decrease to  $1.25 \text{ g/m}^3$  occurs in the BCR, continuing into the first part of the DDR. As the aircraft progresses into the DDR, vapor increases back to  $1.55 \text{ g/m}^3$  indicating a net loss of  $0.20 \text{ g/m}^3$ . Ice contents are generally lower throughout the 4400 meter flight leg compared to the 4100 meter flight leg with PBR values on the order of  $0.20 \text{ g/m}^3$ . The expected increase in ice occurs in the BCR with ice reaching a maxima of  $0.80 \text{ g/m}^3$ .

Liquid water shows a steady increase in the PBR from  $0.03 \text{ g/m}^3$  to  $0.04 \text{ g/m}^3$  and takes a sharp rise in the BC region to  $0.08 \text{ g/m}^3$ . Values

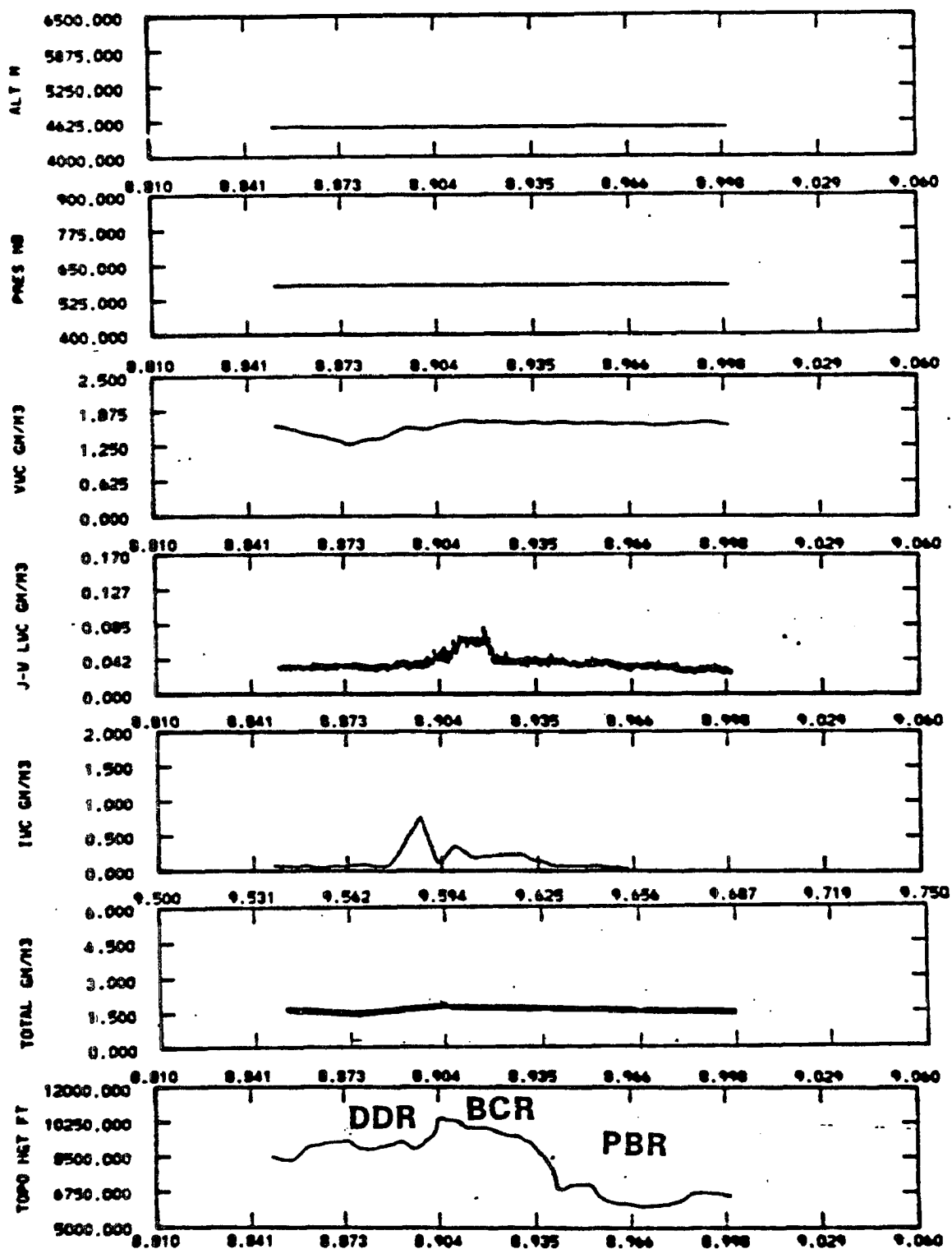


Figure 16A. 4500 Meters MSL Flight Leg: Altitude, Pressure, VWC, LWC, IWC and Topography

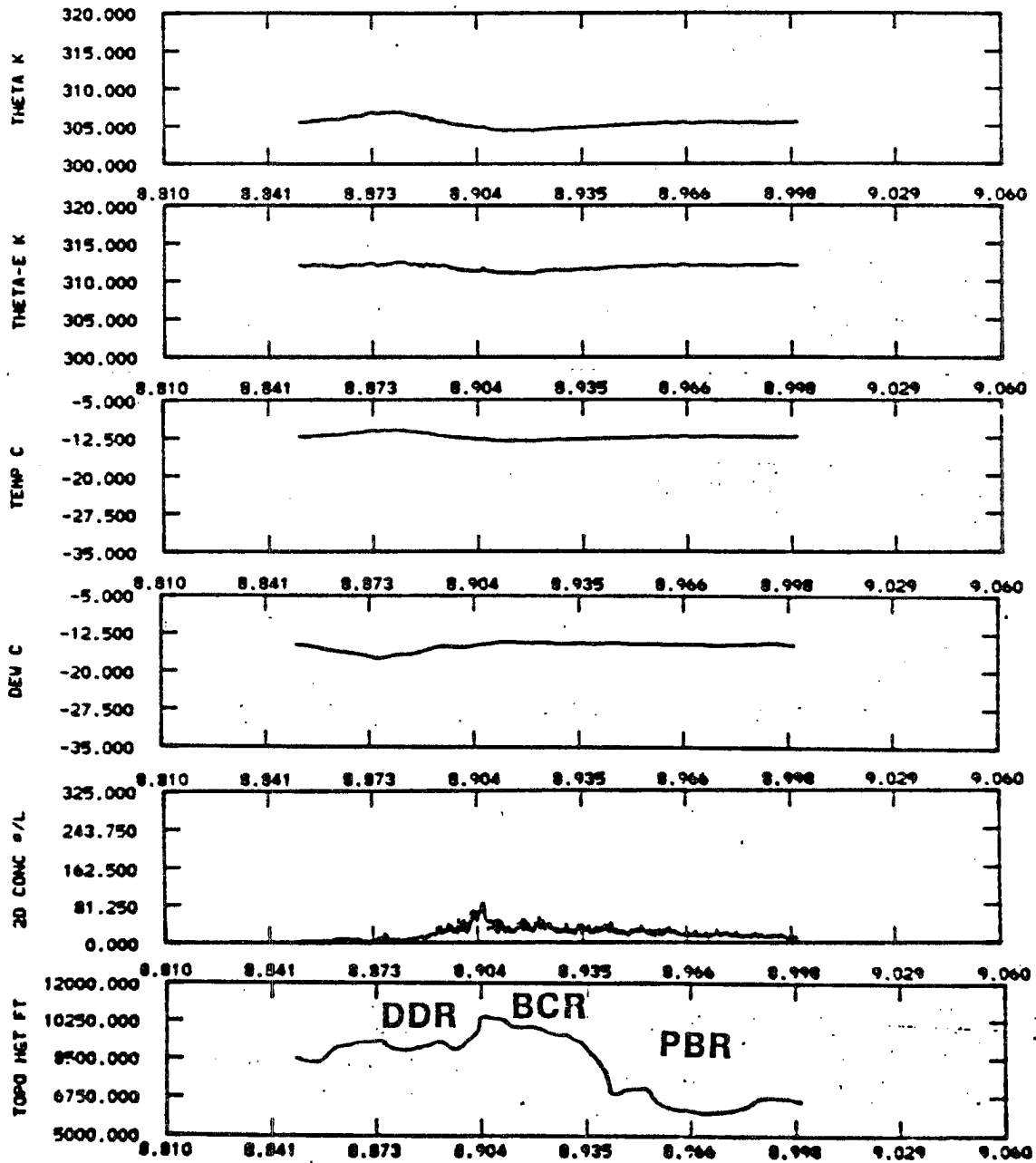


Figure 16B. 4500 Meters MSL Flight Leg: Theta, Theta-e, Temperature, Dewpoint, 2-D Concentration and Topography

again fall off in the DDR, but rather than decreasing all the way to zero, a minimum of around  $0.03 \text{ g/m}^3$  was measured. This value was maintained to the end of the flight segment. Similar to the 4100 meter flight leg, decreases in liquid water seem to lead decreases in ice water content. Total water contents (ice + liquid + vapor) are essentially constant showing only a  $0.30 \text{ g/m}^3$  variation from  $1.5 \text{ g/m}^3$  to  $1.8 \text{ g/m}^3$ . This suggests that a more balanced budget occurs at this altitude, with no significant losses to precipitation.

Crystal concentrations show an increase over the BCR. In the BCR the total loss in vapor mass of  $0.50 \text{ g/m}^3$  is slightly exceeded by the gains in ice and liquid which collectively increase by  $0.65 \text{ g/m}^3$ . As in the 4100 m MSL flight leg this indicates that some vapor advection might be occurring from out of the vertical plane of the aircraft to supply additional growth. The excess may also be a function of the combined inaccuracy of the three measurements.

### iii. The 4800 Meter Flight Leg (Fig. 17A and 17B)

Vapor contents in the 4800 meter flight leg hold steady in the PBR at  $1.5 \text{ g/m}^3$ . Decreases to  $1.0 \text{ g/m}^3$  which begin in the BCR and Continue into the DDR and are quickly followed by a increase back to  $1.25 \text{ g/m}^3$ . Ice water throughout the region is minimal, at less than  $0.07 \text{ g/m}^3$  and shows no detectable trends.

Liquid is much more prominent at this level, with PBR values starting at a maxima of  $.06 \text{ g/m}^3$ , decreasing, and then reaching a maxima of  $0.14 \text{ g/m}^3$  in the BCR. While this value is still small with respect to vapor water contents, they indicate a significant increase by a

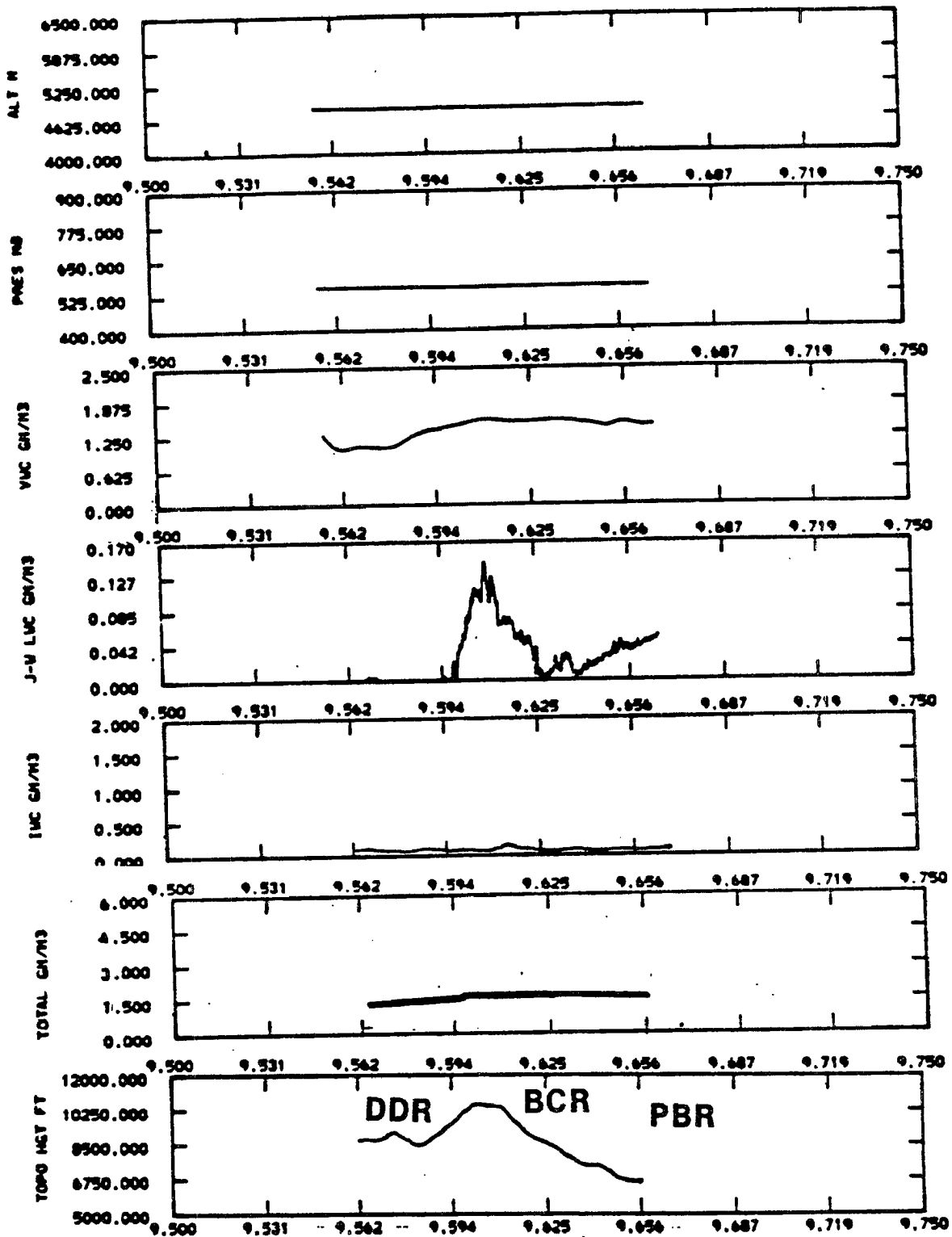


Figure 17A. 4800 Meters MSL Flight Leg: Altitude, Pressure, VWC, LWC, IWC and Topography

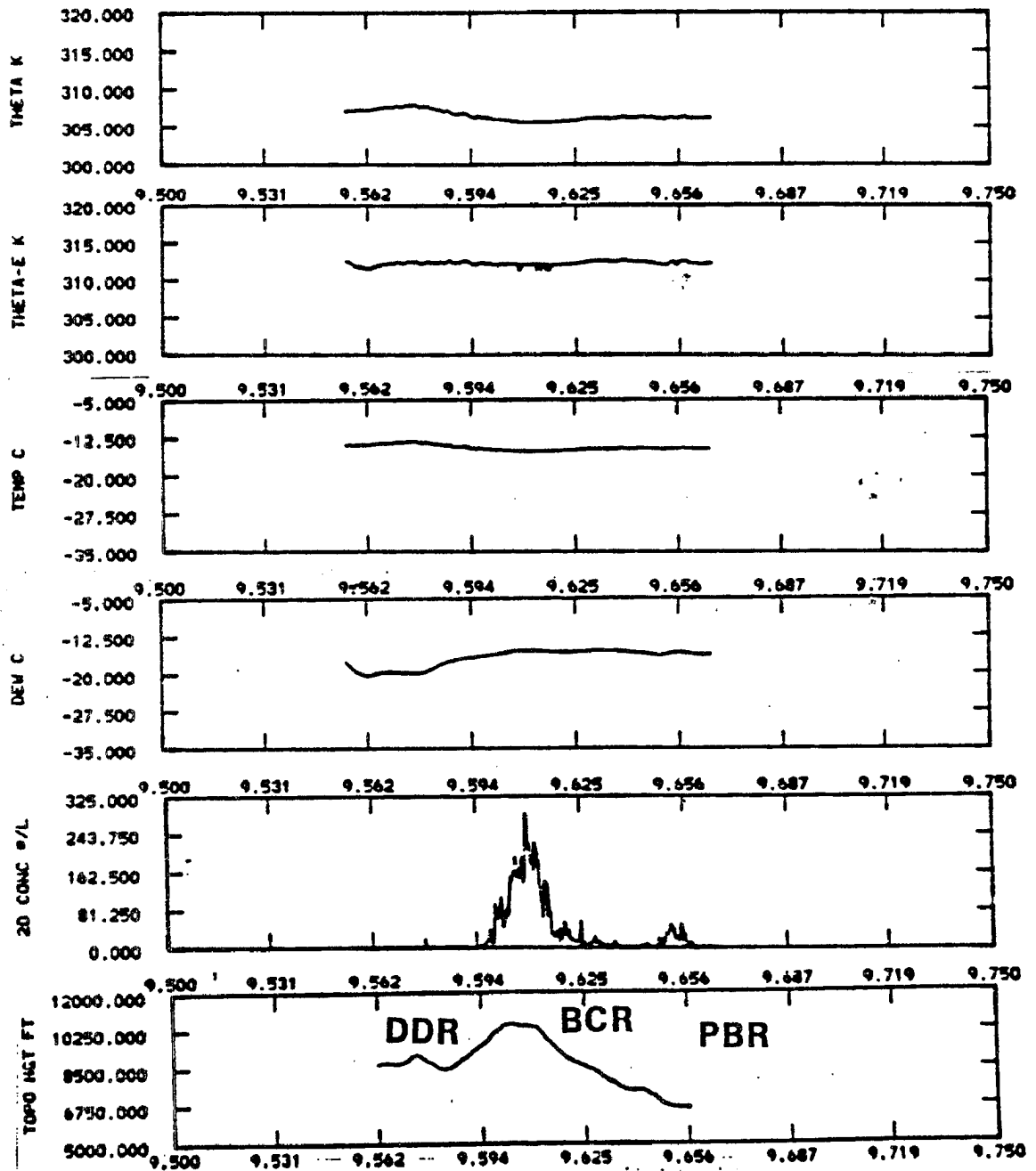


Figure 17B. 4800 Meters MSL Flight Leg: Theta, Theta-e, Temperature, Dewpoint, 2-D Concentration and Topography

factor of two from liquid contents in the lower two flight legs. In this flight leg liquid contents exceed ice contents. This flight leg occurs at the  $-10^{\circ}\text{C}$  temperature level which is one of slow growth rates for ice, which would account for the increased amounts of liquid water. An extremely strong increase in the crystal concentrations from 12/liter to 260/liter in the BCR which is not reflected by a corresponding increase in ice contents indicate that there is an abundance of very tiny crystal that collectively do not have significant mass, and which do not have sufficient time or growth conditions to increase in size. Total water contents (liquid + ice + vapor) remain constant in the PBR and BCR with a  $0.50 \text{ g/m}^3$  decrease in the DDR suggesting precipitation of the water mass out of the cloud.

#### iv. The 5100 Meter Flight Leg (Fig. 18A and 18B)

The 5100 meter leg is a somewhat anomalous leg. While vapor water contents showed the expected trend of decrease in total content from  $1.25 \text{ g/m}^3$  to  $0.80 \text{ g/m}^3$  with a total loss of  $0.45 \text{ g/m}^3$ , ice contents were virtually zero throughout the flight and liquid water contents decrease steadily throughout the PBR to zero and remain at zero. Since this flight leg was performed only eight minutes before the start of the anomalous portion of the data set that was deleted, it is quite possible that synoptic influences were at work. Ice water contents showed a slight increase through the BCR and the beginning of the DDR, reaching a maximum of  $0.12 \text{ g/m}^3$ .

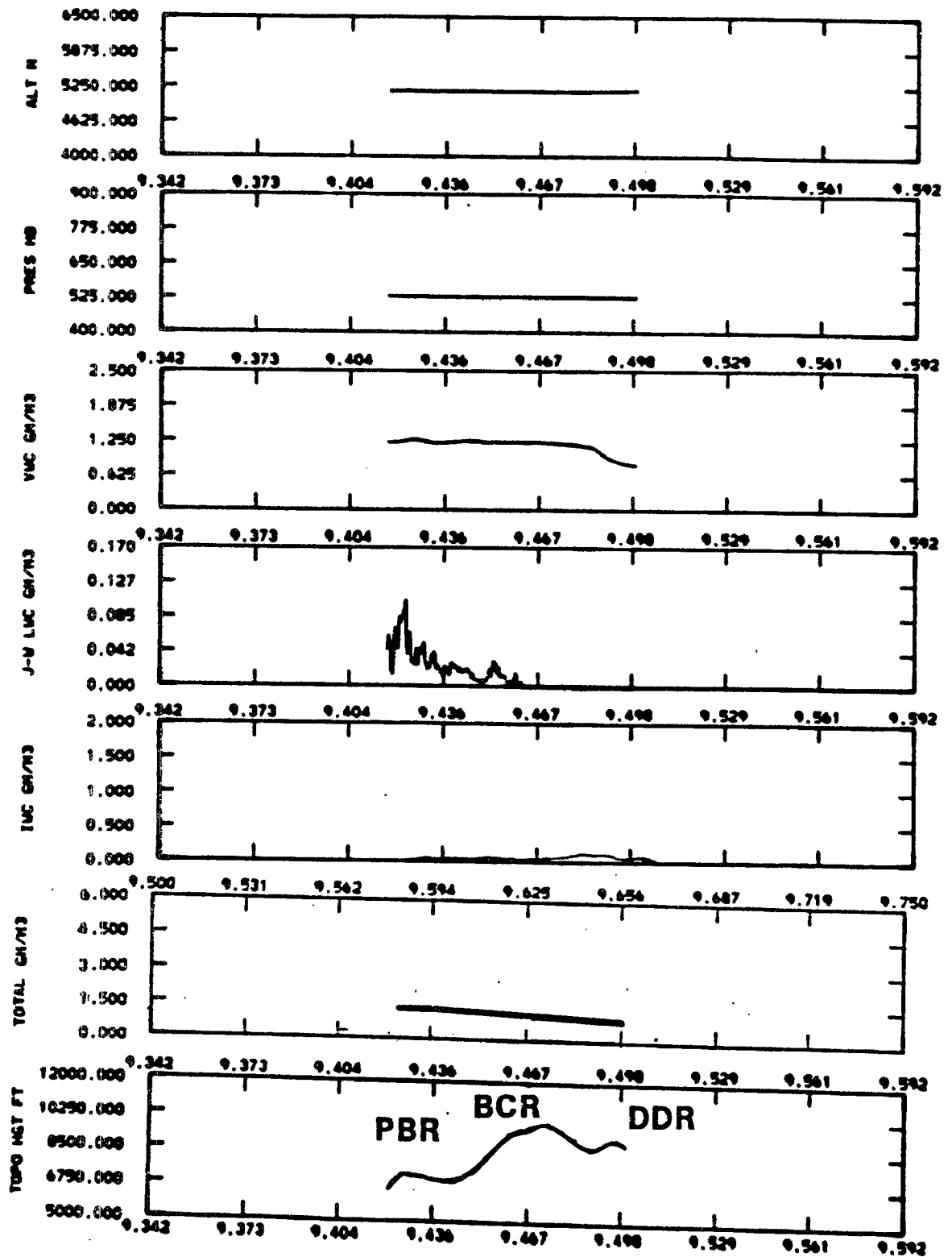


Figure 18A. 5100 Meter MSL Flight Leg: Altitude, Pressure, VWC, LWC, IWC and Topography



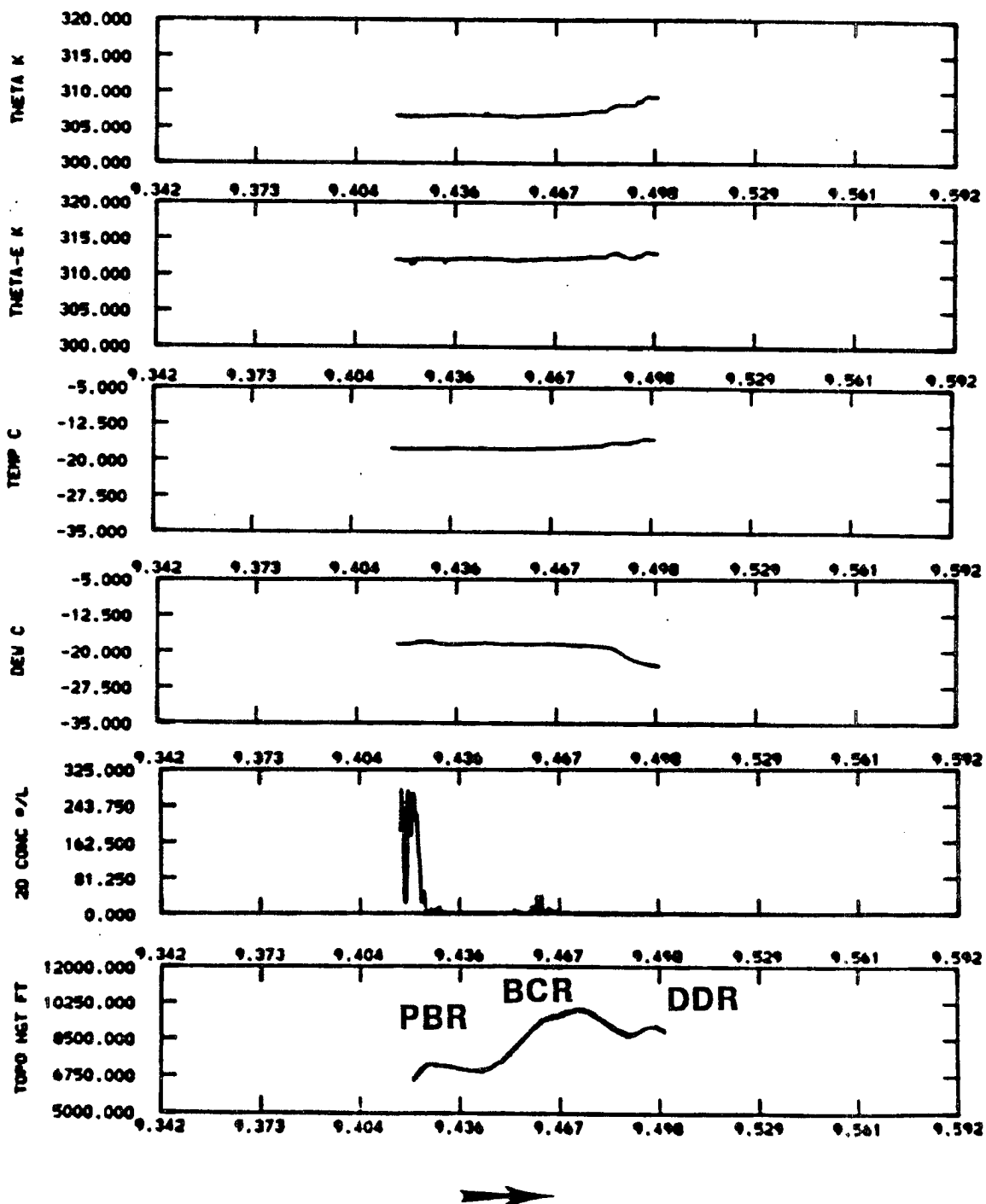


Figure 18B. 5100 Meter MSL Flight Leg: Theta, Theta-e, Temperature, Dewpoint, 2-D Concentration and Topography

## v. The 5400 Meter Flight Leg (Fig. 19A and 19B)

Liquid water contents were extremely low throughout the leg, holding steady at  $.02 \text{ g/m}^3$ . Vapor water contents decreased in the DDR from  $1.09 \text{ g/m}^3$  to  $0.60 \text{ g/m}^3$  with a total loss of  $0.50 \text{ g/m}^3$ . Ice contents increased from near zero values in the PBR to  $0.11 \text{ g/m}^3$ . Liquid mass exhibited an extremely small, transitory increase in the BCR of  $0.01 \text{ g/m}^3$ . The increases in ice and liquid did not account for the losses in vapor. As described in the 4500 m MSL flight leg, it is possible that the lack of balance can be accounted for by advective processes. This is supported by the total water content (liquid + ice + vapor) which starts at a low value of  $0.82 \text{ g/m}^3$  and increases to a maxima of  $1.32 \text{ g/m}^3$  in the BCR and decreases to  $1.02 \text{ g/m}^3$  in the DDR.

## vi. The 5700 Meter Flight Leg (Fig. 20A and 20B)

In this flight leg vapor water contents, liquid water contents and ice water contents all increase through the PBR. This reflects some effect other than topography which is increasing the vapor, the liquid and the ice cloud simultaneously. Vapor contents show a slight decrease from  $0.80 \text{ g/m}^3$  to  $0.60 \text{ g/m}^3$  in the DDR. Liquid contents peak at about  $.02 \text{ g/m}^3$  and ice shows a peak at  $0.16 \text{ g/m}^3$ . The increase in total water through the PBR is  $0.20 \text{ g/m}^3$ , with a loss through the DDR of  $0.15 \text{ g/m}^3$ . Maxima value attained is  $0.85 \text{ g/m}^3$ .

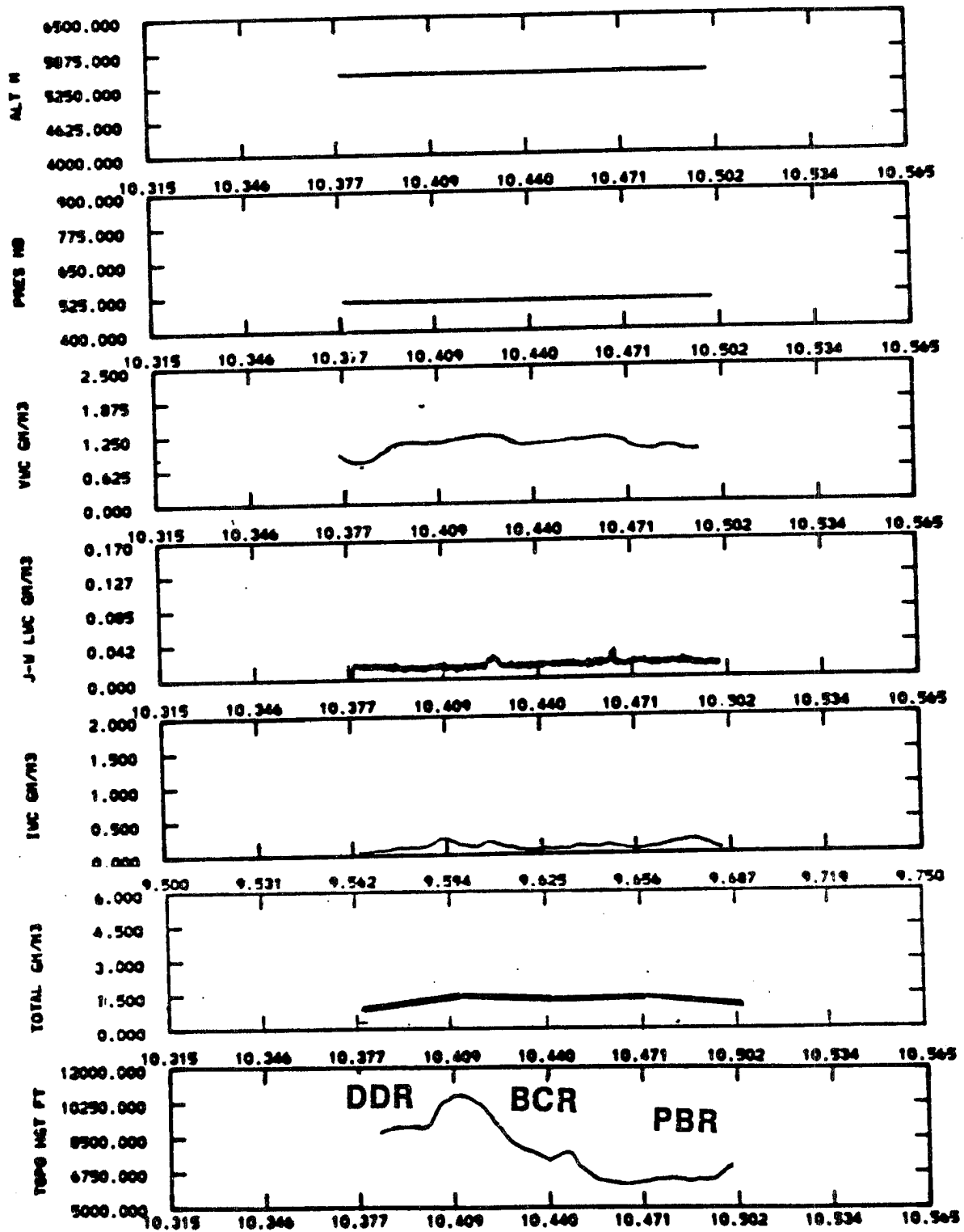


Figure 19A. 5400 Meter MSL Flight Leg: Altitude, Pressure, VWC, LWC, IWC and Topography

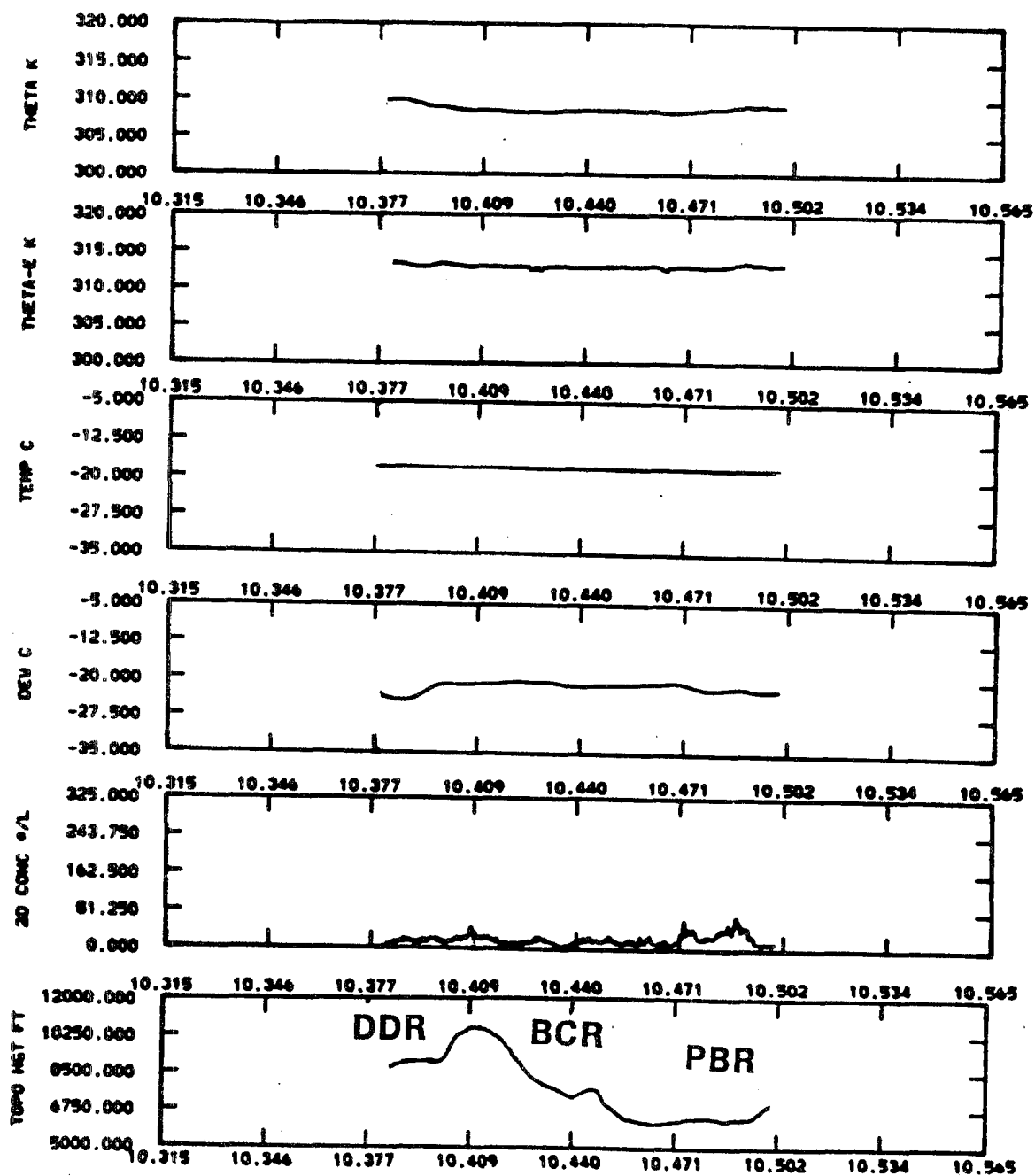


Figure 19B. 5400 Meter MSL Flight Leg: Theta, Theta-e, Temperature, Dewpoint, 2-D Concentration and Topography

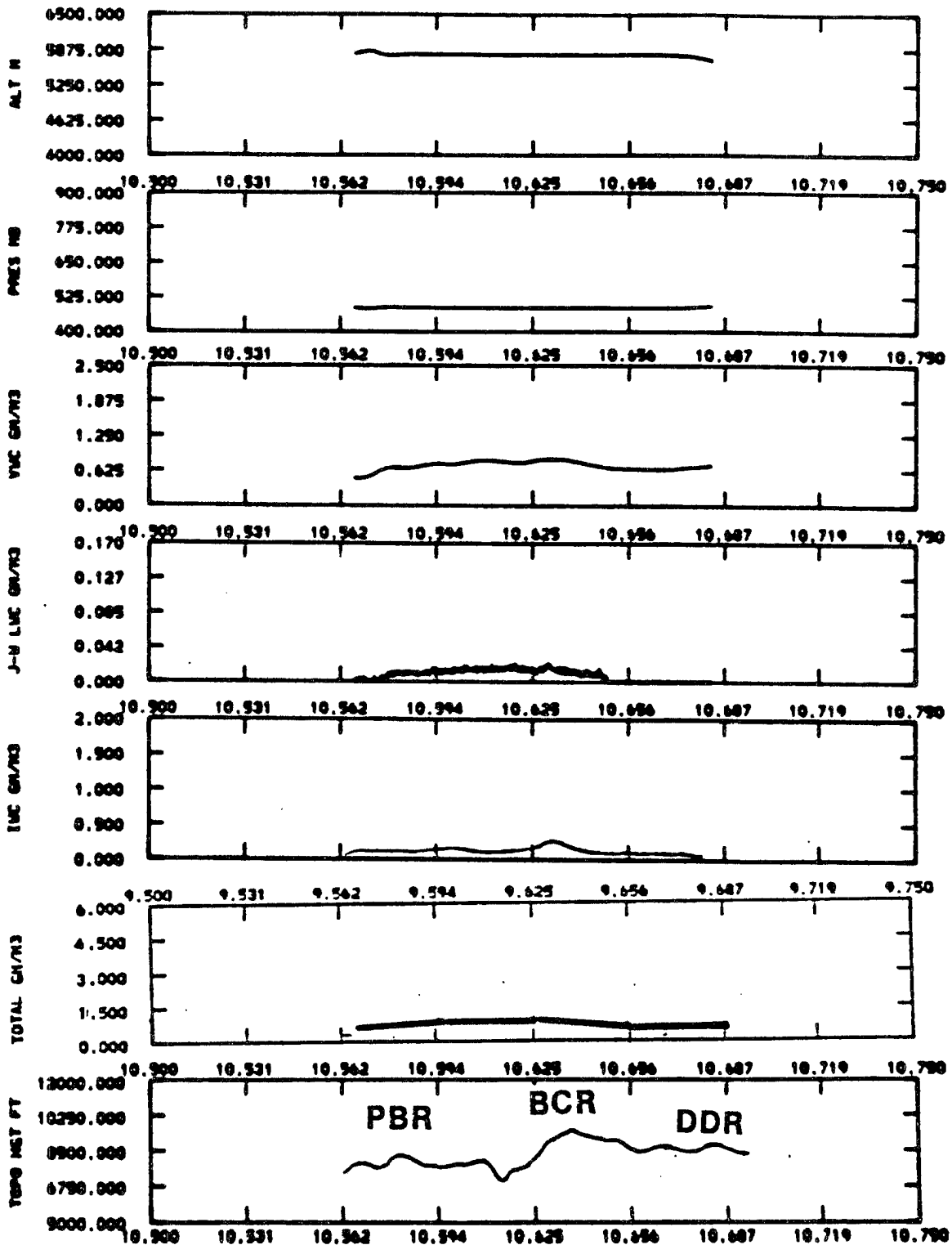


Figure 20A. 5700 Meter MSL Flight Leg: Altitude, Pressure, VWC, LWC, IWC and Topography

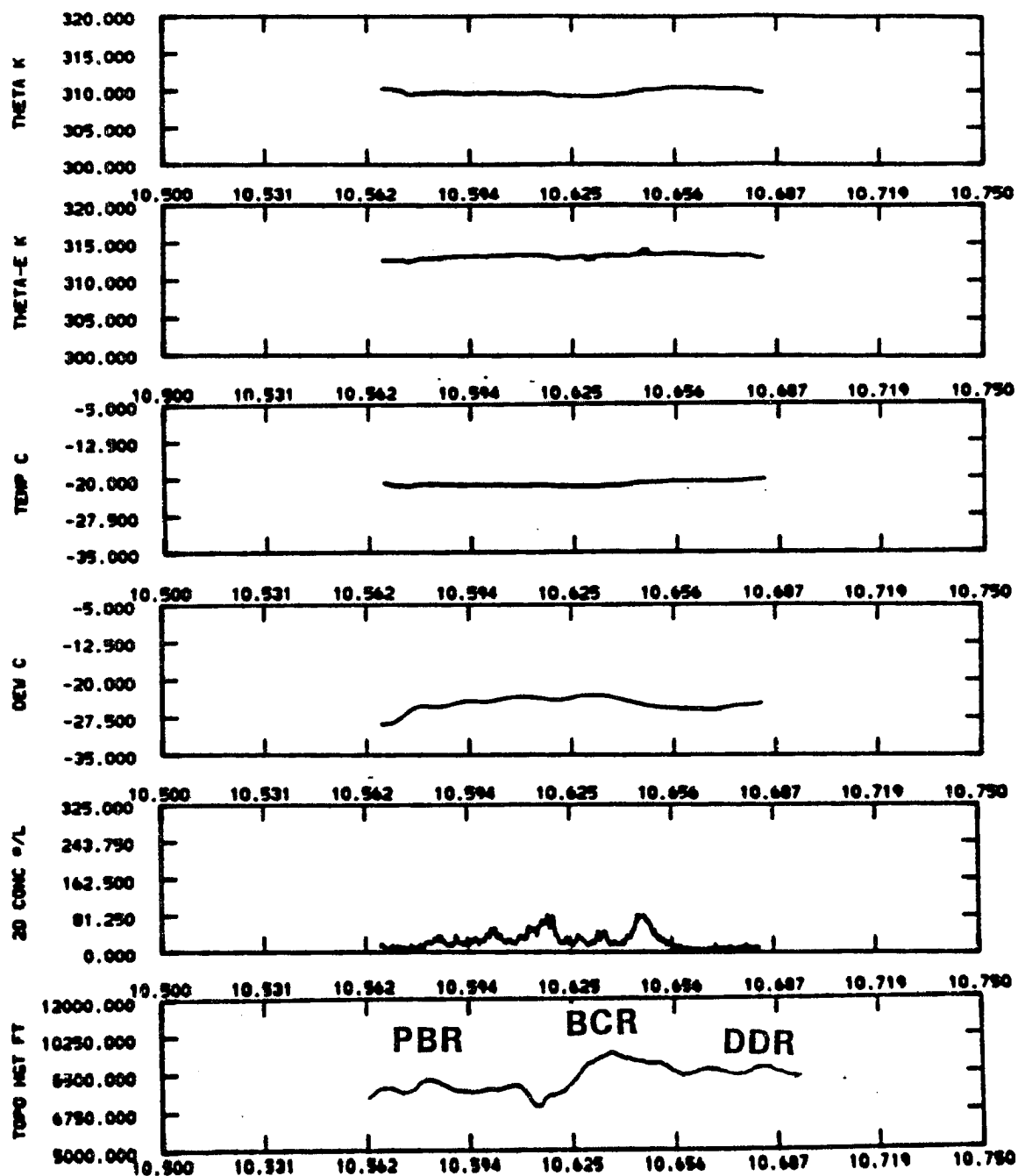


Figure 20B. 5700 Meter MSL Flight Leg: Theta, Theta-e, Temperature, Dewpoint, 2-D Concentration and Topography

vii. The 6000 Meter Flight Leg (Fig. 21A and 21B)

All components of the water budget have decreased in mass in the upper reaches of the cloud. Vapor water contents are on the order of  $0.50 \text{ g/m}^3$ , and show only a small decrease to  $0.40 \text{ g/m}^3$  in the BCR. This dip in values corresponds to an increase in liquid contents from  $0.01 \text{ g/m}^3$  to  $0.03 \text{ g/m}^3$ . Ice water contents are again negligible, less than  $0.08 \text{ g/m}^3$ , and no detectable trend emerges with respect to the underlying topography. The orographic effect is substantially lower at this higher altitude where forcing from below is not as pronounced. Total water contents are extremely stable at  $0.6 \text{ g/m}^3$ .

#### 5.5 Two Dimensional Distributions of Vapor, Liquid, Ice, Total Water and Associated Microphysical Data

Several trends have emerged in the previous section. These are best discussed in the context of contour maps of the liquid, vapor, ice, crystal concentrations, and average crystal sizes. These data are presented in Figs. 22 through 26. Vapor contents (Fig. 22) shows three major trends. 1) Decreases with height at a rate of  $0.5 \text{ g/m}^3/1000$  meters, 2) decreases at all levels over the barrier crest as a result of the condensation induced by the forced orographic lifting and 3) decreases in the down draft region as a result of permanent losses to precipitation out of the cloud. Liquid contents (Fig. 23) also decrease with height diminishing to negligible values at the 6000 MSL level. A strong maxima in water mass exists over the BCR between 4000 meters MSL

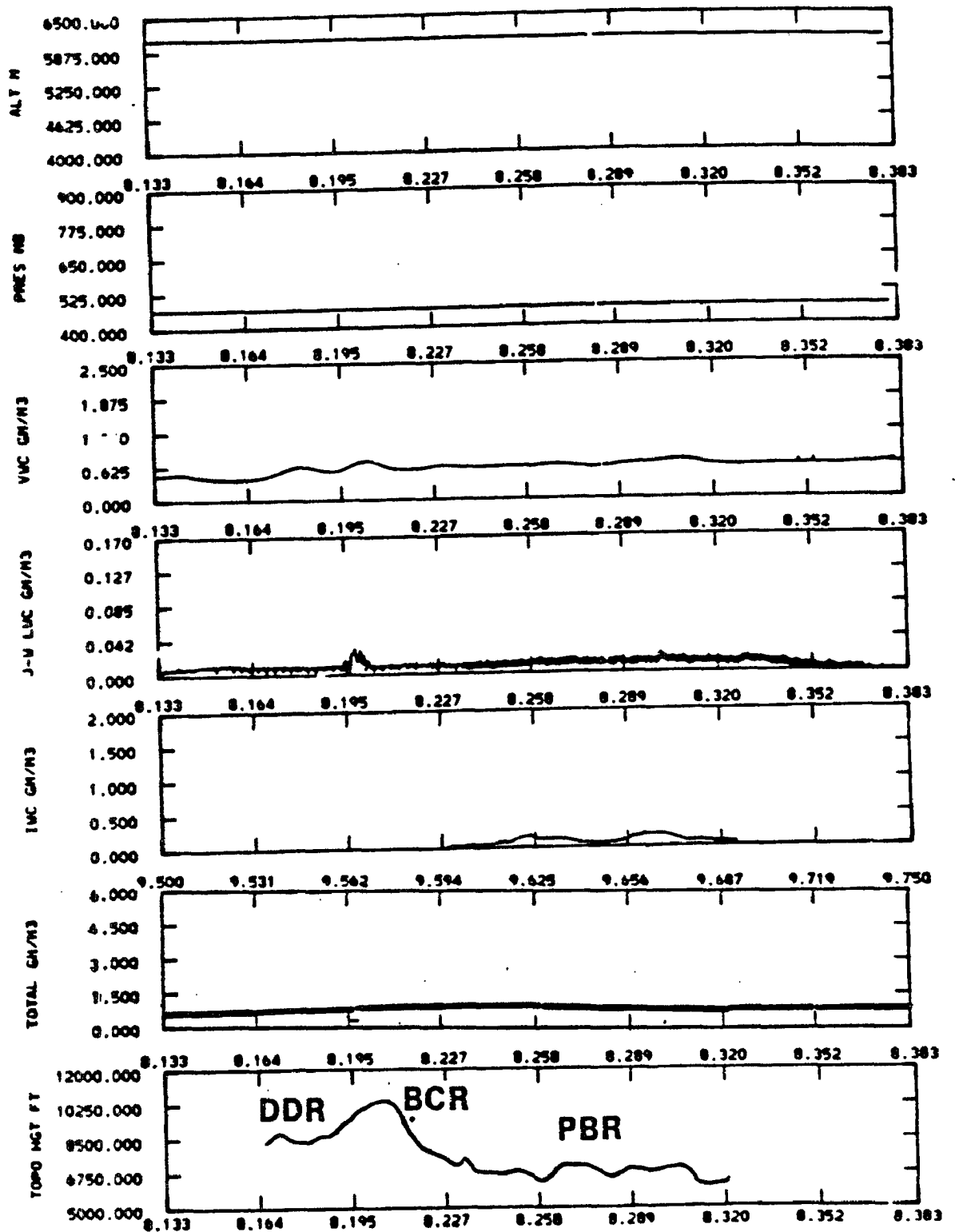


Figure 21A. 6000 Meter MSL Flight Leg: Altitude, Pressure, VWC, LWC, IWC and Topography



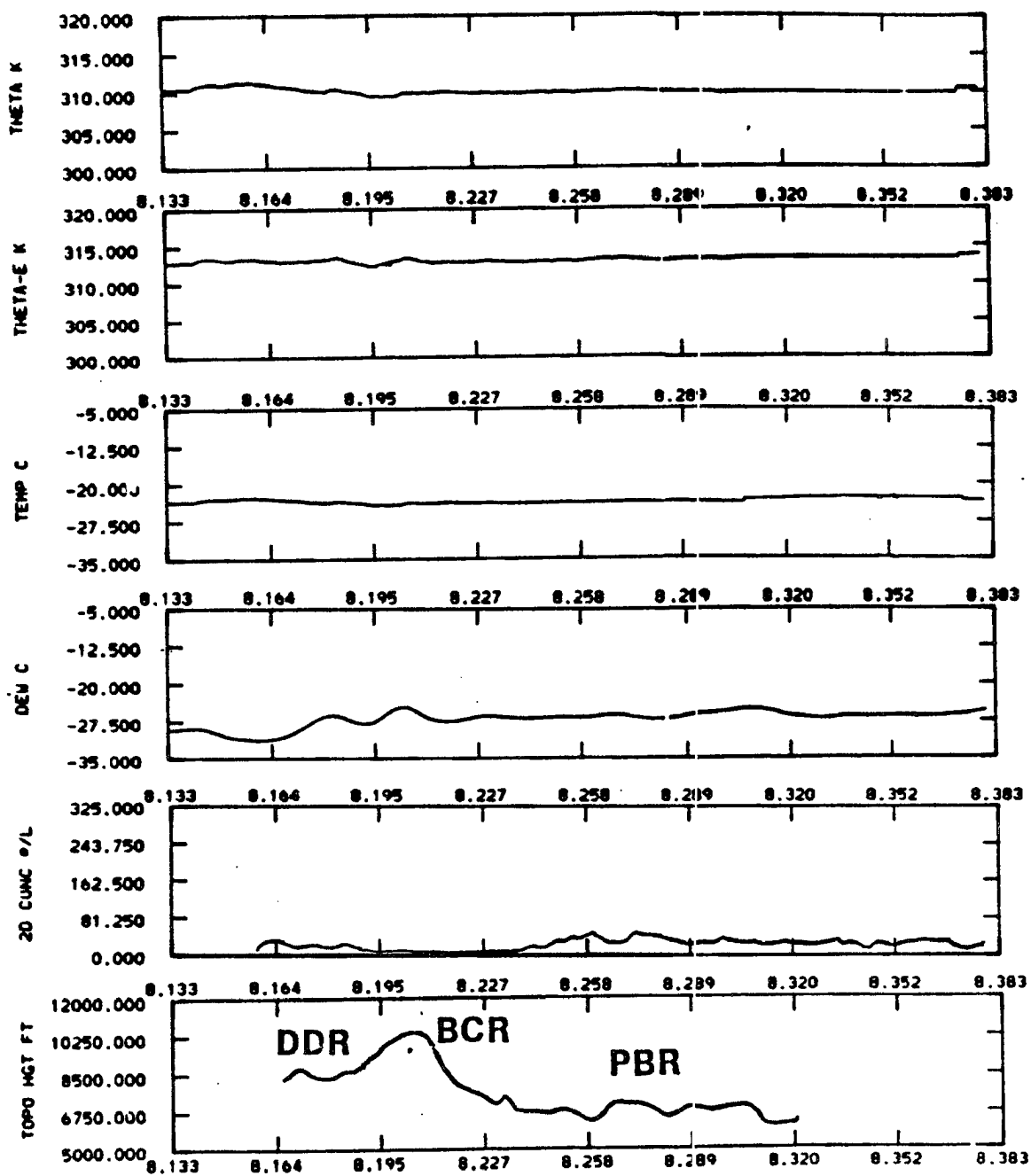


Figure 21B. 6000 Meter MSL Flight Leg: Theta, Theta-e, Temperature, Dewpoint, 2-D Concentration and Topography

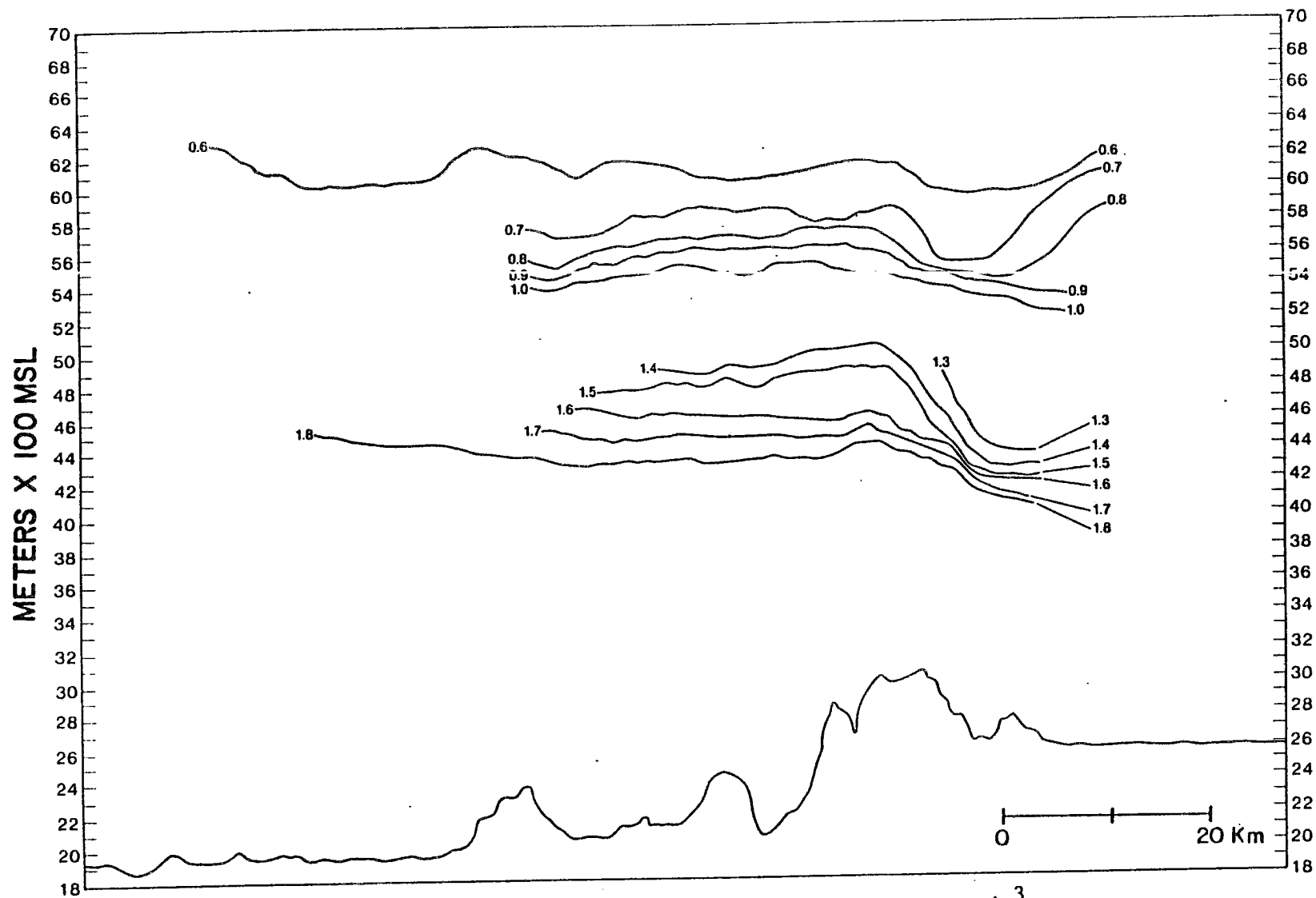
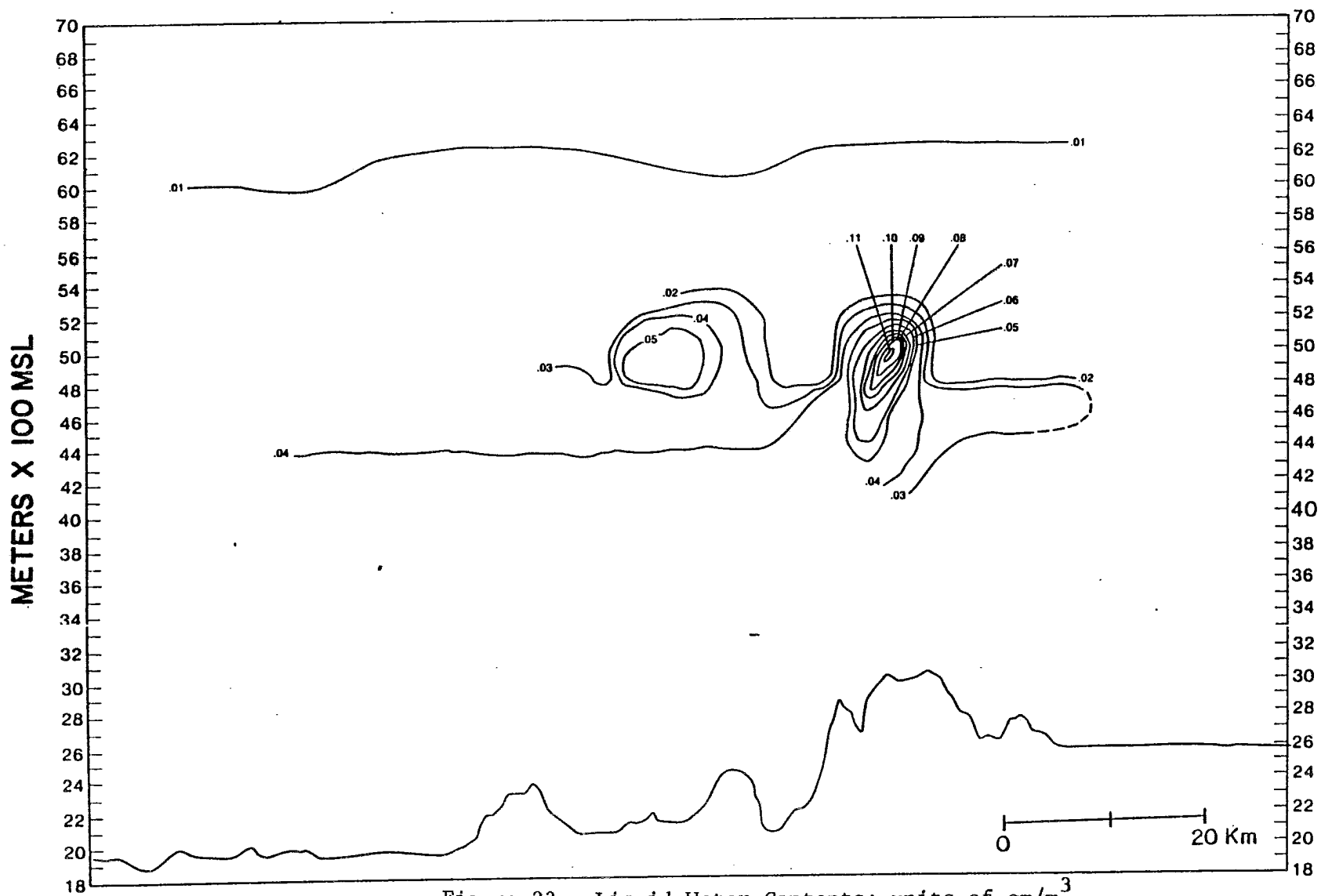


Figure 22. Vapor Water Contents: units of  $\text{gm/m}^3$



and 5000 meters MSL, with a secondary maxima over the smaller upwind barrier. These results are in good agreement with previous studies which have consistently found increased amounts of liquid water immediately over the crests of mountain barriers. Ice water mass (Fig. 24) parallels liquid and vapor in that substantial decreases occur with height, with values falling off by a factor of ten between the 4000 meter MSL and the 6000 meter MSL levels. Near 4500 meter MSL above the barrier crest ice attains a maximum value of  $1.5 \text{ g/m}^3$ . Similar to liquid contents, a small secondary maxima in ice contents is found over the crest of the smaller upwind mountain. The maxima in ice is lower in altitude, and downwind of the maxima in liquid. This phenomena is discussed further in section 6.2.

Total water contents (ice + liquid + vapor) decrease substantially with height with an average value of  $2.6 \text{ g/m}^3$  at the 4100 m MSL level and an average value of  $0.62 \text{ g/m}^3$  at 6000 m MSL. In all but the lower flight legs, the total water content was quasi-constant throughout the pre-barrier region and the barrier crest region. Slight decreases in total water mass were apparent over the down draft region indicating the effects of precipitation. In the lower flight legs, increases in total water mass due to increases in ice mass suggested advection of water substance from out of the plane of the aircraft cross section to support ice growth processes.

At lower levels, average ice crystal sizes (Fig. 25) parallel trends in ice mass with a maximum size of 450 microns occurring coincidentally with the maxima in ice water contents. Average crystal sizes and crystal concentrations (Fig. 26) both decrease with height indicating that decreases in ice mass is a function of both decreasing number density as well as smaller crystal sizes.

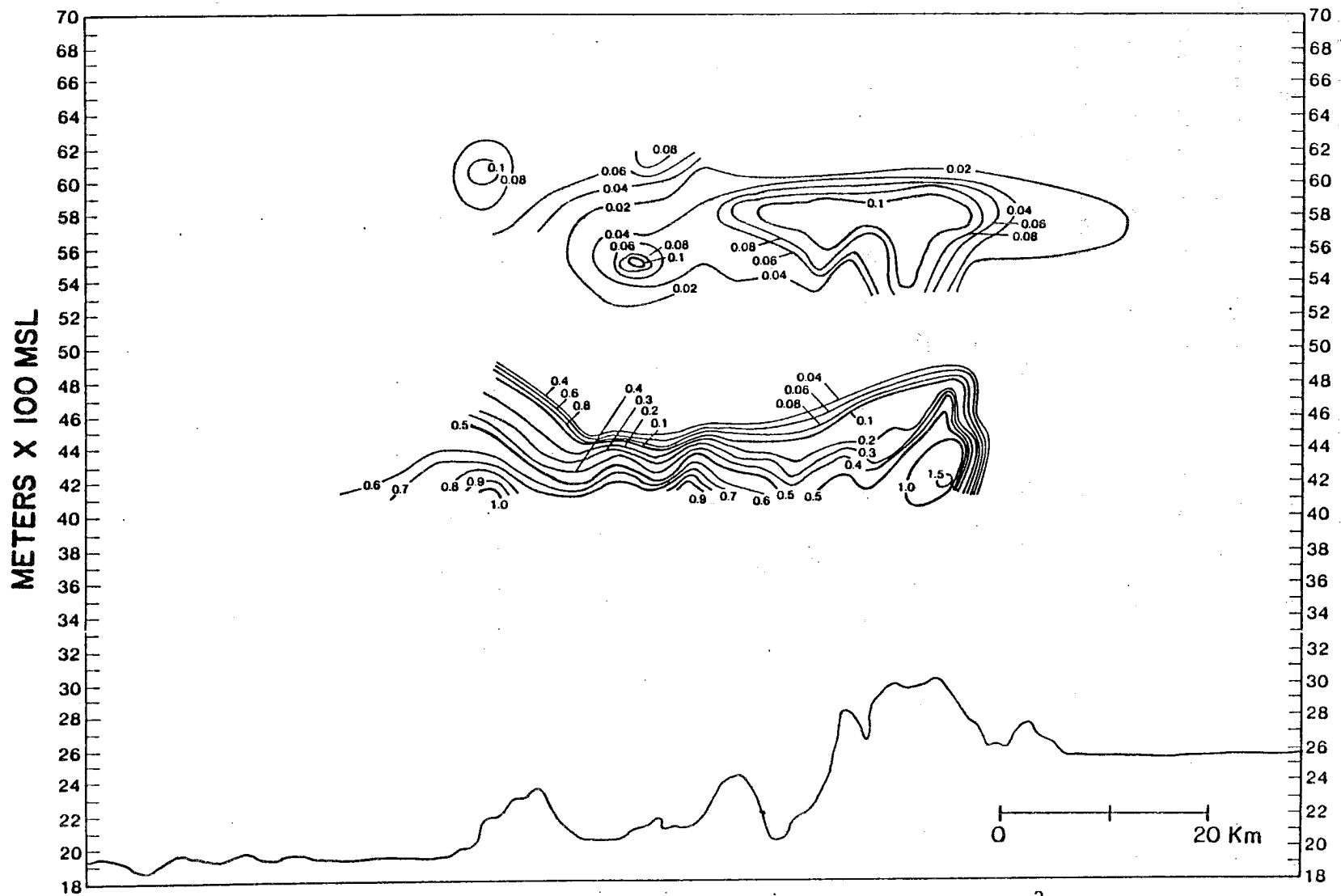


Figure 24. Ice Water Contents: units of  $\text{gm/m}^3$

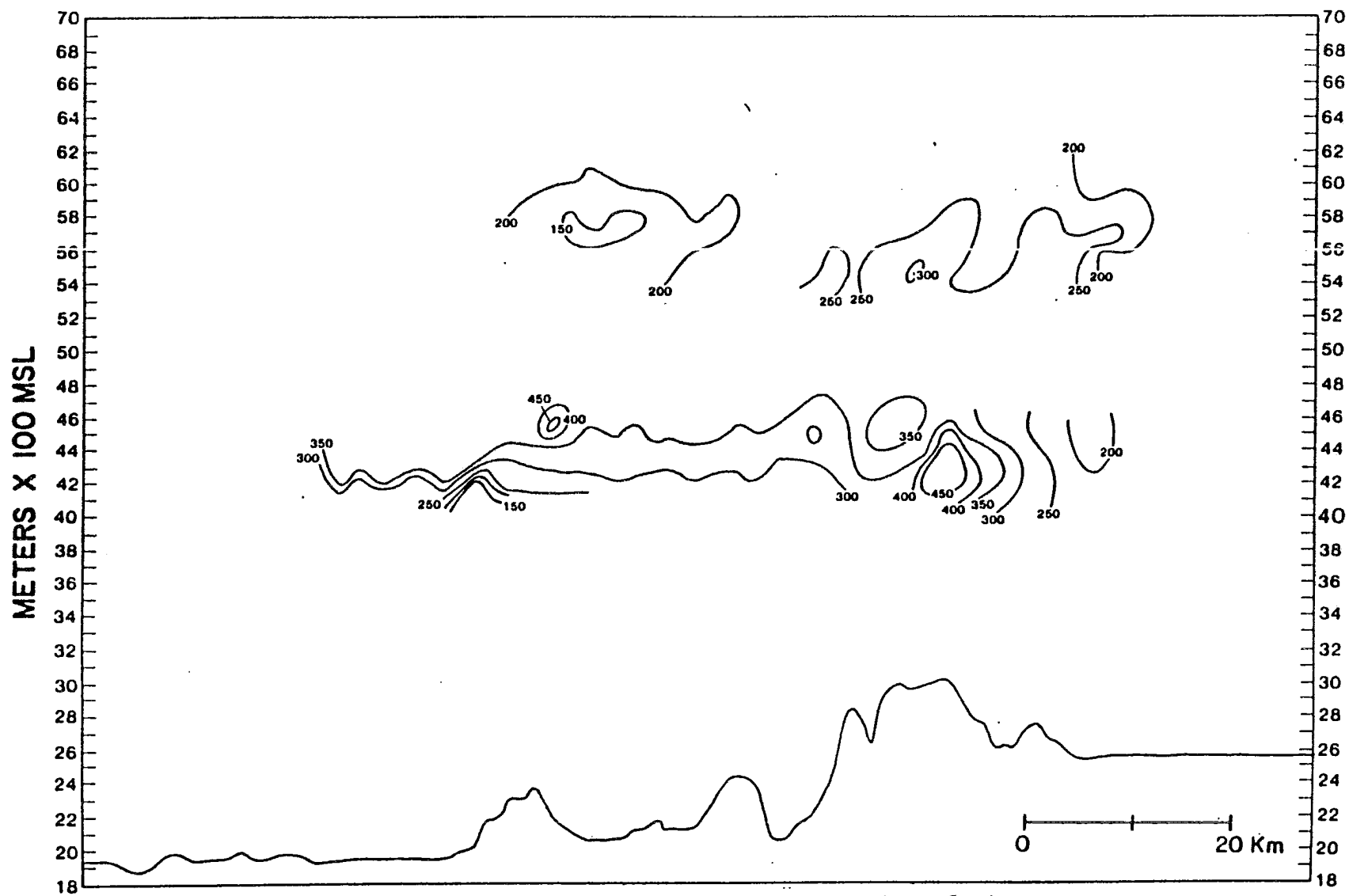


Figure 25. Average Crystal Sizes: units of microns

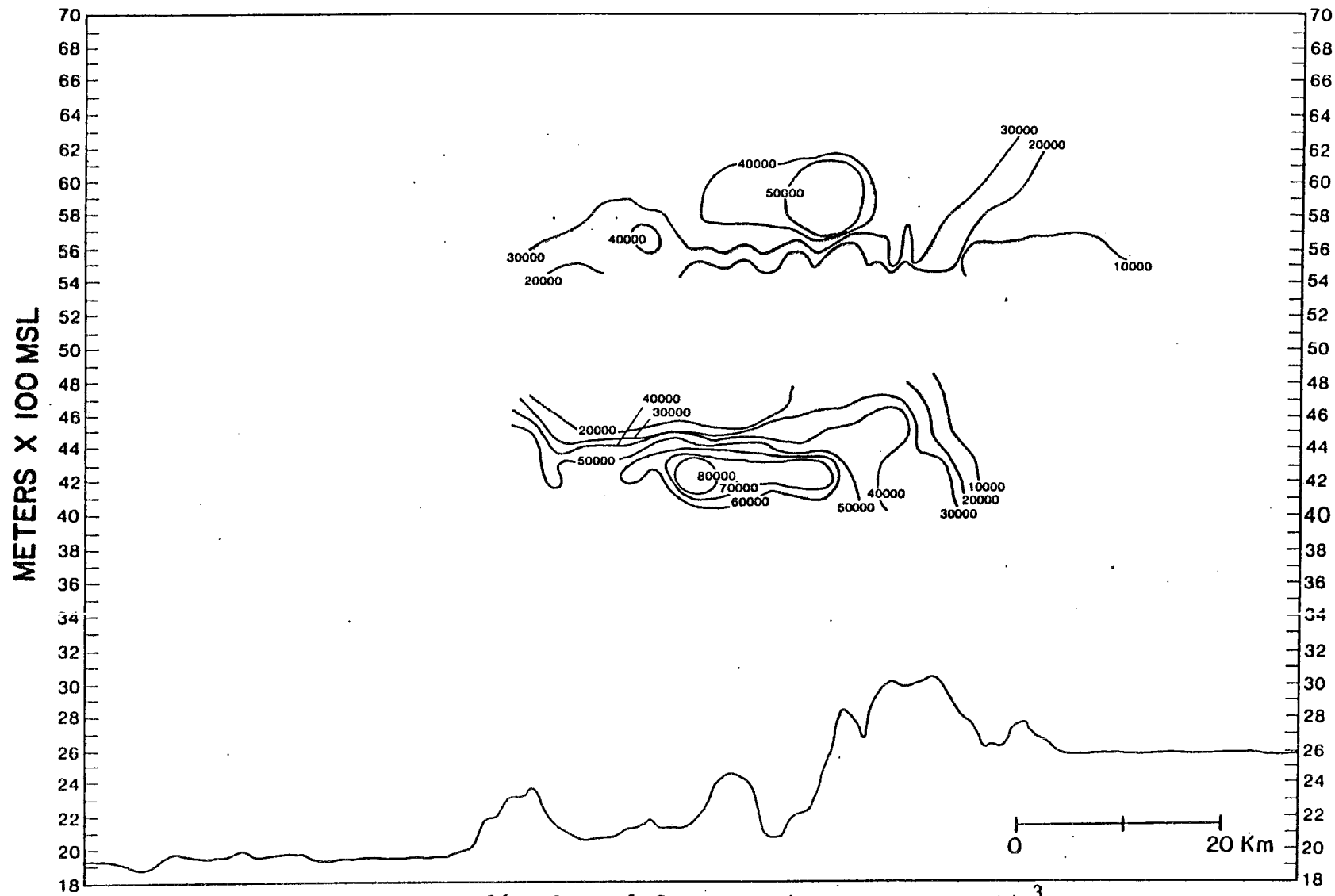


Figure 26. Crystal Concentrations: units of  $\#/\text{m}^3$

## 6. DISCUSSION AND CONCLUSIONS

In this section, the results are summarized and their implications are discussed.

### 6.1 Particle Trajectories

Particle trajectories are predicted using a simple model developed by Rauber (1981), and verified on the basis of in-cloud measurements by decelerator slides. These particle trajectories considered within the context of the temperature structure of the cloud provide information on particle habits. Predictions by the model and measurements with the decelerator in-cloud show that for the particular case under study, extremely regular and predictable habit stratification occurs throughout the portion of the cloud upwind of the mountain. This allows the use of temperature to parameterize crystal habit throughout this part of the cloud to calculate ice water contents. This was possible because at aircraft altitudes, horizontal wind speeds on December 15, 1981, from 0800 MST to 1100 MST ( $\sim 25$  m/sec) were great enough, and crystal sizes ( $\sim 250$  microns) and resulting fall velocities were small enough for crystal to move quasi-horizontally, paralleling the horizontal isotherms. The use of the model was extended to the slightly more complicated but equally predictable region of the cloud where a



significant downdraft occurs under the influence of gravity waves forced by the topography. In this region, it is apparent that crystals from the lower growth regimes are effectively removed from the cloud by rapid descent forced by the downdraft. This precipitation process occurs downwind of the crest of the barrier on the leeward slope of the mountain.

Several conclusions can be drawn from the particle trajectory study: 1) Mountain barriers create favorable conditions for the growth of cloud droplets and ice particles by forcing air parcels upward. Depending on characteristics of the airflow and the shape of the barrier, this effect can be significant. 2) Since particle trajectories are essentially horizontal from sixty km upwind of the mountain to the barrier crest, at aircraft altitudes snowfall received at the ground prior to the mountain originates from other parts of the cloud. These include ice crystals growing in the lower levels of the cloud, ice crystals caught in smaller but significant downdrafts created by secondary upwind barriers, or ice particles which originate very far upwind of the mountain. The decelerator data on particle habits showed evidence for riming over the crests of the topography. This riming undoubtedly aids the precipitation process. 3) The particle trajectories also indicate the important role that the gravity waves play in the intensity and location of snow fall rates on the ground. The strong downdraft on the lee side of the mountain as computed by the model and verified by in-cloud observations suggests that heaviest snowfall rates in such cloud systems will occur just to the lee side of the mountain. 4) The trajectories described in this study covered a simple case, one of horizontal stratified flow. Crystal distributions in

the upper levels of the cloud are extremely predictable, varying as a function of particle trajectory and temperature. Observations suggest that the structure of the flow field can be inferred from an examination of habit distributions in the cloud. The exciting possibility arises that such trajectory studies could be applied to more complicated cases and that ice crystals by virtue of their habits could be used as tracers of the airflow and the environmental conditions.

## 6.2 Ice Studies

The habit information from the trajectory study is coupled with data from the 2D-C cloud probe to calculate ice water contents. The trends in ice contents parallel those of liquid but there are indications that different mechanisms are in effect in the down draft region affecting the relative position of the ice and the liquid maxims. In the barrier crest region liquid water and ice water contents both are significantly enhanced in the zone of strongest lifting created by the mountain. In this region rapid condensation occurs as the air is lifted quickly to colder temperatures and saturations with respect to ice and to water are increased. In the down draft region however, values of liquid mass decrease more rapidly than those of ice. The position of the maxima in ice mass is lower in altitude and downwind of the liquid maximum. This results in part from the fact that average ice crystal sizes are larger than average cloud droplet sizes and therefore they do not evaporate as quickly. However, while liquid water contents are depleted by simple evaporation, the decreases in ice water probably reflect a more complicated process.

In the downdraft region, supersaturations with respect to ice fall off more slowly than supersaturations with respect to water. DeMott et. al. (1982) have hypothesized that this downdraft region may be one of enhanced contact nucleation by virtue of thermophoretic collection. This process is not likely to be a factor in the observations presented, since even large numbers of small crystals would not contribute significantly to the total ice mass. The parcel trajectory model (Fig. 12) predicts that the streamlines will become compacted on the lee side of the mountain. As the ice mass moves into the downdraft, apparent increases occur due to local accumulation resulting from the compressed airflow. This effect is rapidly counteracted as the ice eventually evaporates and precipitates out of the cloud.

When comparing ice content to other crystal parameters it is found that a strong correlation existed between ice water contents and average ice crystal sizes in the lower levels of the cloud. Ice mass, crystal concentration, and crystal sizes all decrease with increasing altitude.

Conclusions of the ice study are as follows: 1) Information from the Knollenberg 2-Dc particle probe is not sufficient to determine particle habits for storms with a large percentage of irregularly shaped crystals. Various computer programs have been developed for form recognition, however the probe does not provide sufficient information for these programs to be consistently successful. This limitation required the development of an alternative method of determining ice water contents. The method developed is not fully evaluated in terms of accuracy, but it shows that reasonable trends and magnitudes emerge from the calculations described in this paper. 2) Ice masses are an important parameter characterizing the structure of the cloud. Despite

its importance, ice contents are not a routine measurement in cloud physics. Since the ice mass is physically interconnected with trends and magnitudes of liquid contents which are often used to assess cloud modification potential, it cannot be overlooked as an important cloud parameter. 3) The correlation between ice crystal sizes and ice contents implies that increases in ice mass are primarily a function of growth processes rather than of nucleation of new particles.

### 6.3 Budget Studies

Information is obtained on spatial distribution of vapor contents, liquid contents and ice contents. These comprise all the parts of a total water budget excluding precipitation. The balance at different levels varied with ice mass usually exceeding, but sometimes being exceeded by liquid mass in the competition for the condensed vapor mass. Total water mass showed two consistent trends, decreasing with height and decreases over the down draft region indicating precipitation processes. On most of the flight legs a reasonably good budget that accounted for losses and gains was found between the three competing elements and the water balance described by Fig. 1 was approximated.

Maximum ice water contents attained a value of  $1.54 \text{ g/m}^3$  which is comparable in magnitude to vapor water contents of  $2.0 \text{ g/m}^3$ . Maximum liquid water contents are at least an order of magnitude lower at a maxima of  $0.11 \text{ g/m}^3$ . The following conclusions are drawn from the budget calculation: 1) In the cloud studied, liquid is a small difference resulting from the competition between two large factors, vapor and ice. This balance suggests that significant amounts of liquid

water can only result when ice growth processes are operating inefficiently. 2) A remarkably high precipitation efficiency, defined as ice (potential precipitation) divided by ice plus liquid (total available condensate) already existed. Values of total water content stayed quasi-constant, especially in the upper levels of the cloud, upwind of the mountain indicating that there were no significant losses to precipitation. If artificial seeding techniques had worked perfectly, ice water contents could not have been enhanced significantly. Since it is not likely that all of the additional ice could have been induced to fall out of the cloud, precipitation amounts would not have been detectably increased. 3) It is apparent that the upper levels of the cloud which existed on December 15, 1981 did not have the requirements for weather modification operations to increase precipitation. However, it is extremely important to note that these results do not preclude the possibility that modification potential existed in the lower levels of the cloud. The study presented is limited to logistically feasible aircraft altitudes. Similar studies are necessary, perhaps utilizing a different set of instruments to evaluate the water balance in the lower levels of the cloud. 4) It has been shown that a phase water budget for a cloud can be evaluated. This water budget has been shown to be useful for evaluating dynamical and microphysical characteristics of the cloud. These properties can be used to develop quantitative measurements of modification potential in the cloud.

## 7. SUGGESTIONS FOR FUTURE RESEARCH

This study revealed important information about the specific cloud with regards to it's physical structure. This suggests that phase budgets can be used to study the physical structure and estimate the modification potential of different types of cloud systems. It would be ideal if operational seeders could be provided with information allowing them to make decisions on what kinds of cloud systems are worthwhile to target with seeding operations, and which ones are not. Such a study would require a comprehensive cataloging of case studies of water budgets for different storm types, such as orographic, convective and frontal. To do such studies, calculations of ice water contents throughout the cloud are an imperative. Use of particle trajectories through temperature refined growth regimes will undoubtedly be a less tractable method when applied to complicated situations involving increased local updraft and downdraft motion and/or increased turbulence. Three other methods of determining ice water contents, are suggested as having potential. These are: 1) improvement of detection techniques to increase image resolution; 2) use of radars to attempt to correlate reflectivities to ice water contents; and, 3) development of an airborne collector of ice particles to directly measure ice water contents.

Cloud models also provide an important application for case studies such as the one presented. Cloud models are an important tool in the

interpretation of cloud processes, and can be used to assess the mechanisms operating in the cloud system on December 15th 1981. At the same time, the distributions of the different phases of the water substance and the in-cloud measurements of crystal habits in the cloud provide an excellent opportunity for verification and initialization of cloud models with realistic parameters.

Finally, it has been shown that ice crystals by virtue of their habit characteristics, size, and riming characteristics can be excellent indicators of the environmental conditions in cold clouds. In theory, one should be able to stand on the ground, to catch a few flakes, and have as much information as can be reduced from a whole array of radars, radiometers, rawinsondes and cloud microphysics aircraft. The studies that are dedicated to revealing the host of information in a single snow crystal are considered by this author to be both aesthetically pleasing and extremely practical.

# CIC CHEYENNE DATA ACQUISITION SYSTEM SENSOR SPECIFICATIONS

Parameter Measured	Instrument Type	Manufacturer and Model Number	Combined Performance of Transducer, Signal Conditioning and Conversion				Useable Resolution (s)
			Range	Accuracy	Time Constant (s)	Sample Rate (s)	
Time	Crystal osc	PHS	12 mo	1 s	N/A	0.1s	0.1 s
Temperature	Platinum resistance	Rosemount Eng. Co. 510BF9 Bridge Model 102 Probe	±50°C	0.5°C	1	1 Hz	0.1°C
Dew Point <sup>2</sup>	Peltier cooled mirror	Cambridge System Inc. Model 137-C3	±50°C	1°C	1-5 s	1 Hz	0.3°C
Liquid Water <sup>3</sup>	Hot Wire	Cloud Technology Model LWH	0-3 gm/m <sup>3</sup>	0.3 gm/m <sup>3</sup>	0.5	1 Hz	0.01 gm/m <sup>3</sup>
Altitude	Static Pressure	Rosemount Eng. Co. Model 830BA	0-15 psia	0.015 psia	0.1	1 Hz	0.007 psia
Altitude	Static Pressure	Setra Systems	0-20 psia	0.015 psia	0.1	1 Hz	0.010 psia
Indicated	Differential pressure	Rosemount Eng. Co. Model 1332B1	±2.5 psid	0.0025 psid	0.1	10 Hz	0.0025 psid
Heading	Gyro	Sperry	0-360°	±2°	0.1	1 Hz	0.1°

8. APPENDIX 1





Parameter Measured	Instrument Type	Manufacturer and Model Number	Combined Performance of Transducer, Signal Conditioning and Conversion				Useable Resolution (s)
			Range	Accuracy	Time Constant (s)	Sample Rate (s)	
Pitch	Gyro	Sperry	$\pm 85^\circ$	$\pm 2^\circ$	0.1	1 Hz	0.1°
Roll	Gyro	Sperry	$\pm 180^\circ$	$\pm 2^\circ$	0.1	1 Hz	0.1°
Position (azimuth)	VOR	King Radio (HTI Digital Interface)	0-360°	$\pm 2^\circ$	1	1 Hz	0.1°
Position (distance)	DME	ARC Radio Corp.	225 km	0.5 km	1	1 Hz	0.01 km
Vertical Acceleration <sup>5</sup>	Pendulous Mass	Sundstrand Corp.	$\pm 2$ g	0.001 g	0.1	1 Hz	0.0001 g
Cloud Particle Size & Concentration <sup>6</sup>	Optical Array	PMS 2-D OAP	37.5-1200 $\mu$ 0.1-10,000 $\text{L}^{-1}$		Discrete Event	Continuous Continuous	37.5 $\mu$ 0.1 $\text{L}^{-1}$
Cloud Droplet Size & Concentration <sup>7</sup>	Optical Forward Scattering	PMS FSSP	2-45 $\mu$ 0.1-10,000 $\text{cm}^{-3}$		Discrete	Continuous	0.5 to 3 $\mu$
Ice Nucleus Concentration <sup>9</sup>	Optical Scattering	HEE/CSU	30-30,000 $\text{L}^{-1}$		Discrete	Continuous	30 $\text{L}^{-1}$



## 9. REFERENCES

- Balick, L.K. and J.L. Rasmussen, 1972: A Case Study of the Water Budget of an Orographic Cloud, Atmospheric Science Paper No. 187, Dept. of Atmospheric Science, Colorado State University, Fort Collins, Colorado.
- Baumgardner, D. and J.E. Dye, 1983: Cloud Particle Measurement Symposium: Summaries and Abstracts, NCAR Technical Note, 103 pp. (NCAR/TN - 199 + PROC).
- Beard, K.V., 1983: Reorientation of Hydrometeors in Aircraft Accelerated Flow. J. Climate Appl. Meteor., 22, 1961-1963.
- Cooper, W.A. and G. Vali, 1981: The Origin of Ice in Mountain Cap Clouds. J. Atmos. Sci., 38, 1244-1259.
- Demott, P.J., Finnegan, W.G., and L.O. Grant, 1982: A Study of Ice Crystal Formation in Stably Stratified Orographic Cloud. Conf. on Cloud Physics, Chicago, IL, November 15-18, 1982, 488-490.
- Demott, P.J., Personal Communication, 1984.
- Duroure, M.C., 1982: An Automatic Method of Pattern Recognition for 2D Images based on Radial and Harmonic Analysis of Image Outline. Cloud Particle Measurement Symposium: Summaries and Abstracts. NCAR/TN-199 & PROC., September 1982.
- Dirks, R.A., 1973: Precipitation Efficiency of Orographic Clouds. J. Rech. Atmos., 7, 177-184.
- Elliot, R.D. and R.W. Shaffer, 1962: The Development of Quantitative Relationships Between Orographic Precipitation and Air Mass Parameters for Use in Forecasting and Cloud Seeding Evaluation. J. Appl. Meteor., 1, 218-228.
- Elliot, R.D. and E.L. Hovind, 1964: The Water Balance of Orographic Clouds, J. Appl. Meteor., 3, 235-239.
- Fukuta, N., G.D. Swoboda and A.S. Wang, 1982: Experimental and Theoretical Studies of Ice Crystal Habit Development. Conf. on Cloud Physics, Chicago, IL, November 15-18, 1982, 329-332.
- Fukuta, N. and A.S. Wang, 1984: The Mechanism of Habit Development in Diffusional Ice Crystal Growth. International Conference on Cloud Physics, Tallinn, Russia, August 21-28, 1984, 194-198.



- Heymsfeld, A.J., 1972: Ice Crystal Terminal Velocities. J. Atmos. Sci., 29, 1348-1357.
- Heymsfeld, A.J. and R.G. Knollenberg, 1972: Properties of Cirrus Generating Cells. J. Atmos. Sci., 29, 1358-1366.
- Heymsfeld, A.J. and J.L. Parrish, 1979: Techniques Employed in the Processing of Particle Size Spectra and State Parameter Data Obtained with T-28 Aircraft Platform. NCAR Technical Note, 78 pp. (NCAR/TN-137 + 1A).
- Hindman, E.W., P.J. DeMott and L.O. Grant, 1981: Precipitation Efficiency Studies of Colorado Mountain Winter Storms and Storm Stages. Eighth Conference on Inadvertant and Planned Weather Modification, Reno, NV, October 15-17, 1981, 56-57.
- Hobbs, P.V. and T.J. Mateyka, 1982: Precipitation Efficiencies and the Potential for Artificially Modifying Extratropical Cyclones. Third WMO Scientific Conference on Weather Modification, 1, 9-15.
- Hogg, D.C. F.O. Guiraud, J.B. Snider, M.T. Decker and E.R. Westwater: A Steerable Dual-Channel Microwave Radiometer for Measurement of Water Vapor and Liquid in the Troposphere, J. of Appl. Meteor., vol. 22, no. 5, May 1983.
- Hunter, H.E., 1982: Machine Classification of Cloud Particle Types. Air Force Geophysics Laboratory, (AFGL-TR-82-0298).
- Jiusto, J.E. and H.K. Weickmann, 1973: Types of Snowfall. Bull Amer. Meteor. Soc., 11, 1148-1162.
- Knollenberg, R.G., 1972: Comparative Liquid Water Content Measurements of Conventional Investments with an Optical Array Spectrometer. J. Appl. Meteor., 11, 501-508.
- Knollenberg, R.G., 1972: Measurements of Growth of an Ice Budget in Persisting Cumuli. J. Atmos. Sci., 29, 1367-1374.
- Knollenberg, R.G., 1976: Three New Instruments for Cloud Physics Measurements. Preprints Int. Conf. Cloud Physics, Boulder, Colorado, Amer. Meteor. Soc., 554-561.
- Kobayashi, T., 1961: The Growth of Snow Crystals at Low Supersaturations. Phil Mag., 6, 1363-1370.
- Lowe, P.R., 1976: An Approximating Polynomial for the Computation of Saturation Vapor Pressure. J. Appl. Meteor., 16, 100-103.
- Magono, C. and C.W. Lee, 1966: Meteorological Classification of Natural Snow Crystals, J. Fac. Sci., Hokkaido University, Sec. 7, 2, no. 4, 321-362.



- Magono, C. and C.W. Lee, 1973: The Vertical Structure of Snow Cloud as Revealed by "Snow Crystal Sondes," Part II. J. Meteor. Soc. Japan, 51, no. 3, 176-189.
- Nakaya, U., 1954: Snow Crystals, Harvard University Press, Cambridge.
- Nakaya, U., M. Hanajiwa and J. Muguruma, 1958: Physical Investigations on the Growth of Snow Crystals. J. Fac. Soc., Hokkaido University, Ser. II, 5, 87-118.
- Queney, P., 1948: The Problem of Airflow over Mountains: A Sumamry of Theoretical Studies. Bull. Amer. Meteor. Soc., 20, 16-26.
- Rasmussen, J.L., R.W. Furman and H. Riehl, 1969: Moisture Analysis of an Extratropical Cyclone. Arch. Meteor. Geoph. Biokl. Ser., A, 18:275-298.
- Rauber, R.M., 1981: Microphysical Processes in Two Stably Stratified Orographic Cloud Systems. M.S. Dissertation, Dept. of Atmos. Science, Colorado State University, Fort Collins, CO, 151 pp.
- Rauber, R.M. and L.O. Grant, 1982: COSE III Operation Lob, December 1, 1981 to February 28, 1982. Department of Atmospheric Science, Colorado State University, Fort Collins, Colorado.
- Riehl, H. and G. Williams, 1981: On the Determination of Precipitation Efficiency. Weather Modification Program Office, National Oceanic and Atmospheric Administration Tech. Memorandum, 29 pp., (ERL/WMPO-46).
- Snider, J.B., H.M. Burdick and D.C. Hogg, 1980: Cloud Liquid Measurements with a Ground-based Microwave Instrument. Radio Sci., 15, no. 3, 683-693.
- Smith, R.B., 1979: The Influence of Mountains on the Atmosphere, Advances in Geophysics, vol. 21, Academic Press, 87-127.
- Tazawa, S. and C. Magono, 1973: The Vertical Structure of Snow Clouds, as Revealed by "Snow Crystal Sondes" Part I. J. Met. Soc. Japan, 51, no. 3, 168-174.



